

# Fundamental Limits of Deep Learning-Based Binary Classifiers Trained with Hinge Loss

Tilahun M. Getu, *Member, IEEE* and Georges Kaddoum, *Senior Member, IEEE*

## Abstract

Although deep learning (DL) has led to several breakthroughs in many disciplines as diverse as chemistry, computer science, electrical engineering, mathematics, medicine, neuroscience, and physics, a comprehensive understanding of why and how DL is empirically successful remains fundamentally elusive. To attack this fundamental problem and unravel the mysteries behind DL's empirical successes, significant innovations toward a unified theory of DL have been made. These innovations encompass nearly fundamental advances in optimization, generalization, and approximation. Despite these advances, however, no work to date has offered a way to quantify the testing performance of a DL-based algorithm employed to solve a pattern classification problem. To overcome this fundamental challenge in part, this paper exposes the fundamental testing performance limits of DL-based binary classifiers trained with hinge loss. For binary classifiers that are based on deep rectified linear unit (ReLU) feedforward neural networks (FNNs) and ones that are based on deep FNNs with ReLU and Tanh activation, we derive their respective novel asymptotic testing performance limits. The derived testing performance limits are validated by extensive computer experiments.

## Index Terms

DL, the (unified) theory of DL, interpretable AI/ML, interpretable DL, fundamental limits.

T. M. Getu is with the Electrical Engineering Department, École de Technologie Supérieure (ETS), Montréal, QC H3C 1K3, Canada. He was with the Communications Technology Laboratory, National Institute of Standards and Technology (NIST), Gaithersburg, MD 20899, USA, and the Electrical Engineering Department, ETS, Montréal, QC H3C 1K3, Canada (e-mail: tilahun-melkamu.getu.1@ens.etsmtl.ca).

G. Kaddoum is with the Electrical Engineering Department, École de Technologie Supérieure (ETS), Montréal, QC H3C 1K3, Canada, and the Cyber Security Systems and Applied AI Research Center, Lebanese American University, Beirut, Lebanon (e-mail: georges.kaddoum@etsmtl.ca).

## I. INTRODUCTION

### A. *Related Works*

As the most popular and powerful contemporary technology behind artificial intelligence (AI) / machine learning (ML), deep learning (DL) [1]–[3] has led to numerous 21st-century breakthroughs in many disciplines. Among those disciplines, chemistry [4]; computer science [5], [6]; electrical engineering [7]–[14]; mathematics [15], [16]; medicine [17], [18]; neuroscience [19]–[21]; and physics [22]–[24] have witnessed breakthroughs that have been made possible because of advancements in DL. In chemistry, DL has been deployed to accurately predict the structure of proteins [4] and facilitate drug discovery by improving prospective predictions [25]. In computer science, DL has been used to solve several remarkably challenging problems related to computer vision and image classification [2], [3]; object recognition [26]; natural language processing [27], [28]; and game intelligence [5], [6].

In electrical engineering, DL has been hugely successful for speech processing and recognition [29]; wireless communication, signal processing, and networking [7]–[14]; and sparse signal and image processing [30], [31]. In mathematics, DL has been a major advancement for solving high-dimensional partial differential equations [15] and approximating functions [16]. In medicine, DL has led to breakthroughs in skin cancer classification [17] and the diagnosis of retinal disease [18]. In neuroscience, DL has been successfully deployed to capture various phenomena with respect to (w.r.t.) semantic development and cognition [19], to implement associative memory [20], and to unify DL and neuroscience [21]. In physics, DL has been successfully used for the variational representation of quantum states toward overcoming the quantum many-body problem [22], to represent entangled quantum systems [23], and to enhance the power of collider searches for exotic particles in high-energy physics [24]. DL (and deep reinforcement learning) have also been applied in finance, energy, and healthcare [32].

Despite DL's many newsworthy successes, a comprehensive understanding of *why* and *how* DL is empirically successful in astronomically many AI/ML problems remains fundamentally elusive. Nevertheless, it is widely believed that DL's empirical successes are attributable to its ability to learn salient hidden representations from the training data [33]. The training data goes through networked layers of interconnected “black box” [34] processing that is at the heart of DL's remarkable successes when it comes to solving both classification and regression AI/ML problems. The mysteries of this black box processing are also the mysteries behind DL's empirical

successes. To uncover these mysteries, significant theoretical advancements have been made by the interdisciplinary<sup>1</sup> AI/ML research communities toward interpretable (or explainable) AI/ML. Toward explainable AI/ML, a new research field has emerged that is widely recognized as the *theory of DL* [36]–[39]. The theory of DL is concerned with three fundamental problems related to DL: *generalization*, *optimization*, and *approximation (representation)* [36].

Inspired by the classical works [40]–[45] that have established that feedforward neural networks (FNNs) with one hidden layer are *universal approximators*, approximation problems, in the theory of DL, deal with deriving the approximation error bounds of one or more function approximation(s) using deep networks. In this vein, a number of recent works have established that deep FNNs – as opposed to shallow FNNs – have the power of *exponential expressivity* [46]–[51]. In light of exponential expressivity, the state-of-the-art literature includes many works on deep approximation such as: the width efficiency of *rectified linear unit* (ReLU) FNNs [52]; the quasi-equivalence of depth and width [53]; the universal approximation capability of slim (and sparse) networks [54] and residual neural network (*ResNet*) with one-neuron hidden layers [55]; the approximation of univariate functions by deep ReLU FNNs [56]; *un-rectifying* signal representation [57]; approximation (and estimation) using high-dimensional DL networks [58]; the improving effect of depth and width [59]; matrix-vector product approximation using deep ReLU FNNs [60]; universal function approximation by deep ReLU FNNs [61]; deep FNN approximation theory [62], [63]; and optimal approximation of piece-wise smooth functions using deep ReLU FNNs [64], [65].

Apart from the aforementioned works on approximation in the context of the theory of DL, there also exist informative works (e.g., [66]–[68]) on optimization in the context of the theory of DL. The authors of [69] highlight these works starting with useful developments for shallow FNNs and corroborate that there exist optimization landscape regions for discrete FNNs with only one or two layers that are both robust and accessible, and their existence is central to good training/testing performance. In addition, the authors of [70] derive various basic geometric and algorithmic features for nonconvex one- and two-layer FNNs that learn random patterns. These crucial advancements are applicable exclusively to shallow networks rather than the state-of-

<sup>1</sup>As more interdisciplinary researchers are getting involved in DL, physics-based DL is becoming popular. There exist intriguing connections between DL and a variety of mathematical physics themes such as random landscapes, spin glasses, jamming, dynamical phase transitions, chaos, Riemannian geometry, random matrix theory, free probability, and non-equilibrium statistical mechanics [35].

the-art practical deep networks that are often over-parameterized [67], [68]. Even though over-parameterized deep (and shallow) networks must be *overfitted* per the classical bias–variance tradeoff [71], [72], over-fitting does not often happen with practical deep networks [67], [68]. This discrepancy<sup>2</sup> remains as one of the fundamental issues in the theory of DL [67], [68]. Meanwhile, several theoretical works have been published on over-parameterized deep (and shallow) networks: convergence theory for deep ReLU FNNs [75], [76]; convergence theory for an over-parameterized ResNet [77]; the optimization landscape of over-parameterized shallow FNNs [78]; global convergence guarantees for training shallow over-parameterized FNNs [79]; and how much over-parameterization is sufficient to learn deep ReLU FNNs [80]. Moreover, the recent theoretical works [81], [82] affirm that over-parameterization improves generalization. In harmony with this theory, the authors of [83] corroborate empirically that over-parameterized DL models can – remarkably – fit the training data and generalize well even when the labels are substituted by noise. Meanwhile, when it comes to generalization via implicit regularization and tractability via over-parametrization, the authors of [39] provide a statistical viewpoint. This leads to our brief discussion of works pertaining to the theory of DL and generalization.

When it comes to generalization, state-of-the-art AI/ML research incorporates interesting works that exploit local Rademacher complexities, algorithmic stability, compression bounds, and algorithmic robustness to derive the generalization error bounds of deep (as well as shallow) networks [38], [39]. The authors of [71], on the other hand, expose the existence of *double descent* that amalgamates the classical U-shaped test risk curve and the modern interpolating regime (with zero training error) for over-parameterized DL models. The authors of [84] took inspiration from double descent and revealed *triple descent*, which also comprises a superabundant parameterization regime corresponding to a deterministic NTK [73]. NTK is the limiting kernel of wide FNNs as their width approaches infinity [73]. When it comes to infinitely wide FNNs, crucial *mean field limits* are derived for two-layer FNNs [85] and multi-layer FNNs [86]. Meanwhile, the fundamental phenomena of *neural collapse* and *minority collapse* are unveiled

<sup>2</sup>Over-parameterized deep networks need to move only a tiny distance, and linearization can be a good approximation (also concerning the *neural tangent kernel* (NTK) [73]). Nonetheless, because deep networks are not necessarily ultra-wide in practice, their parameters will likely move a great distance and hence more than the linearization regimes permit [67], [68]. On the other hand, the authors of [74] reveal an implicit bias phenomenon dubbed *lazy training* that applies when a non-linear parametric model behaves like a linear one. This can occur implicitly under some choices of hyper-parameters governing normalization, initialization, and the number of iterations when the model is large [74].

in [87] and [88], respectively. Neural collapse is a fundamentally pervasive inductive bias that occurs during the terminal phase of training beginning at the epoch in which training error first vanishes while training loss is driven to zero [87], whereas minority collapse is the fundamental limit on the minority classes of DL models that are trained for an adequately long time on class-imbalanced datasets [88].

Despite the many state-of-the-art works on approximation, optimization, and generalization in the context of the theory of DL, quantifying the fundamental limits of deep networks and hence deep FNNs remains a very challenging fundamental problem. This motivates our work and its context, as explained below.

### B. Motivation and Context

Foundational themes on the achievements of DL focus on the following questions: *i*) how can training forward-propagating data through deep networks impact the optimization landscape to such an extent that viable solutions (such as *good local minima*) are attained? *ii*) If a viable solution is attained w.r.t. the training data, how can we generalize it well for unseen testing data? *iii*) When it comes to learning using the *back-propagation algorithm* [89] to solve both classification and regression AI/ML problems, how does a network trainer’s choice of DL architecture, initializer, optimizer, normalization scheme, and regularization scheme interact with the training dataset(s) to influence the optimization landscape and the generalizability of a trained DL model? These questions must be carefully addressed should one aim to reveal the fundamental testing performance limits of a DL-based AI/ML algorithm. Quantifying the fundamental testing performance limits of a deep FNN-based AI/ML algorithm therefore entails the quantification of the attainable optimization landscape during training and the subsequent generalization error bound.

It is widely believed that there could be infinitely many local minima [90] for an FNN architecture and a loss function, some of which can lead to efficient learning. However, we lack a fundamental understanding of which minima the optimization algorithm selects due to a lack of: *i*) understanding of training dynamics, and *ii*) mathematical tools to describe the landscape of the loss function of large FNNs [91]. Apart from these formidable challenges, the back-propagating gradients that are involved in error back-propagation are often random gradients with unknown distributions. These render the development of almost all *high-dimensional statistics* [92], [93] nearly useless, especially when one is trying to determine the non-asymptotic testing performance

limits of an FNN-based classification AI/ML algorithm.<sup>3</sup> These fundamental testing performance limits may pave the way to being able to interpret trained deep networks that solve classification AI/ML problems. Nonetheless, no fundamental works have been managed yet – to the best of our knowledge – to quantify the testing performance limits of DL-based classifiers trained with *cross-entropy loss* or *hinge loss*. This is the motivation and context behind our work on the fundamental testing performance limits of FNN-based binary classifiers trained with hinge loss. Consequently, this paper’s key contributions are outlined below.

### C. Contributions

In this fundamental work, we investigate two kinds of DL-based binary classifiers: *i*) ones that are based on a deep ReLU FNN, and *ii*) ones that are based on a deep FNN that has a ReLU activation function in all layers except the output layer which is instead equipped with a hyperbolic tangent activation function – hereinafter referred to as *deep FNN with ReLU and Tanh activation*. We uncover these classifiers’ fundamental asymptotic testing performance limits, which leads to the following contributions.

- 1) We derive the asymptotic testing performance limits of binary classifiers that are based on a deep ReLU FNN.
- 2) We conduct extensive computer experiments on a binary phase shift keying (BPSK) detector/classifier that is based on a (deep) ReLU FNN, the results of which corroborate our derived asymptotic testing performance limits, especially as the ReLU FNN gets deeper and wider.
- 3) We derive the asymptotic testing performance limits of binary classifiers that are based on a deep FNN with ReLU and Tanh activation.
- 4) We carry on extensive computer experiments on a BPSK detector that is based on a (deep) FNN with ReLU and Tanh activation, the results of which validate our derived asymptotic testing performance limits, especially as the FNN gets deeper and wider.

Following this introduction, the remainder of this paper is organized as follows. Section II presents the prelude of this paper. Section III outlines the system setup for generic DL-based

<sup>3</sup>For a regression AI/ML algorithm, on the other hand, the authors of [94] are the first to provide asymptotic and non-asymptotic fundamental testing performance limits for a ReLU FNN-based regression AI/ML algorithm. The authors of [95], meanwhile, derive the asymptotic performance limits on a DL-based text semantic communication system subjected to interference.

binary classification. Section IV formulates problems regarding the fundamental testing performance limits of binary classifiers that are based on deep FNNs. Section V presents the asymptotic testing performance limits of binary classifiers based on deep FNNs. Section VI reports on the extensive computer experiments conducted in the context of BPSK detection. Finally, Section VII sets out our concluding remarks and this paper's research outlook.

*Notation:* scalars, row and column vectors, and matrices are represented by italic letters, bold lowercase letters, and bold uppercase letters, respectively. Uppercase italic letters denote random variables. Uppercase calligraphic letters denote events, hypotheses, and training/testing sets.  $\mathbb{R}$ ,  $\mathbb{R}^n$ , and  $\mathbb{R}^{m \times n}$  denote the sets of real numbers,  $n$ -dimensional real vectors, and  $m \times n$  real matrices, respectively.  $\mathbb{R} \setminus \{0\}$ ,  $\mathbb{R}_+$ ,  $\mathbb{N}$ , and  $\mathbb{N}_0$  stand for the sets of real numbers excluding zero, positive real numbers, natural numbers, and natural numbers including zero, respectively.

$\sim$ ,  $:=$ ,  $\equiv$ ,  $\mathbf{0}$ ,  $\mathbf{I}_n$ ,  $\exp(\cdot)$ , and  $\mathbb{P}(\cdot)$  stand for distributed as, equal by definition, equivalent to, a zero vector/matrix whose dimension will be clear from the context, an  $n \times n$  identity matrix, exponential function, and probability, respectively.  $\text{diag}(\cdot)$ ,  $\text{sgn}(\cdot)$ ,  $\max(\cdot, \cdot)$ ,  $\mathcal{N}(\mu, \sigma^2)$ ,  $(\cdot)^\top$ ,  $\mathbb{I}\{\cdot\}$ , and  $|\cdot|$  stand for a diagonal matrix, the sign function, the maximum of two numbers, Gaussian distribution with mean  $\mu$  and variance  $\sigma^2$ , transpose, a (component-wise) indicator function that returns 1 if the argument is true and 0 otherwise, and cardinality, respectively.  $\arg \max$ ,  $\arg \min$ ,  $\cap$ ,  $\cup$ ,  $\|\cdot\|$ ,  $\delta(\cdot)$ , and  $\ln(\cdot)$  stand for the arguments of the maxima, the arguments of the minima, the intersection of two sets/events, the union of two sets/events, a vector norm, the Dirac delta function, and the natural logarithm, respectively. For a function  $f(x, y) \in \mathbb{R}$ ,  $f'(x, y) := \frac{\partial}{\partial x} f(x, y)$  denotes its partial derivative w.r.t.  $x \in \mathbb{R}$ . Meanwhile,  $\mathcal{Q}(\cdot)$  denotes the  $Q$ -function defined for  $x \in \mathbb{R}$  as [96]

$$\mathcal{Q}(x) := \frac{1}{\sqrt{2\pi}} \int_x^\infty \exp(-t^2/2) dt. \quad (1)$$

$\mathbb{N}_{\geq k} := \{k, k+1, \dots\}$  denotes the sets of natural numbers greater than or equal to  $k$  with  $k \in \mathbb{N}_0$ . For  $n \in \mathbb{N}_{\geq 1}$ ,  $[n] := \{1, \dots, n\}$ . For  $\mathbf{A} \in \mathbb{R}^{m \times n}$  and  $\mathbf{a} \in \mathbb{R}^n$ ,  $(\mathbf{A})_{i,j}$  and  $(\mathbf{a})_i$  denote the  $(i, j)$ -th element of  $\mathbf{A}$  and the  $i$ -th entry of  $\mathbf{a}$ , respectively. Per the MATLAB<sup>®</sup> syntax,  $\mathbf{A}(i, :)$  denotes the  $i$ -th row of  $\mathbf{A} \in \mathbb{R}^{m \times n}$ . For  $\mathbf{A} \in \mathbb{R}^{m \times n}$  and  $\mathbf{a} \in \mathbb{R}^n$ ,  $\|\mathbf{A}\|_{\ell_0} := |\{(i, j) : (\mathbf{A})_{i,j} \neq 0\}|$ ,  $\|\mathbf{a}\|_\infty := \max_{i=1, \dots, n} |(\mathbf{a})_i|$ , and  $\|\mathbf{A}\|_\infty := \max_{i,j} |(\mathbf{A})_{i,j}|$ . The Hadamard product (or element-wise product) of two conformable matrices  $\mathbf{A}$  and  $\mathbf{B}$  is denoted by  $\mathbf{A} \odot \mathbf{B}$ . For  $n \in \mathbb{N}_{\geq 2}$ , the horizontal concatenation of  $n$  conformable vectors and matrices is written as  $[\mathbf{a}_1 \ \mathbf{a}_2 \ \dots \ \mathbf{a}_n]$  and  $[\mathbf{A}_1 \ \mathbf{A}_2 \ \dots \ \mathbf{A}_n]$ , respectively. A sequence of  $K$  matrix-vector tuples is

expressed as  $[[\mathbf{W}_1, \mathbf{b}_1], \dots, [\mathbf{W}_K, \mathbf{b}_K]]$ . For  $N_k$  being the number of neurons of the  $k$ -th layer, a  $K$ -layer FNN is denoted by a sequence of matrix-vector tuples as  $\Phi := [[\mathbf{W}_1, \mathbf{b}_1], \dots, [\mathbf{W}_K, \mathbf{b}_K]]$  such that  $\mathbf{b}_k \in \mathbb{R}^{N_k}$  and  $\mathbf{W}_k \in \mathbb{R}^{N_k \times N_{k-1}}$  are the biases of the  $k$ -th layer and the weight matrix of the neuronal connections between the  $k$ -th and  $(k-1)$ -th layers,  $k \in [K]$ , respectively.

## II. PRELUDE

This section documents preliminaries concerning the mathematics of FNNs, the basics of probability theory, and definitions of DL, which are presented in Sections II-A, II-B, and II-C, respectively.

### A. The Mathematics of FNNs

We state below a definition of ReLU FNNs that has been adopted from [64, Definition 2.2].

**Definition 1.** Let  $K, N_0, N_1, \dots, N_K \in \mathbb{N}$  and  $K \geq 2$ . A FNN  $\Phi$  is a sequence of matrix-vector tuples defined as

$$\Phi := [[\mathbf{W}_1, \mathbf{b}_1], [\mathbf{W}_2, \mathbf{b}_2], \dots, [\mathbf{W}_K, \mathbf{b}_K]], \quad (2)$$

where  $\mathbf{W}_k \in \mathbb{R}^{N_k \times N_{k-1}}$  and  $\mathbf{b}_k \in \mathbb{R}^{N_k}$  are the weight matrix of the neuronal connections between the  $k$ -th and  $(k-1)$ -th layers and the  $k$ -th layer's biases given  $N_k$  is the number of neurons in the  $k$ -th layer (the input layer is considered the 0-th layer), respectively. For the  $K$ -layer FNN expressed by (2),  $\mathcal{N}(\Phi) := \sum_{k=0}^K N_k$ ,  $\mathcal{M}(\Phi) := \sum_{k=1}^K (\|\mathbf{W}_k\|_{\ell_0} + \|\mathbf{b}_k\|_{\ell_0})$ ,  $\mathcal{W}(\Phi) := \max_{k=0, \dots, K} N_k$ , and  $\mathcal{B}(\Phi) := \max_{k \in [K]} \{\|\mathbf{W}_k\|_{\infty}, \|\mathbf{b}_k\|_{\infty}\}$  define the total number of neurons, the network connectivity, the maximum width, and the maximum absolute value of the weights, respectively. For an input  $\mathbf{x} \in \mathbb{R}^{N_0}$  and an element-wise activation function  $\rho(\cdot)$ , an FNN map  $\Phi : \mathbb{R}^{N_0} \rightarrow \mathbb{R}^{N_K}$  is defined as  $\Phi(\mathbf{x}) = \mathbf{x}_K$ , where  $\mathbf{x}_K$  is obtained recursively as

$$\mathbf{x}_0 := \mathbf{x}; \quad \mathbf{x}_k := \rho(\mathbf{W}_k \mathbf{x}_{k-1} + \mathbf{b}_k), \quad \forall k \in [K-1] \quad (3a)$$

$$\mathbf{x}_K := \mathbf{W}_K \mathbf{x}_{K-1} + \mathbf{b}_K, \quad (3b)$$

where  $\rho(\mathbf{y}) = [\rho(y_1), \dots, \rho(y_m)]^\top$  for  $\mathbf{y} = [y_1, \dots, y_m]^\top \in \mathbb{R}^m$ . For  $\rho(y_i) := \max(y_i, 0)$ , the FNN in (2) is known as a ReLU FNN. This type of FNN is often termed a deep ReLU neural network when  $K$  is very large. When  $N_k$ ,  $k \in [K]$ , is very large (often a polynomial order of the input number of neurons and the data points [75], [76]), the FNN is usually termed an

over-parameterized ReLU neural network if  $K$  is small and an over-parameterized deep ReLU neural network if  $K$  is very large.

As an alternative to Definition 1, we state the following definition that is adopted from [62, Definition II.1].

**Definition 2.** Let  $\mathbf{x} \in \mathbb{R}^{N_0}$ ,  $K \in \mathbb{N}_{\geq k}$ , and  $\rho(y) := \max(0, y)$ . Suppose  $N_0, N_k \in \mathbb{N}$  for  $k \in [K]$ . A map  $\Phi : \mathbb{R}^{N_0} \rightarrow \mathbb{R}^{N_K}$  defined as

$$\Phi(\mathbf{x}) := \mathbf{A}_K(\rho(\mathbf{A}_{K-1}(\rho(\dots\rho(\mathbf{A}_1(\mathbf{x})))))), \quad (4)$$

with affine linear maps  $\mathbf{A}_k : \mathbb{R}^{N_{k-1}} \rightarrow \mathbb{R}^{N_k}$  defined as  $\mathbf{A}_k(\mathbf{x}_{k-1}) = \mathbf{W}_k \mathbf{x}_{k-1} + \mathbf{b}_k$  – with  $\mathbf{W}_k \in \mathbb{R}^{N_k \times N_{k-1}}$ ,  $\mathbf{x}_{k-1} \in \mathbb{R}^{N_{k-1}}$ , and  $\mathbf{b}_k \in \mathbb{R}^{N_k}$  – and an element-wise ReLU activation function  $\rho(\mathbf{x}) := [\rho(x_1), \dots, \rho(x_{N_0})]^\top$  is called a ReLU FNN. Regarding  $\mathbf{W}_k$  and  $\mathbf{b}_k$ ,  $(\mathbf{W}_k)_{i,j}$  denotes the weight associated with the edge between the  $j$ -th node of the  $(k-1)$ -th layer and the  $i$ -th node of the  $k$ -th layer, and  $(\mathbf{b}_k)_i$  is the weight associated with the  $i$ -th node of the  $k$ -th layer.

**Remark 1.** According to Definitions 1 and 2, and the works in [56], [62]–[65], [75], [76], [88], and [97], a standard ReLU FNN is an FNN model that has a ReLU activation function in all of its layers except its output layer.

We now highlight the basics of probability theory that have informed our theoretical developments reported further down.

### B. The Basics of Probability Theory

In what follows, we define probability space, probability axioms, conditional probability, the probability density function (PDF) of a continuous random variable (RV), the properties of PDF, the cumulative distribution function (CDF) of a continuous RV, and the properties of CDF. In addition, we state the main results of the multiplication rule, the law of total probability (discrete case), and the law of total probability (continuous case).

We begin with the definition of probability space.

**Definition 3 (Probability space [98], [99]).** In probability theory, a probability space or a probability triple  $(\Omega, \mathcal{F}, \mathbb{P})$  is a mathematical construct that provides a formal model of a random process or experiment. It comprises three elements:

- A sample space  $\Omega$ , which is the set of all possible outcomes of a random process or experiment.
- An event space  $\mathcal{F}$ , which is a set of events (an event is a set of outcomes in the sample space  $\Omega$ ).
- A probability function (probability law)  $\mathbb{P}$ , which assigns each event in the event space  $\mathcal{F}$  a probability (between 0 and 1). A probability function must satisfy the three foundational probability axioms stated below.

**Definition 4 (Probability axioms [99, p. 9], [100, Ch. 2]).** Probability axioms (or the Kolmogorov axioms [101]) are the foundations of probability theory. The three axioms are:

- 1) Non-negativity: for any event  $\mathcal{A}$ ,  $\mathbb{P}(\mathcal{A}) \geq 0$ .
- 2) Additivity: if  $\mathcal{A}$  and  $\mathcal{B}$  are two disjoint events, then

$$\mathbb{P}(\mathcal{A} \cup \mathcal{B}) := \mathbb{P}(\mathcal{A}) + \mathbb{P}(\mathcal{B}). \quad (5)$$

In general, if the sample space has an infinite number of elements  $\mathcal{A}_1, \mathcal{A}_2, \dots$  that are all disjoint events, then

$$\mathbb{P}(\mathcal{A}_1 \cup \mathcal{A}_2 \cup \dots) := \mathbb{P}(\mathcal{A}_1) + \mathbb{P}(\mathcal{A}_2) + \dots. \quad (6)$$

- 3) Normalization: the probability of the whole sample space  $\Omega$  is equal to one, i.e.,  $\mathbb{P}(\Omega) = 1$ .

We now move on to the definition of conditional probability.

**Definition 5 (Conditional probability [99, p. 20], [102, p. 9]).** Consider an event  $\mathcal{A}$  and an event  $\mathcal{B}$  with  $\mathbb{P}(\mathcal{B}) > 0$  in a probability model. The conditional probability of  $\mathcal{A}$  conditioned on  $\mathcal{B}$  is defined as

$$\mathbb{P}(\mathcal{A}|\mathcal{B}) := \frac{\mathbb{P}(\mathcal{A} \cap \mathcal{B})}{\mathbb{P}(\mathcal{B})}. \quad (7)$$

Note that  $0 \leq \mathbb{P}(\mathcal{A}|\mathcal{B}) \leq 1$  and  $\mathbb{P}(\mathcal{A}|\mathcal{B})$  is undefined if  $\mathbb{P}(\mathcal{B}) = 0$  [103].

Since all of  $\mathbb{P}(\mathcal{A}|\mathcal{B})$  is concentrated on  $\mathcal{B}$ , conditional probabilities such as  $\mathbb{P}(\mathcal{A}|\mathcal{B})$  can also be viewed as a probability law on a new universe  $\mathcal{B}$  [99]. In this vein, for an event  $\mathcal{B}$  and an event  $\mathcal{A}$  with  $\mathbb{P}(\mathcal{A}) > 0$  in a probability model, it follows from Definition 5 that

$$\mathbb{P}(\mathcal{B}|\mathcal{A}) := \frac{\mathbb{P}(\mathcal{A} \cap \mathcal{B})}{\mathbb{P}(\mathcal{A})}. \quad (8)$$

The following multiplication rule then ensues from (7) and (8).

**Rule 1 (The multiplication rule [104, p. 75]).** Consider an event  $\mathcal{A}$  with  $\mathbb{P}(\mathcal{A}) > 0$  and an event  $\mathcal{B}$  with  $\mathbb{P}(\mathcal{B}) > 0$  in a probability model. Then,

$$\mathbb{P}(\mathcal{A} \cap \mathcal{B}) = \mathbb{P}(\mathcal{A}|\mathcal{B})\mathbb{P}(\mathcal{B}) = \mathbb{P}(\mathcal{B}|\mathcal{A})\mathbb{P}(\mathcal{A}). \quad (9)$$

Generalizing Rule 1 to mutually exclusive and exhaustive events [104], the law of total probability (total probability theorem) – for discrete cases – follows.

**Law 1 (Law of total probability (discrete case) [99, p. 28], [105, p. 10]).** Let disjoint events  $\mathcal{A}_1, \dots, \mathcal{A}_n$  constitute a partition of the sample space so that each probable outcome is included in exactly one of  $\{\mathcal{A}_1, \dots, \mathcal{A}_n\}$  and  $\mathbb{P}(\mathcal{A}_j) > 0$  for all  $j$ . Then, for any event  $\mathcal{B}$ ,

$$\mathbb{P}(\mathcal{B}) = \sum_{j=1}^n \mathbb{P}(\mathcal{A}_j \cap \mathcal{B}) = \sum_{j=1}^n \mathbb{P}(\mathcal{B}|\mathcal{A}_j)\mathbb{P}(\mathcal{A}_j). \quad (10)$$

We now proceed to definitions pertaining to continuous RVs. We begin by stating a formal definition of a continuous RV.

**Definition 6 (Continuous RV [99, p. 140]).** An RV  $X$  is called a continuous RV if there exists a non-negative function  $f_X$  called the PDF of  $X$  such that

$$\mathbb{P}(X \in \mathcal{S}) = \int_{\mathcal{S}} f_X(x)dx, \quad (11)$$

where it is valid for each subset  $\mathcal{S}$  of the real line.

When it comes to (11), the probability that a continuous RV  $X$  falls within an interval  $[a, b]$  would be

$$\mathbb{P}(X \in [a, b]) = \mathbb{P}(a \leq X \leq b) = \int_a^b f_X(x)dx, \quad (12)$$

where  $a, b \in \mathbb{R}$ . If we now consider  $[a, b]$  to be  $(-\infty, \infty)$ , (12) leads to

$$\mathbb{P}(-\infty < X < \infty) = 1 = \int_{-\infty}^{\infty} f_X(x)dx. \quad (13)$$

Thus, (13) defines the standard PDF constraint for  $f_X$ . In light of this, the underneath properties of PDF follow.

**Definition 7 (Properties of PDF [99, p. 144]).** Suppose  $X$  is a continuous RV with PDF  $f_X$ . Then,  $f_X(x) \geq 0$  for all  $x$  and  $\int_{-\infty}^{\infty} f_X(x)dx = 1$ . For any subset  $\mathcal{S}$  of the real line,  $\mathbb{P}(X \in \mathcal{S}) = \int_{\mathcal{S}} f_X(x)dx$ . If  $\gamma$  is small,

$$\mathbb{P}(X \in [x, x + \gamma]) = \int_x^{x+\gamma} f_X(x)dx \approx f_X(x) \times \gamma. \quad (14)$$

We now move on to the definition of the CDF of an RV.

**Definition 8 (CDF of an RV [99, P. 148]).** *The CDF of a continuous RV  $X$  denoted by  $F_X(x)$  is defined as  $F_X(x) = \mathbb{P}(X \leq x)$  for any  $x \in \mathbb{R}$ . To this end, if  $X$  is a discrete RV,*

$$F_X(x) = \mathbb{P}(X \leq x) = \sum_{k \leq x} p_X(k). \quad (15)$$

*If  $X$  is a continuous RV, then*

$$F_X(x) = \mathbb{P}(X \leq x) = \int_{-\infty}^x f_X(t) dt, \quad (16)$$

*where  $f_X$  is the PDF of  $X$ .*

In light of Definition 8, the following properties of CDF ensue.

**Definition 9 (Properties of CDF [99, p. 150]).** *Let  $X$  be an RV whose CDF is denoted by  $F_X$ .*

*Then:*

- 1) *If  $F_X$  is monotonically non-decreasing, then  $F_X(x) \leq F_X(y)$  for  $x \leq y$ .*
- 2)  *$\lim_{x \rightarrow -\infty} F_X(x) = 0$  and  $\lim_{x \rightarrow \infty} F_X(x) = 1$ .*
- 3) *If  $X$  is a discrete RV, then  $F_X(x)$  is a piece-wise constant function of  $x$ .*
- 4) *If  $X$  is a continuous RV, then  $F_X(x)$  is a continuous function of  $x$ .*
- 5) *If  $X$  is a continuous RV whose PDF is denoted by  $f_X$ ,*

$$F_X(x) = \int_{-\infty}^x f_X(t) dt \Leftrightarrow f_X(x) = \frac{dF_X(x)}{dx}. \quad (17)$$

Employing the CDF and PDF of a continuous RV per Definition 9 and Definition 7, respectively, makes it possible to extend the law of total probability to a continuous case. The case in point is of conditioning on events generated by a continuous RV and stated below.

**Law 2 (Law of total probability (continuous case) [106], [107]).** *Let  $(\Omega, \mathcal{F}, \mathbb{P})$  be a probability space. Assume  $X$  is an RV with CDF  $F_X$  and an event  $\mathcal{A}$  in  $(\Omega, \mathcal{F}, \mathbb{P})$ . Then,*

$$\mathbb{P}(\mathcal{A}) = \int_{-\infty}^{\infty} \mathbb{P}(\mathcal{A}|X = x) dF_X(x). \quad (18)$$

*If  $X$  admits a PDF denoted by  $f_X$ , then it follows from (18) that*

$$\mathbb{P}(\mathcal{A}) = \int_{-\infty}^{\infty} \mathbb{P}(\mathcal{A}|X = x) f_X(x) dx. \quad (19)$$

*Furthermore, if  $\mathcal{A} = \{\mathcal{Y} \in \mathcal{B}\}$  for  $\mathcal{B}$  being a Borel set, then it follows from (19) that*

$$\mathbb{P}(\mathcal{Y} \in \mathcal{B}) = \int_{-\infty}^{\infty} \mathbb{P}(\mathcal{Y} \in \mathcal{B}|X = x) f_X(x) dx. \quad (20)$$

With the aforementioned basics of probability theory defined, we now move on to DL-related definitions.

### C. Definitions Pertaining to Deep Learning

In this subsection, we outline DL-related definitions and assumptions that will be exploited in our subsequent theoretical developments.

**Definition 10 (Gaussian initializers [108]–[110]).** For  $N_k$  and  $N_{k-1}$  which denote the number of neurons in the  $k$ -th and  $(k-1)$ -th layers, respectively, of an FNN expressed in (2), Gaussian initialization for a weight matrix  $\mathbf{W}_k \in \mathbb{R}^{N_k \times N_{k-1}}$  constitutes one of the following initialization techniques:

- He normal:  $\mathbf{W}_k(i, :) \sim \mathcal{N}(\mathbf{0}, \frac{2}{N_{k-1}} \mathbf{I}_{N_{k-1}})$  for  $i \in [N_k]$  and  $k \in [K]$ .
- Lecun normal:  $\mathbf{W}_k(i, :) \sim \mathcal{N}(\mathbf{0}, \frac{1}{N_{k-1}} \mathbf{I}_{N_{k-1}})$  for  $i \in [N_k]$  and  $k \in [K]$ .

**Definition 11 (Hinge loss [90], [111]).** For a target  $t \in \{-1, 1\}$  and an FNN prediction  $y$ , hinge loss  $\ell(t, y)$  is defined as

$$\ell(t, y) = \max(0, 1 - ty). \quad (21)$$

**Definition 12 (FNNs with dual activation functions [111]).** Let  $t \in \mathbb{N}_0$ ,  $n \in \mathbb{N}$ , and  $K \in \mathbb{N}_{\geq 2}$ . Let  $N_1, N_k, N_{k-1} \in \mathbb{N}_{\geq 2}$  for  $k \in [K]$ . Assume a deep FNN training over  $\mathcal{D} := \{(x_n, y_n)\}_{n=1}^N$  with  $x_n$  being the  $n$ -th input generated per (27) and  $y_n \in \{-1, 1\}$  being the  $n$ -th label. For a  $K$ -layer FNN with dual activation functions – denoted by  $\varphi(\cdot)$  and  $\phi(\cdot)$  – and  $N_k$  neurons in its  $k$ -th layer, the network prediction during the  $t$ -th iteration is obtained as<sup>4</sup>

$$\mathbf{y}_{1,n}^{(t)} = \varphi(\mathbf{w}_1^{(t)} x_n) \quad (22a)$$

$$\mathbf{y}_{k,n}^{(t)} = \varphi(\mathbf{W}_k^{(t)} \mathbf{y}_{k-1,n}^{(t)}), \quad \forall k \in \{2, \dots, K-1\} \quad (22b)$$

$$\mathbf{y}_{K,n}^{(t)} = \phi(\mathbf{w}_K^{(t)} \mathbf{y}_{K-1,n}^{(t)}), \quad (22c)$$

where  $\varphi(\mathbf{x}) = [\varphi(x_1), \dots, \varphi(x_m)]^\top \in \mathbb{R}^m$  for  $\mathbf{x} = [x_1, \dots, x_m]^\top \in \mathbb{R}^m$ ;  $\mathbf{w}_1^{(t)} \in \mathbb{R}^{N_1}$ ,  $\mathbf{W}_k^{(t)} \in \mathbb{R}^{N_k \times N_{k-1}}$ , and  $(\mathbf{w}_K^{(t)})^\top \in \mathbb{R}^{N_{K-1}}$ ;  $\mathbf{y}_{1,n}^{(t)} \in \mathbb{R}^{N_1}$ ,  $\mathbf{y}_{k,n}^{(t)} \in \mathbb{R}^{N_k}$ , and  $y_{K,n}^{(t)} \in \mathbb{R}$  are the first,  $k$ -th, and  $K$ -th layers' outputs, respectively, at the  $t$ -th stochastic gradient descent (SGD) iteration<sup>5</sup>

<sup>4</sup>Without loss of generality, the biases are discarded. However, they are often subsumed by a linear model that employs a matrix of non-zero weights and an input equal to 1 [111].

<sup>5</sup>Throughout this paper, the  $t$ -th iteration accounts for the process of forward-propagating all the inputs of a mini-batch randomly chosen prior to forward-propagation.

in response to the  $n$ -th training input drawn from  $\mathcal{D}$ ; and  $\phi(\mathbf{y}) = [\varphi(y_1), \dots, \varphi(y_n)]^\top \in \mathbb{R}^n$  for  $\mathbf{y} = [y_1, \dots, y_n]^\top \in \mathbb{R}^n$ .

**Remark 2.** For a ReLU FNN,  $\varphi(x) = \rho(x) := \max(0, x)$  and  $\phi(x) = x$  for all  $x \in \mathbb{R}$ . For an FNN with ReLU and Tanh activation,  $\varphi(x) = \rho(x)$  and  $\phi(x) = \tanh(x)$  [112] for all  $x \in \mathbb{R}$ .

**Definition 13 (SGD [75], [76], [110]).** Let  $\mathbf{W}_1, \mathbf{W}_2, \dots, \mathbf{W}_K$  be the  $K$ -layer FNN weights at Gaussian initialization per Definition 10. Let  $B \in [N]$  be the size of a minibatch  $\mathcal{B}^{(t)}$  sampled randomly at the  $t$ -th iteration. Let  $T$  be the total number of iterations at convergence. The SGD update rule is then given by

$$\mathbf{W}_k^{(t+1)} = \mathbf{W}_k^{(t)} - \eta_t \times \overbrace{\frac{1}{B} \sum_{i \in \mathcal{B}^{(t)}} \frac{\partial \ell(y_i, f_{\mathbf{W}^{(t)}}(x_i))}{\partial \mathbf{W}_k^{(t)}}}^{\text{Gradient estimate at the } t\text{-th iteration}}, \quad (23)$$

where  $t = 0, 1, \dots, T-1$  and  $k \in [K]$ ;  $\mathbf{W}_k^{(0)} = \mathbf{W}_k$  for  $k \in [K]$ ;  $\mathbf{W}^{(t)} := \{\mathbf{W}_k^{(t)}\}_{k=1}^K$  is the collection of  $\mathbf{W}_1^{(t)}, \dots, \mathbf{W}_K^{(t)}$ ;  $\mathcal{B}^{(t)} \subseteq [N]$ ;  $\eta_t$  is the learning rate at the  $t$ -th iteration;  $f_{\mathbf{W}^{(t)}}(\cdot)$  is the output of the  $K$ -layer FNN with weights  $\mathbf{W}^{(t)}$ ; and  $x_i$  is the  $i$ -th input of the  $t$ -th minibatch.

The following remarks are in order w.r.t. Definition 13.

**Remark 3.**  $B = 1$  and  $B = N$  correspond to ordinary online gradient descent and standard (or “batch”) gradient descent, respectively [110].

**Remark 4.** The gradient  $\frac{\partial \ell(y_i, f_{\mathbf{W}^{(t)}}(x_i))}{\partial \mathbf{W}_k^{(t)}}$  is obtained via the back-propagation algorithm, which is derived in Appendix A for back-propagation with hinge loss, SGD, and dual activation functions.

**Definition 14 (SGD with momentum [3, Algorithm 8.2]).** In light of the settings of Definition 13, the SGD with momentum algorithm’s update rules are:

$$\mathbf{V}_k^{(t+1)} = \alpha \mathbf{V}_k^{(t)} - \eta \times \frac{1}{B} \sum_{i \in \mathcal{B}^{(t)}} \frac{\partial \ell(y_i, f_{\mathbf{W}^{(t)}}(x_i))}{\partial \mathbf{W}_k^{(t)}} \quad (24a)$$

$$\mathbf{W}_k^{(t+1)} = \mathbf{W}_k^{(t)} + \mathbf{V}_k^{(t+1)}, \quad (24b)$$

where  $t = 0, 1, \dots, T-1$ ;  $k \in [K]$ ;  $\eta$  is the learning rate;  $\alpha$  is the momentum parameter;  $f_{\mathbf{W}^{(t)}}(\cdot)$  is the output of the  $K$ -layer FNN with weights  $\mathbf{W}^{(t)}$ ;  $x_i$  is the  $i$ -th input of the  $t$ -th minibatch;  $\mathbf{V}_k^{(t)}$  is the velocity matrix for the  $k$ -th FNN layer at the  $t$ -th iteration; and  $\mathbf{V}_k^{(0)}$  is the initial velocity matrix corresponding to the  $k$ -th FNN layer.

**Definition 15 (RMSP<sub>prop</sub> [3, Algorithm 8.5]).** *Per the settings of Definition 13, the RMSP<sub>prop</sub> algorithm’s update rules are:*

$$\mathbf{G}_k^{(t)} = \frac{1}{B} \sum_{i \in \mathcal{B}^{(t)}} \frac{\partial \ell(y_i, f_{\mathbf{W}^{(t)}}(x_i))}{\partial \mathbf{W}_k^{(t)}} \quad (25a)$$

$$\mathbf{R}_k^{(t+1)} = \rho \mathbf{R}_k^{(t)} + (1 - \rho) \mathbf{G}_k^{(t)} \odot \mathbf{G}_k^{(t)} \quad (25b)$$

$$\Delta \tilde{\mathbf{W}}_k^{(t+1)} = -\frac{\eta}{\sqrt{\delta + \mathbf{R}_k^{(t+1)}}} \odot \mathbf{G}_k^{(t)} \quad (25c)$$

$$\mathbf{W}_k^{(t+1)} = \mathbf{W}_k^{(t)} + \Delta \tilde{\mathbf{W}}_k^{(t+1)}, \quad (25d)$$

where  $t = 0, 1, \dots, T - 1$ ;  $k \in [K]$ ;  $\eta$  is the (global) learning rate;  $\rho$  is the decay rate;  $\delta$  is a small constant (often  $10^{-6}$ ) used to stabilize division by small numbers;  $f_{\mathbf{W}^{(t)}}(\cdot)$  is the output of the  $K$ -layer FNN with weights  $\mathbf{W}^{(t)}$ ;  $x_i$  is the  $i$ -th input of the  $t$ -th minibatch;  $\mathbf{R}_k^{(t)}$  is the accumulation matrix for the  $k$ -th FNN layer at the  $t$ -th iteration; and  $\mathbf{R}_k^{(0)}$  is the initial accumulation matrix corresponding to the  $k$ -th FNN layer and equal to  $\mathbf{0}$ . In (25c),  $\frac{1}{\sqrt{\delta + \mathbf{R}_k^{(t+1)}}}$  is applied element-wise.

**Definition 16 (Adam [3, Algorithm 8.7]).** *Bearing in mind the settings of Definition 13, the Adam algorithm’s update rules are:*

$$\mathbf{G}_k^{(t)} = \frac{1}{B} \sum_{i \in \mathcal{B}^{(t)}} \frac{\partial \ell(y_i, f_{\mathbf{W}^{(t)}}(x_i))}{\partial \mathbf{W}_k^{(t)}} \quad (26a)$$

$$\mathbf{S}_k^{(t+1)} = \rho_1 \mathbf{S}_k^{(t)} + (1 - \rho_1) \mathbf{G}_k^{(t)} \quad (26b)$$

$$\mathbf{R}_k^{(t+1)} = \rho_2 \mathbf{R}_k^{(t)} + (1 - \rho_2) \mathbf{G}_k^{(t)} \odot \mathbf{G}_k^{(t)} \quad (26c)$$

$$\hat{\mathbf{S}}_k^{(t+1)} = \frac{\mathbf{S}_k^{(t+1)}}{1 - \rho_1^{t+1}} \quad \text{and} \quad \hat{\mathbf{R}}_k^{(t+1)} = \frac{\mathbf{R}_k^{(t+1)}}{1 - \rho_2^{t+1}} \quad (26d)$$

$$\Delta \hat{\mathbf{W}}_k^{(t+1)} = -\eta \frac{\hat{\mathbf{S}}_k^{(t+1)}}{\sqrt{\hat{\mathbf{R}}_k^{(t+1)} + \delta}} \quad (\text{element-wise operations}) \quad (26e)$$

$$\mathbf{W}_k^{(t+1)} = \mathbf{W}_k^{(t)} + \Delta \hat{\mathbf{W}}_k^{(t+1)}, \quad (26f)$$

where  $t = 0, 1, \dots, T - 1$ ;  $k \in [K]$ ;  $\eta$  is the step size (default: 0.001);  $\rho_1$  and  $\rho_2$  are exponential decay rates for moment estimates (defaults: 0.9 and 0.999, respectively);  $\delta$  denotes a small constant deployed for numerical stabilization (default:  $10^{-8}$ );  $f_{\mathbf{W}^{(t)}}(\cdot)$  is the output of the  $K$ -layer FNN with weights  $\mathbf{W}^{(t)}$ ;  $x_i$  is the  $i$ -th input of the  $t$ -th minibatch;  $\mathbf{S}_k^{(t)}$  is the biased first-moment estimate matrix for the  $k$ -th FNN layer at the  $t$ -th iteration;  $\mathbf{S}_k^{(0)} = \mathbf{0}$ ;  $\mathbf{R}_k^{(t)}$  is the

biased second-moment estimate matrix for the  $k$ -th FNN layer at the  $t$ -th iteration;  $\mathbf{R}_k^{(0)} = \mathbf{0}$ ; and  $\hat{\mathbf{S}}_k^{(t+1)}$  and  $\hat{\mathbf{R}}_k^{(t+1)}$  are the bias matrices in the first and second moments, respectively.

Following the preliminaries highlighted in Sections II-A, II-B, and II-C, we now consider a generic DL-based binary classification problem to enhance our foundational understanding of the fundamental limits of DL-based classification algorithms as they are applied to wireless communications and networking, signal processing, neuroscience, and quantum communications and networking. Thus, we begin with our system setup.

### III. SYSTEM SETUP: GENERIC DEEP LEARNING-BASED BINARY CLASSIFICATION

We consider a generic DL-based binary classification problem on hypotheses  $\mathcal{H}_{-1}$  and  $\mathcal{H}_1$  regarding the input data point  $x_n$  defined through binary hypothesis testing as

$$x_n = \begin{cases} f(-\beta_n) + z_n & : \mathcal{H}_{-1} \\ f(\beta_n) + z_n & : \mathcal{H}_1, \end{cases} \quad (27)$$

where  $n \in \mathbb{N}$  and  $x_n \in \mathbb{R}$ ;  $f$  is an unknown generic function whose noisy outputs give rise to  $x_n$ ;  $\beta_n \in \mathbb{R}$  is an unknown data-generating input variable that is assumed to be independent of  $z_n \in \mathbb{R}$ ; and  $z_n$  is additive white Gaussian noise (AWGN) with zero mean and variance  $\sigma^2$ , i.e.,  $z_n \sim \mathcal{N}(0, \sigma^2)$ .<sup>6</sup> As is hypothesized in (27), whenever  $\sigma^2$  is large,  $x_n$  would be contaminated by this swaying noise and correspond to the label  $y_n \in \{-1, 1\}$ . This binary pattern classification problem can be solved as a DL-based binary classification problem. To solve this classification problem, we consider a deep FNN-based binary classifier by training a deep FNN using a training set  $\mathcal{D} := \{(x_n, y_n)\}_{n=1}^N$  such that  $x_n$  is the  $n$ -th input generated via (27) and  $y_n \in \{-1, 1\}$  is the  $n$ -th label for all  $n \in [N]$ . Deploying this training set ensures the deep FNN-based binary classifier considered is trained with hinge loss and optimizers such as SGD, SGD with momentum, RMSProp, or Adam using the back-propagation algorithm [89].<sup>7</sup>

<sup>6</sup>For a non-linear  $f$ , our generic model  $f(\beta_n) + z_n$  matches non-linear additive noise models [113, Definition 4.4] that are the less severe cases of the class of SCMs (structural causal models) that are strong enough to yield a feasible cause-effect inference [113, p. 50]. However, we don't deal with causality or causal inference that can be the backbone of *Causal ML* (see [114]).

<sup>7</sup>The back-propagation algorithm (using square loss) has been around since about 1986 [89], and its derivation is often documented using scalar calculus for an FNN equipped with the same activation function throughout all its layers [111, Ch. 4]. For completeness and clarity, however, we employ *matrix calculus* to derive – as detailed in Appendix A – the update rules for back-propagation w.r.t. hinge loss and SGD for FNNs with dual activation functions.

To *mathematicize* our DL-based classification problem, let  $(\mathbf{w}_K^{(t)})^\top \in \mathbb{R}^{2H}$ ,  $\mathbf{W}_{K-k}^{(t)} \in \mathbb{R}^{2H \times 2H}$  for all  $k \in [K-2]$ , and  $\mathbf{w}_1^{(t)} \in \mathbb{R}^{2H}$  be the weight matrices of the  $K$ -th layer, the  $k$ -th layer, and the first layer of a *biasless* deep ReLU FNN (per Definition 1 or 2) under training during the  $t$ -th iteration, respectively. During this iteration,  $\Phi^{(t)} := [[\mathbf{w}_1^{(t)}, \mathbf{0}], [\mathbf{W}_2^{(t)}, \mathbf{0}], \dots, [\mathbf{W}_{K-1}^{(t)}, \mathbf{0}], [\mathbf{w}_K^{(t)}, \mathbf{0}]]$  defines a deep ReLU FNN – with  $2H$  neurons per a hidden layer and no biases – that is under training and whose output is given by

$$\Phi^{(t)}(x_n) := \mathbf{w}_K^{(t)} \mathbf{y}_{K-1,n}^{(t)} \in \mathbb{R}, \quad (28)$$

where, for  $\Sigma_{k,n}^{(t)} = \text{diag}(\mathbb{I}\{\mathbf{W}_k^{(t)} (\prod_{l=1}^{k-2} \Sigma_{k-l,n}^{(t)} \mathbf{W}_{k-l}^{(t)}) \Sigma_{1,n}^{(t)} \mathbf{w}_1^{(t)} x_n \geq 0\}) \in \{0, 1\}^{2H \times 2H}$  and  $\Sigma_{1,n}^{(t)} = \text{diag}(\mathbb{I}\{\mathbf{w}_1^{(t)} x_n \geq 0\}) \in \{0, 1\}^{2H \times 2H}$  [76],

$$\mathbf{y}_{K-1,n}^{(t)} = \left( \prod_{k=1}^{K-2} \Sigma_{K-k,n}^{(t)} \mathbf{W}_{K-k}^{(t)} \right) \Sigma_{1,n}^{(t)} \mathbf{w}_1^{(t)} x_n \in \mathbb{R}^{2H}. \quad (29)$$

Note that the output of the  $(K-1)$ -th deep ReLU FNN layer during the  $t$ -th iteration is given by (29) and denoted by  $\mathbf{y}_{K-1,n}^{(t)}$ .

Similarly, per Definition 12, the output of a deep FNN  $\check{\Phi}^{(t)}$  with ReLU and Tanh activation is given by

$$\check{\Phi}^{(t)}(x_n) := \tanh(\check{\mathbf{w}}_K^{(t)} \check{\mathbf{y}}_{K-1,n}^{(t)}) \in \mathbb{R}, \quad (30)$$

where  $\check{\Phi}^{(t)} := [[\check{\mathbf{w}}_1^{(t)}, \mathbf{0}], [\check{\mathbf{W}}_2^{(t)}, \mathbf{0}], \dots, [\check{\mathbf{W}}_{K-1}^{(t)}, \mathbf{0}], [\check{\mathbf{w}}_K^{(t)}, \mathbf{0}]]$  such that  $(\check{\mathbf{w}}_K^{(t)})^\top \in \mathbb{R}^{2H}$ ,  $\check{\mathbf{W}}_{K-k}^{(t)} \in \mathbb{R}^{2H \times 2H}$  for all  $k \in [K-2]$ , and  $\check{\mathbf{w}}_1^{(t)} \in \mathbb{R}^{2H}$ , and  $\check{\mathbf{y}}_{K-1,n}^{(t)}$  is the output of the  $(K-1)$ -th deep FNN layer during the  $t$ -th iteration, which is given by

$$\check{\mathbf{y}}_{K-1,n}^{(t)} = \left( \prod_{k=1}^{K-2} \check{\Sigma}_{K-k,n}^{(t)} \check{\mathbf{W}}_{K-k}^{(t)} \right) \check{\Sigma}_{1,n}^{(t)} \check{\mathbf{w}}_1^{(t)} x_n \in \mathbb{R}^{2H}, \quad (31)$$

where  $\check{\Sigma}_{k,n}^{(t)} = \text{diag}(\mathbb{I}\{\check{\mathbf{W}}_k^{(t)} (\prod_{l=1}^{k-2} \check{\Sigma}_{k-l,n}^{(t)} \check{\mathbf{W}}_{k-l}^{(t)}) \check{\Sigma}_{1,n}^{(t)} \check{\mathbf{w}}_1^{(t)} x_n \geq 0\}) \in \{0, 1\}^{2H \times 2H}$  and  $\check{\Sigma}_{1,n}^{(t)} = \text{diag}(\mathbb{I}\{\check{\mathbf{w}}_1^{(t)} x_n \geq 0\}) \in \{0, 1\}^{2H \times 2H}$ . Meanwhile, the minimization of a training loss manifested by this deep FNN and the aforementioned deep ReLU FNN follows through (30) and (28), respectively, on a mini-batch-by-mini-batch basis.

After forward-propagating the  $t$ -th mini-batch  $\mathcal{B}^{(t)}$  sampled randomly from  $\mathcal{D}$ , the training loss exhibited by the aforementioned deep ReLU FNN and deep FNN – which have been trained using hinge loss  $\ell(t, y) := \max(0, 1 - ty)$  – is defined as

$$L_{\mathcal{B}^{(t)}}(\mathbf{W}^{(t)}) := \frac{1}{B} \sum_{i \in \mathcal{B}^{(t)}} \ell(y_i, f_{\mathbf{W}^{(t)}}(x_i)), \quad (32)$$

where  $\mathbf{W}^{(t)} = [\mathbf{w}_1^{(t)} \mathbf{W}_2^{(t)} \dots \mathbf{W}_{K-1}^{(t)} (\mathbf{w}_K^{(t)})^\top]$  or  $\mathbf{W}^{(t)} = [\check{\mathbf{w}}_1^{(t)} \check{\mathbf{W}}_2^{(t)} \dots \check{\mathbf{W}}_{K-1}^{(t)} (\check{\mathbf{w}}_K^{(t)})^\top]$ ;  $B := |\mathcal{B}^{(t)}|$ ; and  $f_{\mathbf{W}^{(t)}}(x_n) = \Phi^{(t)}(x_n)$  per (28) for the output of a deep ReLU FNN or  $f_{\mathbf{W}^{(t)}}(x_n) = \check{\Phi}^{(t)}(x_n)$  through (30) for the output of a deep FNN with ReLU and Tanh activation. The deep FNNs' overall training error over  $\mathcal{D}$  can be expressed as [115]

$$R_{\mathcal{D}}(\mathbf{W}^{(t)}) := \frac{1}{N} \sum_{n=1}^N \mathbb{I}\{y_n \neq \text{sgn}(f_{\mathbf{W}^{(t)}}(x_n))\}. \quad (33)$$

To minimize (33) while minimizing (32) on a mini-batch-by-mini-batch basis, training would need to be conducted using the back-propagation algorithm. Per this algorithm, the goal of DL-based binary classifiers is to solve the optimization problem  $\mathbf{W}^* := \sum_{t \in \mathbb{N}, \mathcal{B}^{(t)} \subset \mathcal{D}} \arg \min_{\mathbf{W}^{(t)}} L_{\mathcal{B}^{(t)}}(\mathbf{W}^{(t)})$  while learning deep models that generalize better. To reveal the fundamental limits of the aforementioned DL-based binary classifiers, we proceed with the following problem formulation.

#### IV. PROBLEM FORMULATION: FUNDAMENTAL TESTING PERFORMANCE LIMITS OF BINARY CLASSIFIERS THAT ARE BASED ON DEEP FNNs

##### A. Problems in Testing Performance Limits of Deep ReLU FNNs-Based Binary Classifiers

Our problems for the testing performance limits of binary classifiers that are based on deep ReLU FNNs are motivated by letting  $\Phi^{(T)} := [[\mathbf{w}_1^{(T)}, \mathbf{0}], [\mathbf{W}_2^{(T)}, \mathbf{0}], \dots, [\mathbf{W}_{K-1}^{(T)}, \mathbf{0}], [\mathbf{w}_K^{(T)}, \mathbf{0}]]$  be a biasless deep ReLU FNN that has converged after the  $T$ -th iteration and been trained using hinge loss and SGD, SGD with momentum, RMSProp, or Adam after being initialized by a Gaussian initializer such as LeCun normal or He normal (per Definition 10) such that

$$\mathbf{w}_1^{(T)} = \mathbf{w}_1^{(T-1)} + \Delta \mathbf{w}_1^{(T-1)} = \mathbf{w}_1^{(0)} + \sum_{t=0}^{T-1} \Delta \mathbf{w}_1^{(t)} \in \mathbb{R}^{2H} \quad (34a)$$

$$\mathbf{W}_k^{(T)} = \mathbf{W}_k^{(T-1)} + \Delta \mathbf{W}_k^{(T-1)} = \mathbf{W}_k^{(0)} + \sum_{t=0}^{T-1} \Delta \mathbf{W}_k^{(t)} \in \mathbb{R}^{2H \times 2H} \quad (34b)$$

$$\mathbf{w}_K^{(T)} = \mathbf{w}_K^{(T-1)} + \Delta \mathbf{w}_K^{(T-1)} = \mathbf{w}_K^{(0)} + \sum_{t=0}^{T-1} \Delta \mathbf{w}_K^{(t)} \in \mathbb{R}^{1 \times 2H}, \quad (34c)$$

where  $T \in \mathbb{N}$ ;  $\mathbf{w}_1^{(0)}$ ,  $\mathbf{W}_k^{(0)}$ , and  $\mathbf{w}_K^{(0)}$  are weight matrices (or vectors) initialized with Gaussian initializers (per Definition 10); and  $\Delta \mathbf{w}_1^{(t)}$ ,  $\Delta \mathbf{W}_k^{(t)}$ , and  $\Delta \mathbf{w}_K^{(t)}$  are the  $t$ -th back-propagated error matrices (or vectors) accounting for an optimization with SGD (per Definition 13), SGD with momentum (per Definition 14), RMSProp (per Definition 15), or Adam (per Definition 16). Meanwhile, w.r.t. a collected weight matrix  $\mathbf{W}^{(T)} := [\mathbf{w}_1^{(T)} \mathbf{W}_2^{(T)} \dots \mathbf{W}_{K-1}^{(T)} (\mathbf{w}_K^{(T)})^\top]$  of

all the layers' trained weights, the testing error over the testing set  $\mathcal{T} := \{(x_n, y_n)\}_{n=N+1}^{N+\tilde{N}}$  – given that  $x_n$  is the  $n$ -th input generated via (27) and  $y_n \in \{-1, 1\}$  is the  $n$ -th label for all  $n \in \{N+1, \dots, N+\tilde{N}\}$  – can be defined as

$$R_{\mathcal{T}}(\mathbf{W}^{(T)}) := \frac{1}{\tilde{N}} \sum_{n=N+1}^{N+\tilde{N}} \mathbb{I}\{y_n \neq \text{sgn}(\Phi^{(T)}(x_n))\}, \quad (35)$$

where  $\tilde{N} := |\mathcal{T}|$  and  $\Phi^{(T)}(x_n)$  is defined via (28). Regarding the right-hand side (RHS) of (35), we prove the following lemma.

**Lemma 1.** *Suppose  $y_n \in \{-1, 1\}$  for all  $n \in \mathbb{N}$ . Then,*

$$\mathbb{I}\{y_n \neq \text{sgn}(\Phi^{(T)}(x_n))\} \equiv \mathbb{I}\{y_n \Phi^{(T)}(x_n) \leq 0\}. \quad (36)$$

*Proof.* The proof is deferred to Appendix B.

By substituting (36) in the RHS of (35), the testing error can also be expressed as

$$R_{\mathcal{T}}(\mathbf{W}^{(T)}) = \frac{1}{\tilde{N}} \sum_{n=N+1}^{N+\tilde{N}} \mathbb{I}\{y_n \Phi^{(T)}(x_n) \leq 0\}. \quad (37)$$

Hence, the average probability of misclassification error  $\bar{P}_e$  manifested by  $\Phi^{(T)}$  becomes

$$\bar{P}_e = \frac{1}{\tilde{N}} \sum_{n=N+1}^{N+\tilde{N}} \mathbb{P}(y_n \Phi^{(T)}(x_n) \leq 0), \quad (38)$$

where (38) follows from (37). As for (38), the probability of point misclassification error  $P_e$  manifested by  $\Phi^{(T)}$  can be expressed and simplified as follows:

$$P_e = \mathbb{P}(y_n \Phi^{(T)}(x_n) \leq 0) \quad (39a)$$

$$\stackrel{(a)}{=} \mathbb{P}(y_n \Phi^{(T)}(x_n) \geq 0 | \mathcal{H}_{-1}) \mathbb{P}(\mathcal{H}_{-1}) + \mathbb{P}(y_n \Phi^{(T)}(x_n) \leq 0 | \mathcal{H}_1) \mathbb{P}(\mathcal{H}_1) \quad (39b)$$

$$\stackrel{(b)}{=} \frac{1}{2} [\mathbb{P}(\Phi^{(T)}(x_n) \geq 0 | \mathcal{H}_{-1}) + \mathbb{P}(\Phi^{(T)}(x_n) \leq 0 | \mathcal{H}_1)] \quad (39c)$$

$$= \frac{1}{2} [\mathbb{P}(\Phi^{(T)}(x_n) > 0 | \mathcal{H}_{-1}) + \mathbb{P}(\Phi^{(T)}(x_n) < 0 | \mathcal{H}_1) + \sum_{i \in \{-1, 1\}} \mathbb{P}(\Phi^{(T)}(x_n) = 0 | \mathcal{H}_i)], \quad (39d)$$

where (a) is due to the law of total probability (per Law 1) and (b) follows from the equally likely labels that  $\mathbb{P}(y_n = -1) = \mathbb{P}(y_n = 1) = 1/2$ .

To simplify the RHS of (39d), we first underscore that  $\Phi^{(T)}(x_n) | \mathcal{H}_{-1}$  and  $\Phi^{(T)}(x_n) | \mathcal{H}_1$  would be continuous RVs – with a high probability – w.r.t. the binary hypothesis testing problem in

(27). When accounting for the randomness in (27), letting  $f_{\Phi_i^{(T)}}$  be the PDF of  $\Phi^{(T)}(x_n)|\mathcal{H}_i$  for  $i \in \{-1, 1\}$  would then help simplify  $\mathbb{P}(\Phi^{(T)}(x_n) = 0|\mathcal{H}_i)$  as follows:

$$\mathbb{P}(\Phi^{(T)}(x_n) = 0|\mathcal{H}_i) = \lim_{\delta \rightarrow 0} \left\{ \mathbb{P}(\Phi^{(T)}(x_n)|\mathcal{H}_i \in [0, \delta]) \right\} \quad (40a)$$

$$\stackrel{(a)}{=} \lim_{\delta \rightarrow 0} \left\{ f_{\Phi_i^{(T)}}(\Phi^{(T)}(x_n)|\mathcal{H}_i) \times \delta \right\} \quad (40b)$$

$$\stackrel{(b)}{=} \lim_{\delta \rightarrow 0} f_{\Phi_i^{(T)}}(\Phi^{(T)}(x_n)|\mathcal{H}_i) \times \lim_{\delta \rightarrow 0} \delta \quad (40c)$$

$$= 0, \quad (40d)$$

where (a) is due to the PDF property stated in (14) and (b) is because of the limit property. Meanwhile, substituting (40d) into the RHS of (39d) leads to the expression

$$P_e = \frac{1}{2} [\mathbb{P}(\Phi^{(T)}(x_n) > 0|\mathcal{H}_{-1}) + \mathbb{P}(\Phi^{(T)}(x_n) < 0|\mathcal{H}_1)]. \quad (41)$$

We formulate the following problems for (41) w.r.t.  $\mathbf{y}_{K-1,n}^{(T)}$ , which is defined through (29).

**Problem 1.** For the  $P_e$  given by (41), characterize  $\lim_{\|\mathbf{y}_{K-1,n}^{(T)}\|_{\mathcal{H}_{-1}}, \|\mathbf{y}_{K-1,n}^{(T)}\|_{\mathcal{H}_1} \rightarrow \infty} P_e$ .

**Problem 2.** For the  $P_e$  given by (41), quantify  $\lim_{\|\mathbf{y}_{K-1,n}^{(T)}\|_{\mathcal{H}_{-1}}, \|\mathbf{y}_{K-1,n}^{(T)}\|_{\mathcal{H}_1} \rightarrow 0} P_e$ .

Problems 1 and 2 are novel in the sense that a problem solver should address the interpretability of a trained deep ReLU FNN model while also circumventing the random gradients (with unknown distribution) that were back-propagated during training per the back-propagation algorithm. More specifically, Problems 1 and 2 capture the impact of the penultimate layer's output on a ReLU FNN-based classifier when the norm of the penultimate layer's output approaches infinity and zero, respectively, regardless of the input.

In view of Problems 1 and 2, we would also like to understand the fundamental testing performance limits of binary classifiers that are based on deep FNNs with ReLU and Tanh activation. As a result, we continue with the following problem formulation on testing performance limits.

### B. Problems in Testing Performance Limits of Binary Classifiers that are Based on Deep FNNs with ReLU and Tanh Activation

For binary classifiers that are based on deep FNNs with ReLU and Tanh activation, suppose that  $\check{\Phi}^{(T)} := [[\check{\mathbf{w}}_1^{(T)}, \mathbf{0}], [\check{\mathbf{W}}_2^{(T)}, \mathbf{0}], \dots, [\check{\mathbf{W}}_{K-1}^{(T)}, \mathbf{0}], [\check{\mathbf{w}}_K^{(T)}, \mathbf{0}]]$  is a deep FNN that has been trained using hinge loss and SGD, SGD with momentum, RMSProp, or Adam after being initialized

with a Gaussian initializer such as LeCun normal or He normal (per Definition 10) such that

$$\check{\mathbf{w}}_1^{(T)} = \check{\mathbf{w}}_1^{(T-1)} + \Delta\check{\mathbf{w}}_1^{(T-1)} = \check{\mathbf{w}}_1^{(0)} + \sum_{t=0}^{T-1} \Delta\check{\mathbf{w}}_1^{(t)} \in \mathbb{R}^{2H} \quad (42a)$$

$$\check{\mathbf{W}}_k^{(T)} = \check{\mathbf{W}}_k^{(T-1)} + \Delta\check{\mathbf{W}}_k^{(T-1)} = \check{\mathbf{W}}_k^{(0)} + \sum_{t=0}^{T-1} \Delta\check{\mathbf{W}}_k^{(t)} \in \mathbb{R}^{2H \times 2H} \quad (42b)$$

$$\check{\mathbf{w}}_K^{(T)} = \check{\mathbf{w}}_K^{(T-1)} + \Delta\check{\mathbf{w}}_K^{(T-1)} = \check{\mathbf{w}}_K^{(0)} + \sum_{t=0}^{T-1} \Delta\check{\mathbf{w}}_K^{(t)} \in \mathbb{R}^{1 \times 2H}, \quad (42c)$$

where  $\check{\mathbf{w}}_1^{(0)}$ ,  $\check{\mathbf{W}}_k^{(0)}$ , and  $\check{\mathbf{w}}_K^{(0)}$  are weight matrices/vectors initialized with Gaussian initializers (per Definition 10); and  $\Delta\check{\mathbf{w}}_1^{(t)}$ ,  $\Delta\check{\mathbf{W}}_k^{(t)}$ , and  $\Delta\check{\mathbf{w}}_K^{(t)}$  are the  $t$ -th back-propagated error matrices/vectors w.r.t. an optimization with SGD (per Definition 13), SGD with momentum (per Definition 14), RMSProp (per Definition 15), or Adam (per Definition 16).

For the trained deep FNN  $\check{\Phi}^{(T)}$ , its manifested testing error over  $\mathcal{T} := \{(x_n, y_n)\}_{n=N+1}^{N+\tilde{N}}$  – provided that  $x_n$  is the  $n$ -th input generated via (27) and  $y_n \in \{-1, 1\}$  is the  $n$ -th label for all  $n \in \{N+1, \dots, N+\tilde{N}\}$  – is defined similarly to (35) and (37) as

$$R_{\mathcal{T}}(\check{\mathbf{W}}^{(T)}) = \frac{1}{\tilde{N}} \sum_{n=N+1}^{N+\tilde{N}} \mathbb{I}\{y_n \neq \text{sgn}(\check{\Phi}^{(T)}(x_n))\} \stackrel{(a)}{=} \frac{1}{\tilde{N}} \sum_{n=N+1}^{N+\tilde{N}} \mathbb{I}\{y_n \check{\Phi}^{(T)}(x_n) \leq 0\}, \quad (43)$$

where  $\check{\mathbf{W}}^{(T)} = [\check{\mathbf{w}}_1^{(T)} \check{\mathbf{W}}_2^{(T)} \dots \check{\mathbf{W}}_{K-1}^{(T)} (\check{\mathbf{w}}_K^{(T)})^\top]$  and (a) follows from Lemma 1. Consequently, it follows through (43) that the average probability of misclassification error  $\check{P}_e$  exhibited by  $\check{\Phi}^{(T)}$  is given by

$$\check{P}_e = \frac{1}{\tilde{N}} \sum_{n=N+1}^{N+\tilde{N}} \mathbb{P}(y_n \check{\Phi}^{(T)}(x_n) \leq 0). \quad (44)$$

Accordingly, the probability of point misclassification error  $\check{P}_e$  manifested by  $\check{\Phi}^{(T)}$  is given by

$$\check{P}_e = \mathbb{P}(y_n \check{\Phi}^{(T)}(x_n) \leq 0). \quad (45)$$

By using (45) and adopting the simplifications in (39a)-(40d), it follows directly through (41) that

$$\check{P}_e = \frac{1}{2} [\mathbb{P}(\check{\Phi}^{(T)}(x_n) > 0 | \mathcal{H}_{-1}) + \mathbb{P}(\check{\Phi}^{(T)}(x_n) < 0 | \mathcal{H}_1)]. \quad (46)$$

We formulate the following problems for (46) w.r.t.  $\check{\mathbf{y}}_{K-1,n}^{(T)}$ , which is defined via (31).

**Problem 3.** For the  $\check{P}_e$  given by (46), determine 
$$\lim_{\|\check{\mathbf{y}}_{K-1,n}^{(T)}\|_{\mathcal{H}_{-1}}, \|\check{\mathbf{y}}_{K-1,n}^{(T)}\|_{\mathcal{H}_1} \rightarrow \infty} \check{P}_e.$$

**Problem 4.** For the  $\check{P}_e$  given by (46), derive 
$$\lim_{\|\check{\mathbf{y}}_{K-1,n}^{(T)}\|_{\mathcal{H}_{-1}}, \|\check{\mathbf{y}}_{K-1,n}^{(T)}\|_{\mathcal{H}_1} \rightarrow 0} \check{P}_e.$$

Problems 3 and 4 are novel in the sense that a problem solver must tackle the interpretability of a trained deep FNN model with ReLU and Tanh activation while also circumventing the random gradients (with unknown distribution) that were back-propagated during training using the back-propagation algorithm. Problems 3 and 4 capture the impact of the penultimate layer's output on an FNN-based classifier with ReLU and Tanh activation when the norm of the penultimate layer's output approaches infinity and zero, respectively, irrespective of the input.

In light of Problems 1, 2, 3, and 4, we now derive the asymptotic testing performance limits of binary classifiers that are based on deep FNNs.

## V. ASYMPTOTIC TESTING PERFORMANCE LIMITS OF BINARY CLASSIFIERS THAT ARE BASED ON DEEP FNNs

We derive the fundamental asymptotic testing performance limits of the two trained deep FNNs from Section IV (i.e.,  $\Phi^{(T)}$  and  $\check{\Phi}^{(T)}$ ) using the tools of probability theory and high-dimensional statistics. These tools enable us to derive the asymptotic testing performance limits of  $\Phi^{(T)}$  and  $\check{\Phi}^{(T)}$ , beginning with  $\Phi^{(T)}$ .

### A. Asymptotic Testing Performance Limits of Binary Classifiers that are Based on Deep ReLU FNNs

The asymptotic testing performance limits manifested by  $\Phi^{(T)}$  are characterized by the following theorem.

**Theorem 1.** Let  $H, K, N, \tilde{N}, T \in \mathbb{N}$ . Consider a deep ReLU FNN that has been trained over  $\mathcal{D} := \{(x_n, y_n)\}_{n=1}^N$  and tested over  $\mathcal{T} := \{(x_n, y_n)\}_{n=N+1}^{N+\tilde{N}}$ , with  $x_n$  being the  $n$ -th input per (27) and  $y_n \in \{-1, 1\}$  being the  $n$ -th label. Let  $\Phi^{(T)} := [[\mathbf{w}_1^{(T)}, \mathbf{0}], [\mathbf{W}_2^{(T)}, \mathbf{0}], \dots, [\mathbf{W}_{K-1}^{(T)}, \mathbf{0}], [\mathbf{w}_K^{(T)}, 0]]$  be a deep ReLU FNN – such that  $\mathbf{w}_K^{(T)} \in \mathbb{R}^{1 \times 2H}$ ,  $\mathbf{W}_{K-k}^{(T)} \in \mathbb{R}^{2H \times 2H}$  for all  $k \in [K-2]$ , and  $\mathbf{w}_1^{(T)} \in \mathbb{R}^{2H}$  – that has been trained with hinge loss and SGD, SGD with momentum, RMSProp, or Adam after being initialized by a Gaussian initializer such as LeCun normal

or He normal. Then, the following results hold for any  $N, \tilde{N}, T, K \geq 2$ , and  $H < \infty$ :

$$\lim_{\|\mathbf{y}_{K-1,n}^{(T)}\|_{\mathcal{H}_{-1}}, \|\mathbf{y}_{K-1,n}^{(T)}\|_{\mathcal{H}_1} \rightarrow \infty} P_e = 1/2 \quad (47a)$$

$$\lim_{\|\mathbf{y}_{K-1,n}^{(T)}\|_{\mathcal{H}_{-1}}, \|\mathbf{y}_{K-1,n}^{(T)}\|_{\mathcal{H}_1} \rightarrow 0} P_e = 1, \quad (47b)$$

where (47a) and (47b) are valid for all  $n \in \{N + 1, N + 2, \dots, N + \tilde{N}\}$ .

*Proof.* The proof is relegated to Appendix C.

Following Appendix C containing the proof of Theorem 1, the underneath remarks are in order.

**Remark 5.** Eqs. (47a) and (47b) are valid for any  $N, \tilde{N}, T, K \geq 2$ , and  $H < \infty$ . Thus, Theorem 1 is valid regardless of training/testing dataset size, network depth, or (finite) network width.

**Remark 6.** Since Theorem 1 does not make any specific assumptions w.r.t. the input hypotheses, it applies to any binary classification AI/ML problem solved using a deep ReLU FNN that has been trained with hinge loss and SGD, SGD with momentum, RMSProp, or Adam after being initialized with a Gaussian initializer such as LeCun normal or He normal.

**Remark 7.** As  $\|\mathbf{y}_{K-1,n}^{(T)}\|_{\mathcal{H}_{-1}}, \|\mathbf{y}_{K-1,n}^{(T)}\|_{\mathcal{H}_1} \rightarrow \infty$ , the output of the trained deep ReLU FNN will be an infinitely large positive or negative number. Accordingly, the binary classifier will be coin-tossing and hence the derived limit  $P_e = 1/2$  is intuitive w.r.t. (47a).

**Remark 8.** As  $\|\mathbf{y}_{K-1,n}^{(T)}\|_{\mathcal{H}_{-1}}, \|\mathbf{y}_{K-1,n}^{(T)}\|_{\mathcal{H}_1} \rightarrow 0$ , the trained deep ReLU FNN will tend to produce zero as an output. Accordingly, the binary classifier will always be blind and wrong – per the  $P_e$  expression in (41) – and thus, the derived limit  $P_e = 1$  is intuitive w.r.t. (47b).

**Remark 9.** Theorem 1 has limitations when it comes to interpreting the results of a trained ReLU FNN-based binary classifier because (47a) and (47b) can quantify the classifier’s performance only when  $\|\mathbf{y}_{K-1,n}^{(T)}\|_{\mathcal{H}_{-1}}, \|\mathbf{y}_{K-1,n}^{(T)}\|_{\mathcal{H}_1} \rightarrow \infty$  and  $\|\mathbf{y}_{K-1,n}^{(T)}\|_{\mathcal{H}_{-1}}, \|\mathbf{y}_{K-1,n}^{(T)}\|_{\mathcal{H}_1} \rightarrow 0$ , respectively.

Following the aforementioned informative remarks, we move on to derive the asymptotic testing performance limits of  $\check{\Phi}^{(T)}$ , as detailed below.

## B. Asymptotic Testing Performance Limits of Binary Classifiers that are Based on FNNs with ReLU and Tanh Activation

The asymptotic testing performance limits exhibited by  $\check{\Phi}^{(T)}$  are characterized by the following theorem.

**Theorem 2.** *Let  $H, K, N, \tilde{N}, T \in \mathbb{N}$ . Consider a deep FNN that has been trained over  $\mathcal{D} := \{(x_n, y_n)\}_{n=1}^N$  and tested over  $\mathcal{T} := \{(x_n, y_n)\}_{n=N+1}^{N+\tilde{N}}$ , with  $x_n$  being the  $n$ -th input per (27) and  $y_n \in \{-1, 1\}$  being the  $n$ -th label. Let  $\check{\Phi}^{(T)} := [[\check{\mathbf{w}}_1^{(T)}, \mathbf{0}], [\check{\mathbf{W}}_2^{(T)}, \mathbf{0}], \dots, [\check{\mathbf{W}}_{K-1}^{(T)}, \mathbf{0}], [\check{\mathbf{w}}_K^{(T)}, 0]]$  be a deep FNN with ReLU and Tanh activation – such that  $\check{\mathbf{w}}_K^{(T)} \in \mathbb{R}^{1 \times 2H}$ ,  $\check{\mathbf{W}}_{K-k}^{(T)} \in \mathbb{R}^{2H \times 2H}$  for all  $k \in [K-2]$ , and  $\check{\mathbf{w}}_1^{(T)} \in \mathbb{R}^{2H}$  – that has been trained with hinge loss and SGD, SGD with momentum, RMSProp, or Adam after being initialized by a Gaussian initializer such as LeCun normal or He normal. Then, the following results are valid for any  $N, \tilde{N}, T, K \geq 2$ , and  $H < \infty$ :*

$$\lim_{\|\check{\mathbf{y}}_{K-1,n}^{(T)}\|_{\mathcal{H}_{-1}}, \|\check{\mathbf{y}}_{K-1,n}^{(T)}\|_{\mathcal{H}_1} \rightarrow \infty} \check{P}_e = 1/2 \quad (48a)$$

$$\lim_{\|\check{\mathbf{y}}_{K-1,n}^{(T)}\|_{\mathcal{H}_{-1}}, \|\check{\mathbf{y}}_{K-1,n}^{(T)}\|_{\mathcal{H}_1} \rightarrow 0} \check{P}_e = 1, \quad (48b)$$

where (48a) and (48b) are true for all  $n \in \{N+1, N+2, \dots, N+\tilde{N}\}$ .

*Proof.* The proof is deferred to Appendix D.

Following Appendix D containing the proof of Theorem 2, the underneath remarks are in order.

**Remark 10.** *Eqs. (48a) and (48b) are valid for any  $N, \tilde{N}, T, K \geq 2$ , and  $H < \infty$ . Theorem 2 is thus valid irrespective of training/testing dataset size, network depth, or (finite) network width.*

**Remark 11.** *Because Theorem 2 does not make any particular assumptions w.r.t. the input hypotheses, it applies to any binary classification AI/ML problem solved using a deep FNN with ReLU and Tanh activation that has been trained with hinge loss and SGD, SGD with momentum, RMSProp, or Adam after being initialized with a Gaussian initializer such as LeCun normal or He normal.*

**Remark 12.** As  $\|\check{\mathbf{y}}_{K-1,n}^{(T)}\|\mathcal{H}_{-1}, \|\check{\mathbf{y}}_{K-1,n}^{(T)}\|\mathcal{H}_1 \rightarrow \infty$ , the trained deep FNN with ReLU and Tanh activation will produce an infinitely large positive or negative output. Thus, the binary classifier will be coin-tossing and hence the derived limit  $\check{P}_e = 1/2$  is intuitive w.r.t. (48a).

**Remark 13.** As  $\|\check{\mathbf{y}}_{K-1,n}^{(T)}\|\mathcal{H}_{-1}, \|\check{\mathbf{y}}_{K-1,n}^{(T)}\|\mathcal{H}_1 \rightarrow 0$ , the trained deep FNN with ReLU and Tanh activation will tend to deliver zero as an output. Consequently, the binary classifier will always be blind and wrong – per the  $\check{P}_e$  expression in (46) – and thus, the derived limit  $\check{P}_e = 1$  is intuitive w.r.t. (48b).

**Remark 14.** Theorem 2 has limitations when it comes to interpreting the results of a binary classifier that is based on a trained deep FNN with ReLU and Tanh activation because (48a) and (48b) can quantify the classifier’s performance only when  $\|\check{\mathbf{y}}_{K-1,n}^{(T)}\|\mathcal{H}_{-1}, \|\check{\mathbf{y}}_{K-1,n}^{(T)}\|\mathcal{H}_1 \rightarrow \infty$  and  $\|\check{\mathbf{y}}_{K-1,n}^{(T)}\|\mathcal{H}_{-1}, \|\check{\mathbf{y}}_{K-1,n}^{(T)}\|\mathcal{H}_1 \rightarrow 0$ , respectively.

We conducted extensive computer experiments to validate our theory and assess the performance of our proposed DL-based binary classifiers. The results of those experiments are reported below.

## VI. COMPUTER EXPERIMENTS

### A. Context of our Computer Experiments: BPSK Detection

We consider a classical optimum detection problem involving a BPSK signal received over an AWGN channel. For a received AWGN-contaminated BPSK signal having a bit duration of  $T_s$ , we first assume that the received passband signal is down-converted to the received baseband signal. The received baseband signal – denoted by  $r(t)$  – is then assumed to be sampled per the Nyquist rate  $f_s = 1/T_s$  [96]. The sampled baseband signal can be formulated in terms of a binary hypothesis testing problem for  $n \in \mathbb{N}$  as

$$r[n] = \begin{cases} -\sqrt{\mathcal{E}_b} + z[n] & : \mathcal{H}_{-1} \\ \sqrt{\mathcal{E}_b} + z[n] & : \mathcal{H}_1, \end{cases} \quad (49)$$

where  $r[n]$  is the received baseband signal sample obtained by sampling  $r(t)$  as  $r[n] := r(nT_s)$ ;  $\mathcal{E}_b$  is the transmitted energy per bit;  $s_0 = -\sqrt{\mathcal{E}_b}$  and  $s_1 = \sqrt{\mathcal{E}_b}$  are the equally likely samples of the transmitted BPSK signal pertaining to bit 0 and bit 1, respectively;  $z[n]$  denotes the AWGN samples obtained by sampling the AWGN process  $z(t)$  as  $z[n] := z(nT_s)$  and  $z[n] \sim \mathcal{N}(0, N_0/2)$ ,

with  $N_0$  being the power spectral density (PSD) of the noise; and  $\mathcal{H}_{-1}$  and  $\mathcal{H}_1$  are hypotheses corresponding to the transmission of  $s_0$  and  $s_1$ , respectively. In light of the detection problem in (49) and  $\gamma_b$  being the signal-to-noise ratio (SNR) per bit, an optimum *maximum-likelihood* BPSK detector's manifested probability of bit error ( $\tilde{P}_e$ ) is given by  $P_e = \mathcal{Q}(\sqrt{2\gamma_b})$  (see the proof in Appendix E). This optimal performance limit serves as a baseline for our computer experiments to empirically assess our DL-based BPSK detectors' performance. This assessment was carried out using the materials and methods detailed below.

### B. Materials and Methods

Our computer experiments were carried out on the NIST GPU cluster named *Enki* using Keras with TensorFlow as a backend. We used MATLAB<sup>®</sup> to generate our testing and training sets. Our training sets  $\mathcal{D}_1$  and  $\mathcal{D}_2$  were generated by combining the training data generated for each SNR per bit  $\gamma_b \in \{0, 5, 10, 15, 20, 25, 30, 35\}$  dB. For each  $\gamma_b^i = 5(i-1)$  dB given  $i \in [8]$ , we generated training sets  $\mathcal{D}_1^i$  and  $\mathcal{D}_2^i$  made of  $2 \times 10^5$  inputs equal to received baseband signal samples produced at SNR  $\gamma_b^i$  and equally likely labels chosen from  $\{-1, 1\}$  as  $\mathcal{D}_1^i := \{(x_n^i, y_n^i)\}_{n=1}^{200,000}$  and  $\mathcal{D}_2^i := \{(x_{\tilde{n}}^i, y_{\tilde{n}}^i)\}_{\tilde{n}=1}^{200,000}$  such that  $x_n^i = r[n]_{\gamma_b=\gamma_b^i}$  for  $r[n]$  defined in (49);  $y_n^i \in \{-1, 1\}$ ;  $x_{\tilde{n}}^i = r[\tilde{n}]_{\gamma_b=\gamma_b^i}$  for  $r[\tilde{n}]$  defined in (49); and  $y_{\tilde{n}}^i \in \{-1, 1\}$ . For the generation of  $x_n^i = r[n]_{\gamma_b=\gamma_b^i}$  and  $x_{\tilde{n}}^i = r[\tilde{n}]_{\gamma_b=\gamma_b^i}$  w.r.t.  $\gamma_b^i = \mathcal{E}_b^i/N_0$ , we set  $N_0 = 1$  W/Hz such that  $\gamma_b^i = \mathcal{E}_b^i$ ,  $z[n] \sim \mathcal{N}(0, 1/2)$ , and  $z[\tilde{n}] \sim \mathcal{N}(0, 1/2)$ . We used these settings to generate  $\mathcal{D}_1^i$  and  $\mathcal{D}_2^i$  for all  $i \in [8]$  and formed  $\mathcal{D}_1$  and  $\mathcal{D}_2$  as  $\mathcal{D}_1 := \{\mathcal{D}_1^1 \cup \mathcal{D}_1^2 \cup \dots \cup \mathcal{D}_1^7 \cup \mathcal{D}_1^8\}$  and  $\mathcal{D}_2 := \{\mathcal{D}_2^1 \cup \mathcal{D}_2^2 \cup \dots \cup \mathcal{D}_2^7 \cup \mathcal{D}_2^8\}$ , respectively. Similarly, we generated a testing set  $\mathcal{T}$  as  $\mathcal{T} := \{\mathcal{T}^1 \cup \mathcal{T}^2 \cup \dots \cup \mathcal{T}^7 \cup \mathcal{T}^8\}$  for  $\mathcal{T}^i$ ,  $i \in [8]$ , which is the testing set generated at SNR  $\gamma_b^i$  such that  $\mathcal{T}^i := \{(x_n^i, y_n^i)\}_{n=200,001}^{250,000}$  for  $x_n^i = r[n]_{\gamma_b=\gamma_b^i}$ ,  $y_n^i \in \{-1, 1\}$ , and  $\gamma_b^i = 5(i-1)$  dB. We then uploaded  $\mathcal{T}$ ,  $\mathcal{D}_1$ , and  $\mathcal{D}_2$  into Enki and implemented three training strategies.

The three training strategies we implemented in Keras are low SNR training, high SNR training, and all SNR training. For all SNR training, we formed a training (and validation) set  $\mathcal{D}$  as  $\mathcal{D} = \mathcal{D}_1$ . For high SNR training, we generated a training (and validation) set  $\mathcal{D}_{\text{high}}$  as  $\mathcal{D}_{\text{high}} = \mathcal{D}_{1,\text{high}} \cup \mathcal{D}_{2,\text{high}}$ , where  $\mathcal{D}_{1,\text{high}} := \{\mathcal{D}_1^5 \cup \mathcal{D}_1^6 \cup \mathcal{D}_1^7 \cup \mathcal{D}_1^8\}$ ,  $\mathcal{D}_{2,\text{high}} := \{\mathcal{D}_2^5 \cup \mathcal{D}_2^6 \cup \mathcal{D}_2^7 \cup \mathcal{D}_2^8\}$ , and  $|\mathcal{D}_{1,\text{high}}| = |\mathcal{D}|$ . For low SNR training, we created a training (and validation) set  $\mathcal{D}_{\text{low}}$  as  $\mathcal{D}_{\text{low}} = \mathcal{D}_{1,\text{low}} \cup \mathcal{D}_{2,\text{low}}$ , where  $\mathcal{D}_{1,\text{low}} := \{\mathcal{D}_1^1 \cup \mathcal{D}_1^2 \cup \mathcal{D}_1^3 \cup \mathcal{D}_1^4\}$ ,  $\mathcal{D}_{2,\text{low}} := \{\mathcal{D}_2^1 \cup \mathcal{D}_2^2 \cup \mathcal{D}_2^3 \cup \mathcal{D}_2^4\}$ , and  $|\mathcal{D}_{1,\text{low}}| = |\mathcal{D}|$ . Using  $\mathcal{D}_{\text{low}}$ ,  $\mathcal{D}_{\text{high}}$ , and  $\mathcal{D}$ , we carried out exhaustive training that led to the optimized (hyper)parameters set out in Tables VI and VII for the best performing ReLU FNN

models and FNN models with ReLU and Tanh activation, respectively. In addition to the above-mentioned (hyper)parameters, we used four KERAS callbacks [116, Ch. 7]: `TensorBoard`, `ModelCheckpoint`, `EarlyStopping`, and `ReduceLRonPlateau`. `EarlyStopping` and `ReduceLRonPlateau` were set to have patience over 20 and 40 epochs, respectively. `ReduceLRonPlateau` was set to reduce the learning rate by 0.5 for every 20 epochs that witness a performance stagnation.

Finally, we tested the BPSK detection performance of trained (deep) ReLU FNNs and (deep) FNNs with ReLU and Tanh activation by varying  $K$  and  $H$  for each testing SNR. This leads to the main results for ReLU FNNs and those for FNNs with ReLU and Tanh activation which are reported in Sections VI-C and VI-D, respectively.

### C. Main Results for ReLU FNNs

The ReLU FNN-based BPSK detectors' testing and theory validation results were produced using the materials and methods detailed in Section VI-B and the (hyper)parameters set out in Table VI, and are presented in Sections VI-C1 and VI-C2, respectively.

1) *Testing Results for ReLU FNN-Based BPSK Detectors:* Tables I, II, and III contrast the detection performance of the optimum BPSK detector and ReLU FNN-based BPSK detectors. The latter detectors' performance was evaluated by assessing the performance of ReLU FNNs trained using the all SNR training (All-SNR-T), high SNR training (High-SNR-T), and low SNR training (Low-SNR-T) schemes as detailed in Section VI-B. Table I confirms that – as expected – shallow ReLU FNNs with  $K = 3$  perform relatively well with Low-SNR-T better than with All-SNR-T or High-SNR-T for  $\gamma_b \in \{0, 5\}$  dB. Tables II and III validate that deep ReLU FNNs with  $K \in \{7, 9\}$  perform better with All-SNR-T than with Low-SNR-T or High-SNR-T for  $\gamma_b \in \{0, 5\}$  dB. Tables I, II, and III substantiate that High-SNR-T produces the worst performance – as expected – for  $\gamma_b \in \{0, 5\}$  dB. They also corroborate that ReLU FNNs perform identically with All-SNR-T, High-SNR-T, and Low-SNR-T for  $\gamma_b > 5$  dB irrespective of their depth and width.

As Tables I, II, and III attest, the minimum probability of bit error exhibited by a ReLU FNN-based BPSK detector irrespective of its width, depth, and training scheme is almost 0.5 – the chance of getting heads when flipping a coin. Those tables thus illustrate that a ReLU FNN-based BPSK detector trained with hinge loss and Adam fails to learn optimum BPSK detection. Moreover, at high SNRs, a sampled BPSK signal would likely be a large positive

SNR [in dB]	Optimal detector	ReLU FNN-based BPSK detector ( $K, H$ ) = (3, 3)			ReLU FNN-based BPSK detector ( $K, H$ ) = (3, 9)		
		All-SNR-T	High-SNR-T	Low-SNR-T	All-SNR-T	High-SNR-T	Low-SNR-T
$\gamma_b$ [dB]	$\mathcal{Q}(\sqrt{2\gamma_b})$						
0	0.0786	0.56448001	0.75902	0.56411999	0.56411999	0.59154001	0.56402001
5	0.0060	0.50569999	0.57170001	0.50566	0.50566	0.51100001	0.50564
10	$3.8721 \times 10^{-6}$	0.50075999	0.50128001	0.50075999	0.50075999	0.50075999	0.50075999
15	$9.1240 \times 10^{-16}$	0.50338	0.50338	0.50338	0.50338	0.50338	0.50338
20	$1.0442 \times 10^{-45}$	0.49835998	0.49835998	0.49835998	0.49835998	0.49835998	0.49835998
25	$7.3070 \times 10^{-140}$	0.49908	0.49908	0.49908	0.49908	0.49908	0.49908
30	0	0.49677998	0.49677998	0.49677998	0.49677998	0.49677998	0.49677998
35	0	0.50049999	0.50049999	0.50049999	0.50049999	0.50049999	0.50049999

TABLE I: Numerical results I on the probability of bit error manifested by an optimal BPSK detector and by ReLU FNN-based BPSK detectors.

SNR [in dB]	Optimal detector	ReLU FNN-based BPSK detector ( $K, H$ ) = (7, 7)			ReLU FNN-based BPSK detector ( $K, H$ ) = (7, 14)		
		All-SNR-T	High-SNR-T	Low-SNR-T	All-SNR-T	High-SNR-T	Low-SNR-T
$\gamma_b$ [dB]	$\mathcal{Q}(\sqrt{2\gamma_b})$						
0	0.0786	0.56362	0.86848	0.56345999	0.56378001	0.55552	0.56332001
5	0.0060	0.50562	0.65803999	0.50562	0.50564	0.50426	0.50558001
10	$3.8721 \times 10^{-6}$	0.50075999	0.50454	0.50075999	0.50075999	0.50075999	0.50075999
15	$9.1240 \times 10^{-16}$	0.50338	0.50338	0.50338	0.50338	0.50338	0.50338
20	$1.0442 \times 10^{-45}$	0.49835998	0.49835998	0.49835998	0.49835998	0.49835998	0.49835998
25	$7.3070 \times 10^{-140}$	0.49908	0.49908	0.49908	0.49908	0.49908	0.49908
30	0	0.49677998	0.49677998	0.49677998	0.49677998	0.49677998	0.49677998
35	0	0.50049999	0.50049999	0.50049999	0.50049999	0.50049999	0.50049999

TABLE II: Numerical results II on the probability of bit error exhibited by an optimal BPSK detector and by ReLU FNN-based BPSK detectors.

or negative number when bit 1 or bit 0 is transmitted over an AWGN channel, respectively. This detection problem is thus a simple inference problem that can be solved by using the decision threshold  $\tau_{\text{th}} = 0$ . Nonetheless, our best-trained deep (or shallow) ReLU FNNs fail at this common-sense inference task. This may be because FNNs (and deep networks in general) are poor at solving (common-sense) inference tasks [117] such as BPSK signal detection at high SNRs. Meanwhile, how can we interpret our trained ReLU FNNs' performance results using

SNR [in dB]	Optimal detector	ReLU FNN-based BPSK detector ( $K, H$ ) = (9, 9)			ReLU FNN-based BPSK detector ( $K, H$ ) = (9, 18)		
		All-SNR-T	High-SNR-T	Low-SNR-T	All-SNR-T	High-SNR-T	Low-SNR-T
$\gamma_b$ [dB]	$\mathcal{Q}(\sqrt{2\gamma_b})$						
0	0.0786	0.56356001	0.64416	0.56376001	0.56417999	0.55226001	0.565
5	0.0060	0.50562	0.52410001	0.50564	0.50567999	0.50376001	0.50588
10	$3.8721 \times 10^{-6}$	0.50075999	0.50080001	0.50075999	0.50075999	0.50075999	0.50075999
15	$9.1240 \times 10^{-16}$	0.50338	0.50338	0.50338	0.50338	0.50338	0.50338
20	$1.0442 \times 10^{-45}$	0.49835998	0.49835998	0.49835998	0.49835998	0.49835998	0.49835998
25	$7.3070 \times 10^{-140}$	0.49908	0.49908	0.49908	0.49908	0.49908	0.49908
30	0	0.49677998	0.49677998	0.49677998	0.49677998	0.49677998	0.49677998
35	0	0.50049999	0.50049999	0.50049999	0.50049999	0.50049999	0.50049999

TABLE III: Numerical results III on the probability of bit error manifested by an optimal BPSK detector and by ReLU FNN-based BPSK detectors.

a rigorous theory? When it comes to interpreting the performance of binary classifiers that are based on ReLU FNNs trained with hinge loss, the theory developed in this paper is applicable, as described below.

2) *Theory Validation Results for ReLU FNN-Based BPSK Detectors:* to assess the validity of the theory we developed for binary classifiers that are based on ReLU FNNs, which is stated in Theorem 1, we produced many scatter plots of  $\|\mathbf{y}_{K-1,n}^{(T)}\|$  versus  $n$  subject to All-SNR-T, High-SNR-T, and Low-SNR-T for various pairs of  $(K, H)$ . The scatter plots for shallow, deep, and deeper and wider ReLU FNN-based BPSK detectors are shown in Figs. 1-12. When it comes to the shallow ReLU FNN-based BPSK detectors, Figs. 1-3 show the scatter plots of  $\|\mathbf{y}_{K-1,n}^{(T)}\|$  versus  $n$  subject to All-SNR-T, High-SNR-T, and Low-SNR-T, respectively, for  $(K, H) = (8, 8)$ . These scatter plots do not exactly corroborate Theorem 1 and (47a) since  $\|\mathbf{y}_{K-1,n}^{(T)}\|$  doesn't approach infinity, though the testing  $P_e$  does equal 0.5 in all cases.

As for deep ReLU FNN-based BPSK detectors, Figs. 4-6 show the scatter plots of  $\|\mathbf{y}_{K-1,n}^{(T)}\|$  versus  $n$  subject to All-SNR-T, High-SNR-T, and Low-SNR-T, respectively, given that  $(K, H) = (16, 16)$ . The scatter plots in Figs. 5 and 6 also fail to corroborate (47a) because  $\|\mathbf{y}_{K-1,n}^{(T)}\|$  doesn't approach infinity, though the testing  $P_e$  does equal 0.5. Some points in Fig. 4 validate (47b) since  $\|\mathbf{y}_{K-1,n}^{(T)}\|$  approaches zero for those points and  $P_e = 1.0$ .

We now proceed to deep and wider ReLU FNN-based BPSK detectors. Figs. 7-9 show the scatter plots of  $\|\mathbf{y}_{K-1,n}^{(T)}\|$  versus  $n$  subject to All-SNR-T, High-SNR-T, and Low-SNR-T,

respectively, for  $(K, H) = (20, 100)$ . Figs. 7 and 9 precisely validate (47b) because the testing  $P_e$  is always 1 whenever  $\|\mathbf{y}_{K-1,n}^{(T)}\| = 0$  for all  $n$ . Some points in Fig. 8 verify (47b) since  $\|\mathbf{y}_{K-1,n}^{(T)}\|$  approaches zero for those points and  $P_e = 1.0$ .

At last, we move on to deeper and wider ReLU FNN-based BPSK detectors. Figs. 10-12 show the scatter plots of  $\|\mathbf{y}_{K-1,n}^{(T)}\|$  versus  $n$  subject to All-SNR-T, High-SNR-T, and Low-SNR-T, respectively, for  $(K, H) = (50, 50)$ . Figs. 10 and 12 perfectly validate (47b) because the testing  $P_e$  is always 1 whenever  $\|\mathbf{y}_{K-1,n}^{(T)}\| = 0$  for all  $n$ . Some points in Fig. 11 confirm (47a) since  $\|\mathbf{y}_{K-1,n}^{(T)}\|$  tends to infinity for those points and  $P_e = 0.5$ .

Therefore, we can conclude from the above results that ReLU FNN-based BPSK detectors validate our theory whenever the FNN gets deeper and wider.

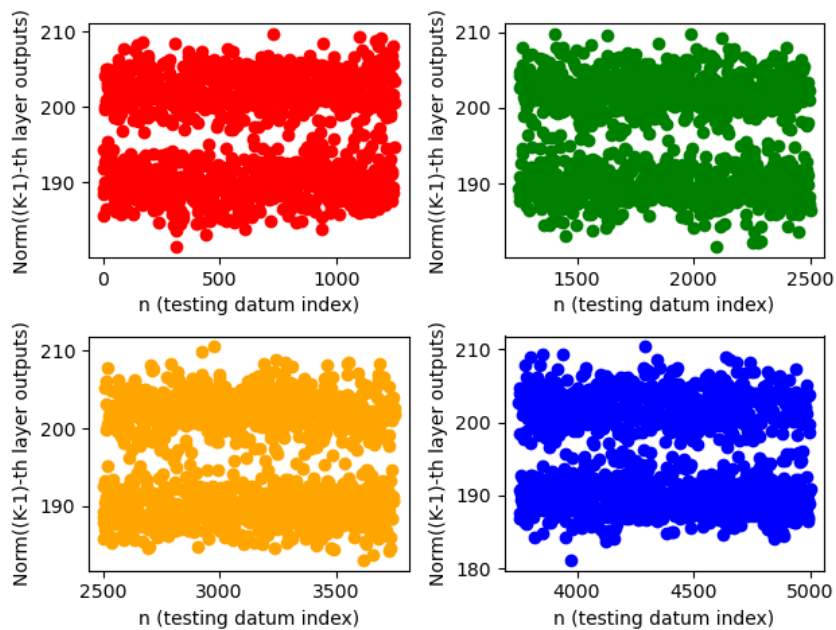


Fig. 1: A scatter plot of  $\|\mathbf{y}_{K-1,n}^{(T)}\|$  versus  $n$  under All-SNR-T,  $(K, H) = (8, 8)$ , and testing at 35 dB: the computed testing  $P_e$  at 35 dB is  $P_e = 0.50049999$ .

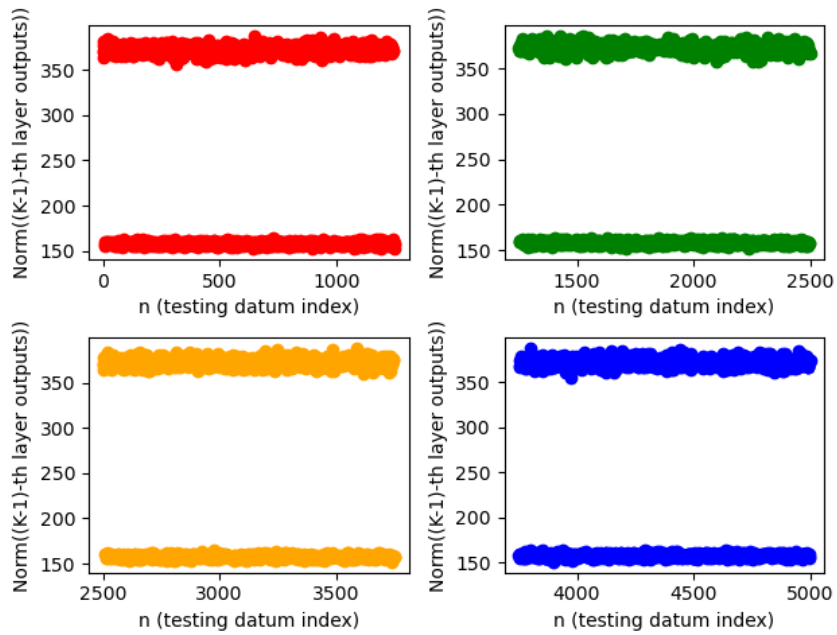


Fig. 2: A scatter plot of  $\|\mathbf{y}_{K-1,n}^{(T)}\|$  versus  $n$  under High-SNR-T,  $(K, H) = (8, 8)$ , and testing at 35 dB: the computed testing  $P_e$  at 35 dB is  $P_e = 0.50049999$ .

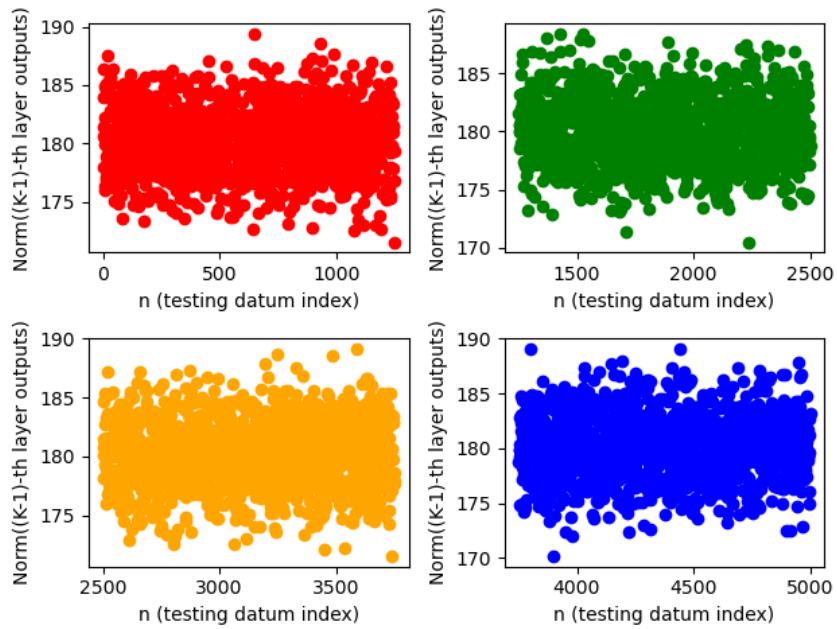


Fig. 3: A scatter plot of  $\|\mathbf{y}_{K-1,n}^{(T)}\|$  versus  $n$  under Low-SNR-T,  $(K, H) = (8, 8)$ , and testing at 35 dB: the computed testing  $P_e$  at 35 dB is  $P_e = 0.50049999$ .

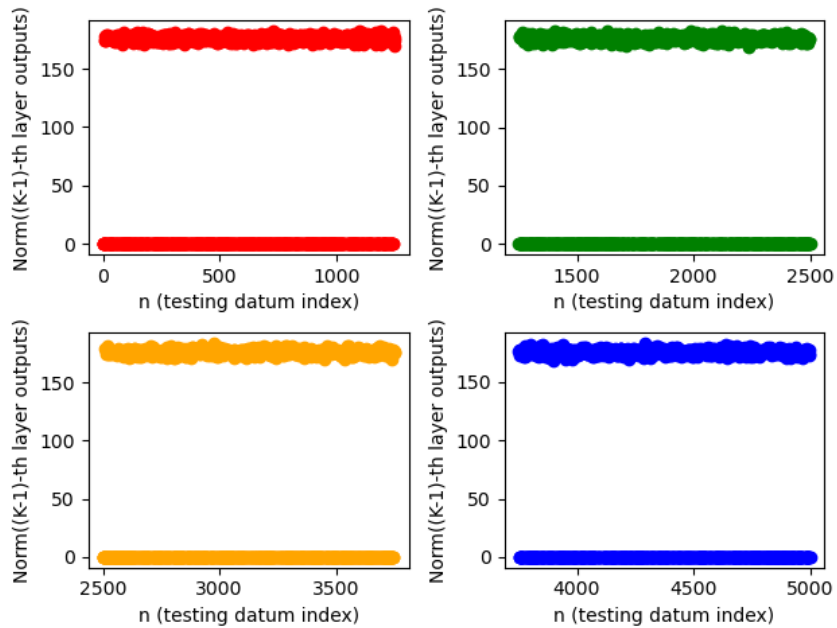


Fig. 4: A scatter plot of  $\|\mathbf{y}_{K-1,n}^{(T)}\|$  versus  $n$  under All-SNR-T,  $(K, H) = (16, 16)$ , and testing at 35 dB: the computed testing  $P_e$  at 35 dB is  $P_e = 1.0$ .

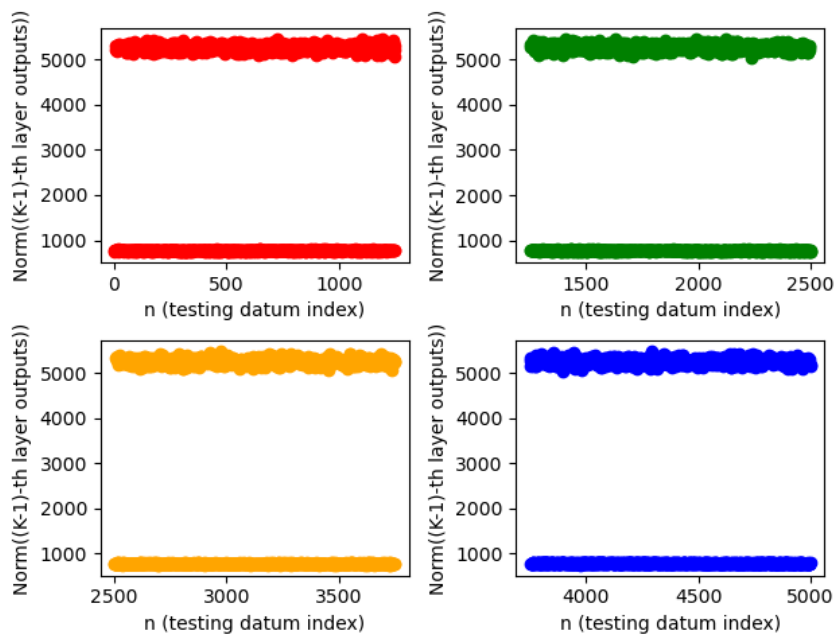


Fig. 5: A scatter plot of  $\|\mathbf{y}_{K-1,n}^{(T)}\|$  versus  $n$  under High-SNR-T,  $(K, H) = (16, 16)$ , and testing at 35 dB: the computed testing  $P_e$  at 35 dB is  $P_e = 0.50049999$ .

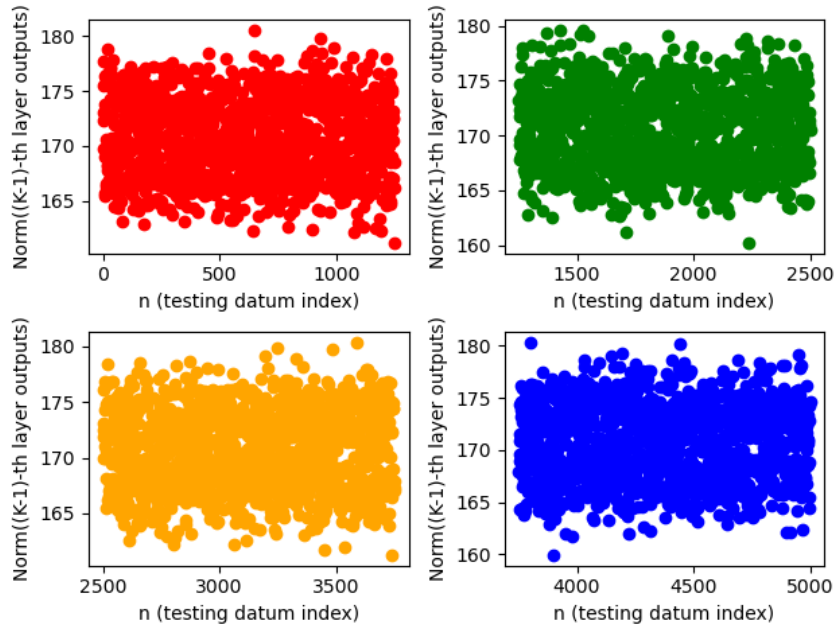


Fig. 6: A scatter plot of  $\|\mathbf{y}_{K-1,n}^{(T)}\|$  versus  $n$  under Low-SNR-T,  $(K, H) = (16, 16)$ , and testing at 35 dB: the computed testing  $P_e$  at 35 dB is  $P_e = 0.50049999$ .

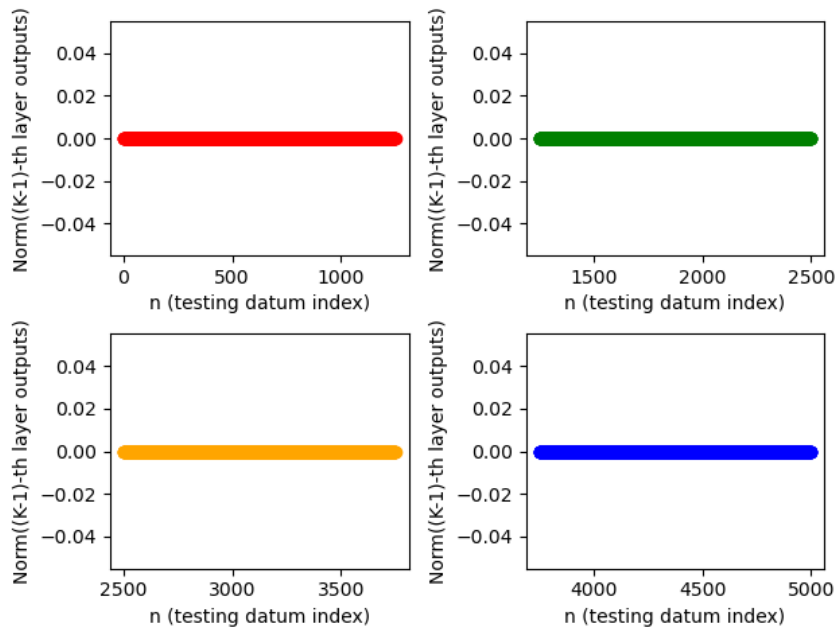


Fig. 7: A scatter plot of  $\|\mathbf{y}_{K-1,n}^{(T)}\|$  versus  $n$  under All-SNR-T,  $(K, H) = (20, 100)$ , and testing at 35 dB: the computed testing  $P_e$  at 35 dB is  $P_e = 1.0$ .

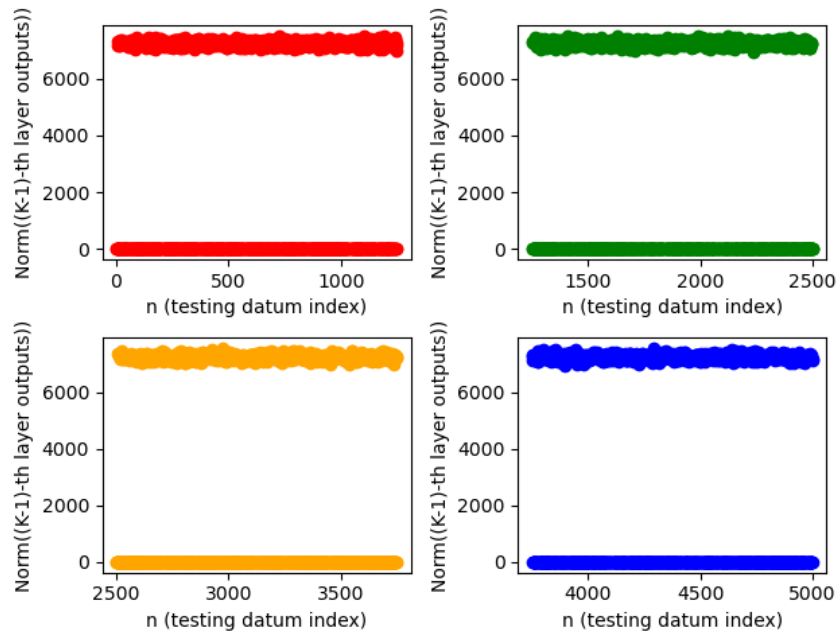


Fig. 8: A scatter plot of  $\|\mathbf{y}_{K-1,n}^{(T)}\|$  versus  $n$  under High-SNR-T,  $(K, H) = (20, 100)$ , and testing at 35 dB: the computed testing  $P_e$  at 35 dB is  $P_e = 1.0$ .

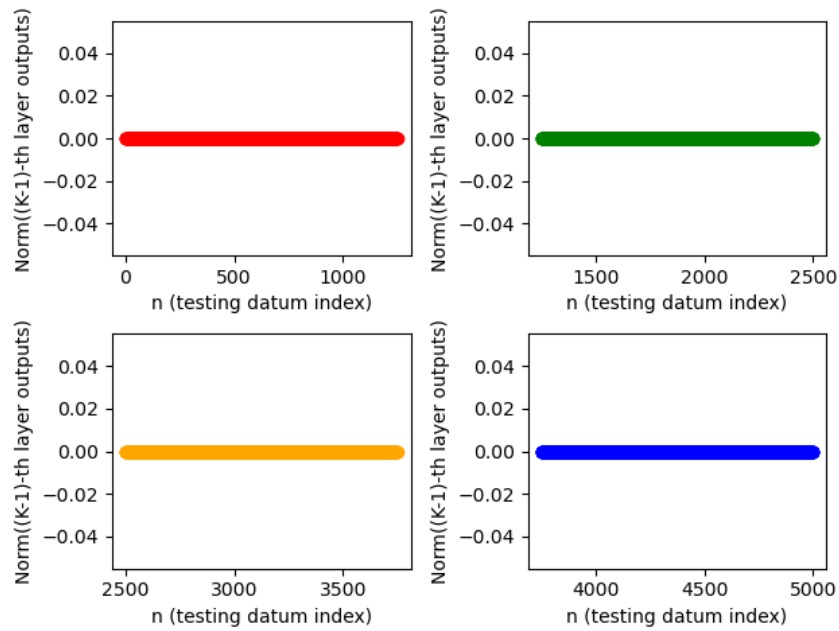


Fig. 9: A scatter plot of  $\|\mathbf{y}_{K-1,n}^{(T)}\|$  versus  $n$  under Low-SNR-T,  $(K, H) = (20, 100)$ , and testing at 35 dB: the computed testing  $P_e$  at 35 dB is  $P_e = 1.0$ .

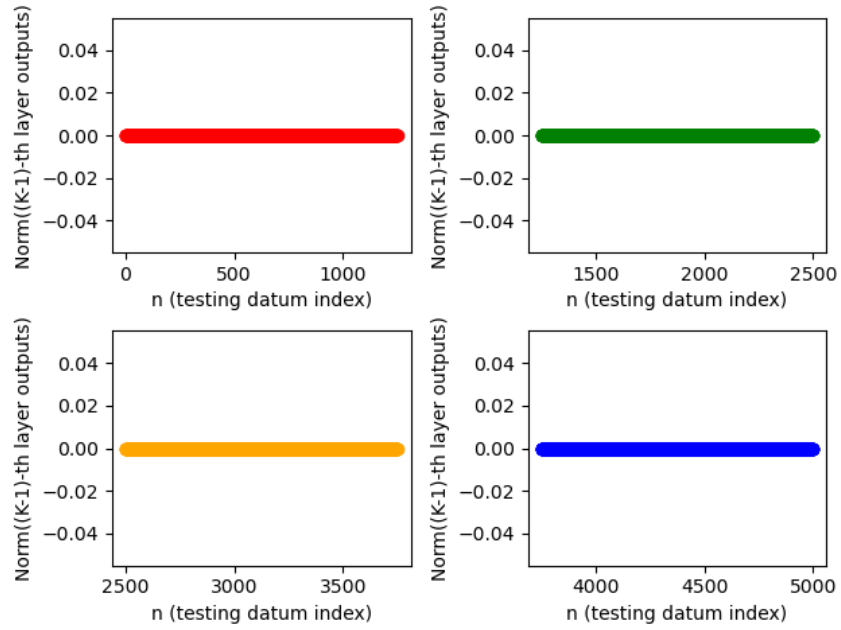


Fig. 10: A scatter plot of  $\|\mathbf{y}_{K-1,n}^{(T)}\|$  versus  $n$  under All-SNR-T,  $(K, H) = (50, 50)$ , and testing at 35 dB: the computed testing  $P_e$  at 35 dB is  $P_e = 1.0$ .

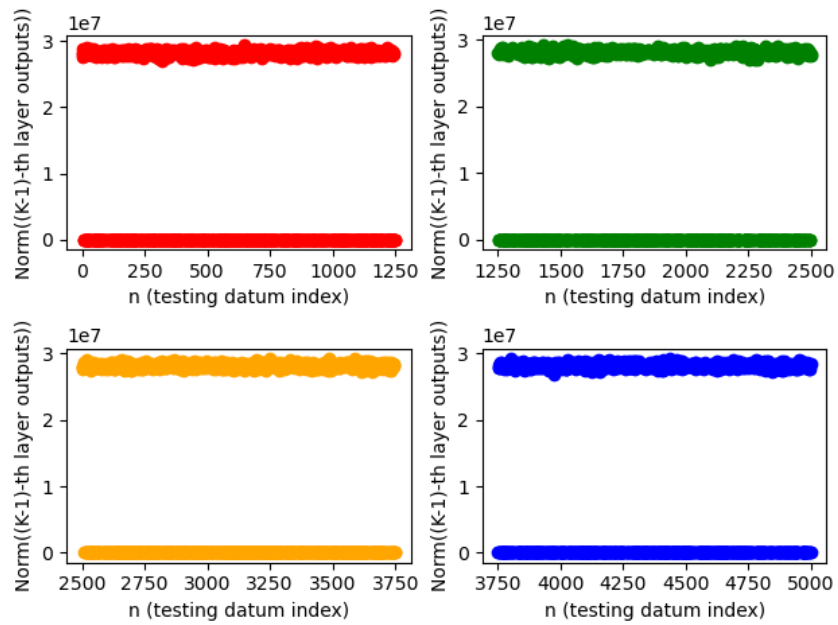


Fig. 11: A scatter plot of  $\|\mathbf{y}_{K-1,n}^{(T)}\|$  versus  $n$  under High-SNR-T,  $(K, H) = (50, 50)$ , and testing at 35 dB: the computed testing  $P_e$  at 35 dB is  $P_e = 0.50049999$ .

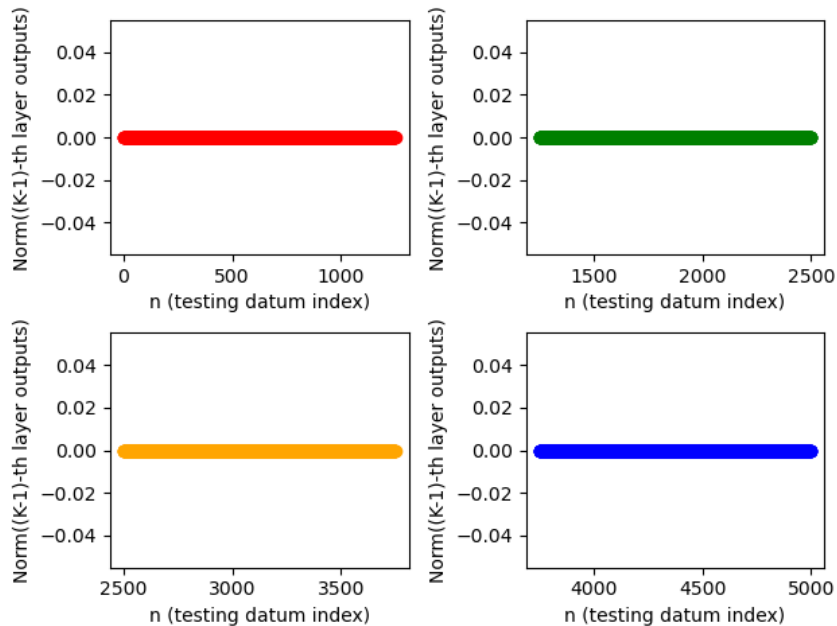


Fig. 12: A scatter plot of  $\|\mathbf{y}_{K-1,n}^{(T)}\|$  versus  $n$  under Low-SNR-T,  $(K, H) = (50, 50)$ , and testing at 35 dB: the computed testing  $P_e$  at 35 dB is  $P_e = 1.0$ .

#### D. Main Results for FNNs with ReLU and Tanh Activation

The testing and theory validation results for BPSK detectors that are based on FNNs with ReLU and Tanh activation were generated using the materials and methods detailed in Section VI-B and the (hyper)parameters set out in Table VII, and are presented in Sections VI-D1 and VI-D2, respectively.

1) *Testing Results for BPSK Detectors that are Based on FNNs with ReLU and Tanh Activation:* the numerical results for BPSK detectors that are based on trained FNNs with ReLU and Tanh activation are provided in Tables IV and V. As can be seen in those tables (like the ReLU FNN-based BPSK detectors from Section VI-C1), BPSK detectors that are based on FNNs with ReLU and Tanh activation and trained with hinge loss and Adam fail to learn optimum BPSK detection for any SNR. This result is affirmed by our developed theory, as highlighted below.

2) *Theory Validation Results for BPSK Detectors that are Based on FNNs with ReLU and Tanh Activation:* to confirm the validity of the theory we developed for binary classifiers that are based on FNNs with ReLU and Tanh activation, which is captured by Theorem 2, we generated many scatter plots of  $\|\check{\mathbf{y}}_{K-1,n}^{(T)}\|$  versus  $n$  subject to All-SNR-T, High-SNR-T, and Low-SNR-T for several pairs of  $(K, H)$ . The scatter plots for BPSK detectors that are based on shallow

SNR [in dB]	Optimal detector	FNN-based BPSK detector ( $K, H$ ) = (3, 3)			FNN-based BPSK detector ( $K, H$ ) = (3, 9)		
		All-SNR-T	High-SNR-T	Low-SNR-T	All-SNR-T	High-SNR-T	Low-SNR-T
$\gamma_b$ [dB]	$\mathcal{Q}(\sqrt{2\gamma_b})$						
0	0.0786	0.54196	0.60334	0.54232001	0.54198	0.57132	0.54192001
5	0.0060	0.50231999	0.51339999	0.50235999	0.50231999	0.50687999	0.50229999
10	$3.8721 \times 10^{-6}$	0.50075999	0.50075999	0.50075999	0.50075999	0.50075999	0.50075999
15	$9.1240 \times 10^{-16}$	0.50338	0.50338	0.50338	0.50338	0.50338	0.50338
20	$1.0442 \times 10^{-45}$	0.49835998	0.49835998	0.49835998	0.49835998	0.49835998	0.49835998
25	$7.3070 \times 10^{-140}$	0.49908	0.49908	0.49908	0.49908	0.49908	0.49908
30	0	0.49677998	0.49677998	0.49677998	0.49677998	0.49677998	0.49677998
35	0	0.50049999	0.50049999	0.50049999	0.50049999	0.50049999	0.50049999

TABLE IV: Numerical results I on the probability of bit error manifested by an optimal BPSK detector and BPSK detectors based on FNNs with ReLU and Tanh activation.

SNR [in dB]	Optimal detector	FNN-based BPSK detector ( $K, H$ ) = (4, 8)			FNN-based BPSK detector ( $K, H$ ) = (7, 7)		
		All-SNR-T	High-SNR-T	Low-SNR-T	All-SNR-T	High-SNR-T	Low-SNR-T
$\gamma_b$ [dB]	$\mathcal{Q}(\sqrt{2\gamma_b})$						
0	0.0786	0.54194	0.58012	0.54179999	0.54192001	0.60139999	0.54192001
5	0.0060	0.50229999	0.50854	0.50226	0.50229999	0.51298001	0.50229999
10	$3.8721 \times 10^{-6}$	0.50075999	0.50075999	0.50075999	0.50075999	0.50075999	0.50075999
15	$9.1240 \times 10^{-16}$	0.50338	0.50338	0.50338	0.50338	0.50338	0.50338
20	$1.0442 \times 10^{-45}$	0.49835998	0.49835998	0.49835998	0.49835998	0.49835998	0.49835998
25	$7.3070 \times 10^{-140}$	0.49908	0.49908	0.49908	0.49908	0.49908	0.49908
30	0	0.49677998	0.49677998	0.49677998	0.49677998	0.49677998	0.49677998
35	0	0.50049999	0.50049999	0.50049999	0.50049999	0.50049999	0.50049999

TABLE V: Numerical results II on the probability of bit error manifested by an optimal BPSK detector and BPSK detectors based on FNNs with ReLU and Tanh activation.

FNNs with ReLU and Tanh activation, deep and wider FNNs with ReLU and Tanh activation, and deeper and wider FNNs with ReLU and Tanh activation are shown in Figs. 13-21. When it comes to the BPSK detectors that are based on shallow FNNs with ReLU and Tanh activation, Figs. 13-15 show the scatter plots of  $\|\tilde{\mathbf{y}}_{K-1,n}^{(T)}\|$  versus  $n$  subject to All-SNR-T, High-SNR-T, and Low-SNR-T, respectively, for  $(K, H) = (8, 8)$ . Some points in Fig. 13 validate (48a) because  $\|\tilde{\mathbf{y}}_{K-1,n}^{(T)}\|$  tends to infinity for them and the testing  $\tilde{P}_e$  equals 0.5. Some points in Fig. 15 also

corroborate (48a) since  $\|\tilde{\mathbf{y}}_{K-1,n}^{(T)}\|$  also tends to infinity for them and the testing  $\check{P}_e$  equals 0.5 – similar to Fig. 14 though  $\|\tilde{\mathbf{y}}_{K-1,n}^{(T)}\|$  does not tend to be infinitely large when subject to High-SNR-T.

As for the BPSK detectors that are based on deep and wider FNNs with ReLU and Tanh activation, Figs. 16-18 show the scatter plots of  $\|\tilde{\mathbf{y}}_{K-1,n}^{(T)}\|$  versus  $n$  subject to All-SNR-T, High-SNR-T, and Low-SNR-T, respectively, for  $(K, H) = (20, 100)$ . Most points in Fig. 16 and all points in Fig. 18 validate (48a) because  $\|\tilde{\mathbf{y}}_{K-1,n}^{(T)}\| \rightarrow \infty$  whenever the testing  $\check{P}_e = 0.5$ . Some points in Fig. 17 validate (48b) since  $\|\tilde{\mathbf{y}}_{K-1,n}^{(T)}\| \rightarrow 0$  whenever the testing  $\check{P}_e = 1$ .

At last, we move on to BPSK detectors that are based on deeper and wider FNNs with ReLU and Tanh activation. Figs. 19-21 show the scatter plots of  $\|\tilde{\mathbf{y}}_{K-1,n}^{(T)}\|$  versus  $n$  subject to All-SNR-T, High-SNR-T, and Low-SNR-T, respectively, for  $(K, H) = (50, 50)$ . These scatter plots fail to validate (48a)-(48b) and hence Theorem 2. Consequently, Theorem 2 fails to interpret the behavior of BPSK detectors that are based on deeper and wider FNNs with ReLU and Tanh activation. This result showcases one of the limitations of our theory.

Therefore, we can conclude from the above results that BPSK detectors that are based on FNNs with ReLU and Tanh activation validate our theory whenever the FNN gets deeper and wider.

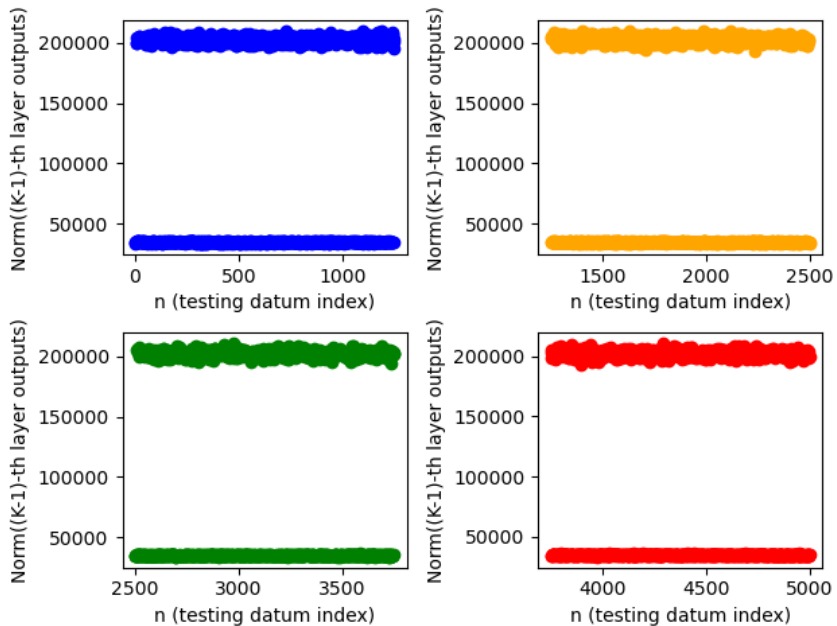


Fig. 13: A scatter plot of  $\|\tilde{\mathbf{y}}_{K-1,n}^{(T)}\|$  versus  $n$  under All-SNR-T,  $(K, H) = (8, 8)$ , and testing at 35 dB: the computed testing  $\check{P}_e$  at 35 dB is  $\check{P}_e = 0.50049999$ .

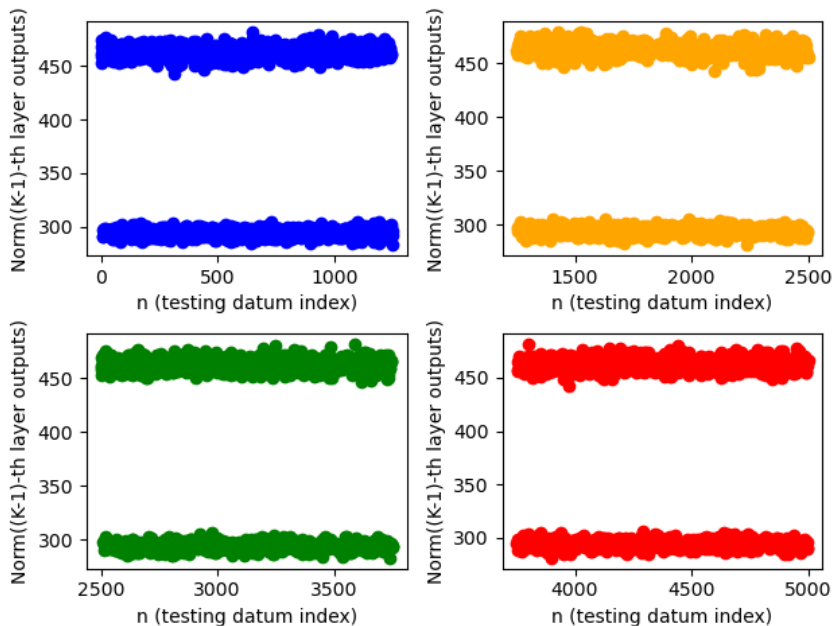


Fig. 14: A scatter plot of  $\|\tilde{\mathbf{y}}_{K-1,n}^{(T)}\|$  versus  $n$  under High-SNR-T,  $(K, H) = (8, 8)$ , and testing at 35 dB: the computed testing  $\check{P}_e$  at 35 dB is  $\check{P}_e = 0.50049999$ .

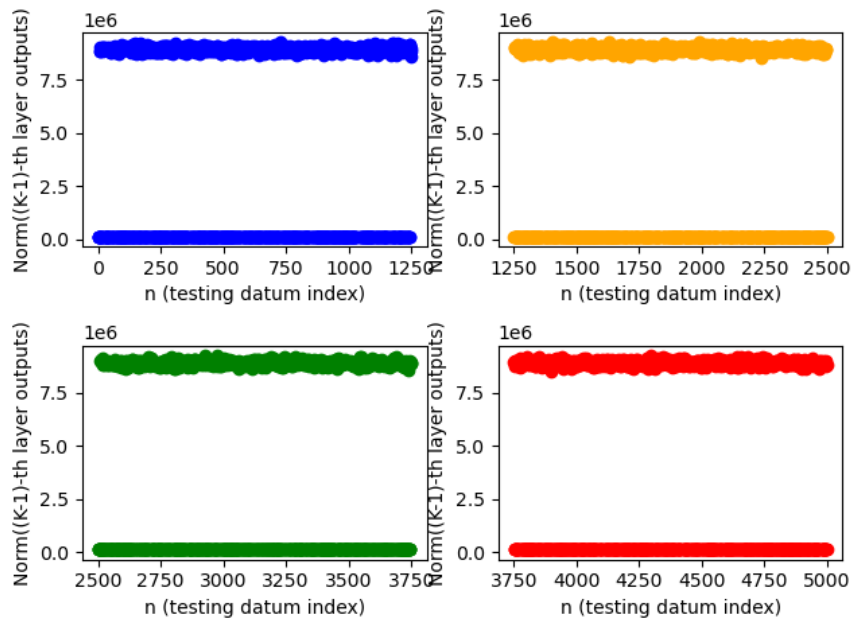


Fig. 15: A scatter plot of  $\|\check{\mathbf{y}}_{K-1,n}^{(T)}\|$  versus  $n$  under Low-SNR-T,  $(K, H) = (8, 8)$ , and testing at 35 dB: the computed testing  $\check{P}_e$  at 35 dB is  $\check{P}_e = 0.50049999$ .

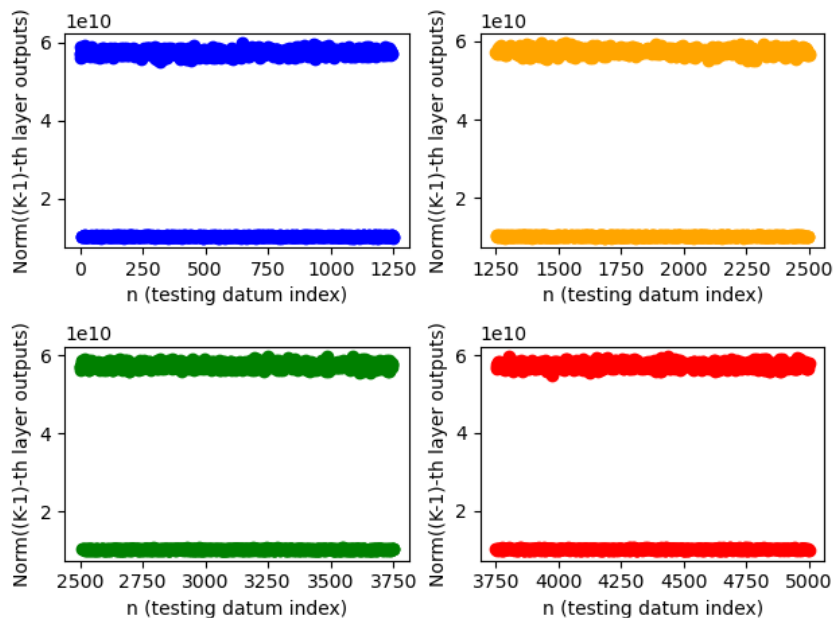


Fig. 16: A scatter plot of  $\|\check{\mathbf{y}}_{K-1,n}^{(T)}\|$  versus  $n$  under All-SNR-T,  $(K, H) = (20, 100)$ , and testing at 35 dB: the computed testing  $\check{P}_e$  at 35 dB is  $\check{P}_e = 0.50049999$ .

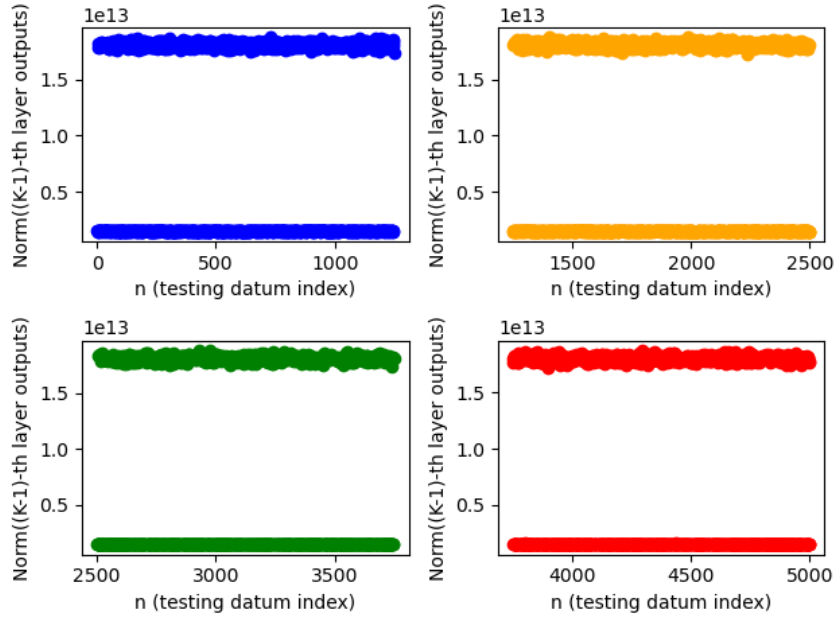


Fig. 17: A scatter plot of  $\|\tilde{\mathbf{y}}_{K-1,n}^{(T)}\|$  versus  $n$  under High-SNR-T,  $(K, H) = (20, 100)$ , and testing at 35 dB: the computed testing  $\check{P}_e$  at 35 dB is  $\check{P}_e = 1.0$ .

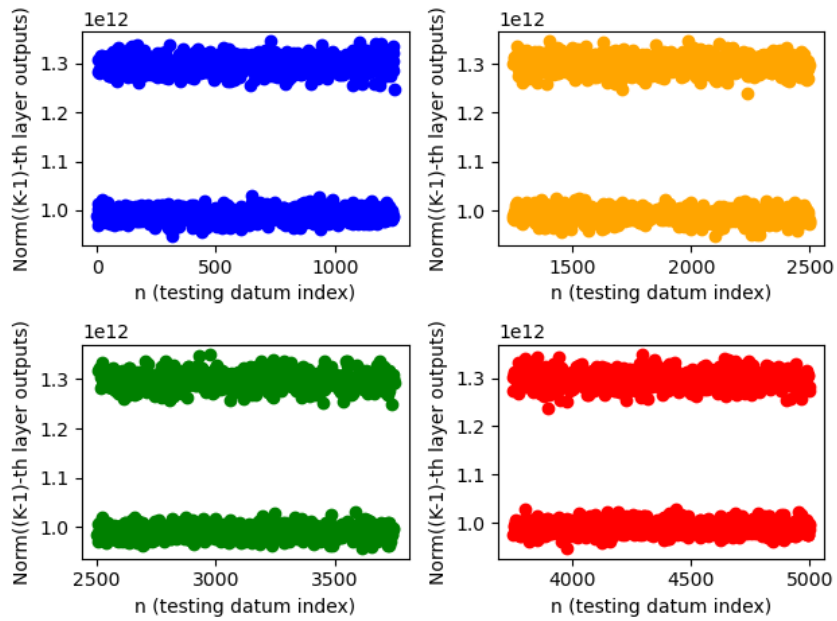


Fig. 18: A scatter plot of  $\|\tilde{\mathbf{y}}_{K-1,n}^{(T)}\|$  versus  $n$  under Low-SNR-T,  $(K, H) = (20, 100)$ , and testing at 35 dB: the computed testing  $\check{P}_e$  at 35 dB is  $\check{P}_e = 0.50049999$ .

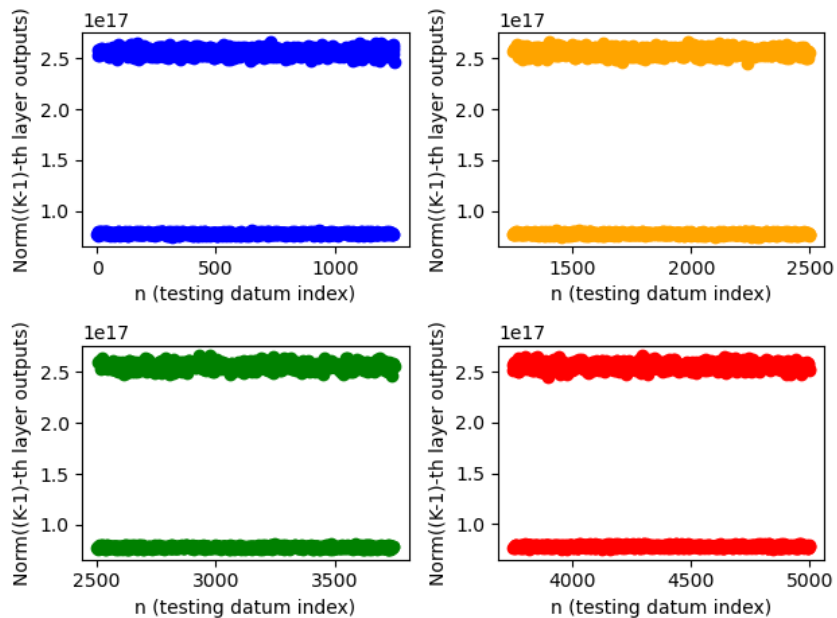


Fig. 19: A scatter plot of  $\|\tilde{\mathbf{y}}_{K-1,n}^{(T)}\|$  versus  $n$  under All-SNR-T,  $(K, H) = (50, 50)$ , and testing at 35 dB: the computed testing  $\check{P}_e$  at 35 dB is  $\check{P}_e = 1.0$ .

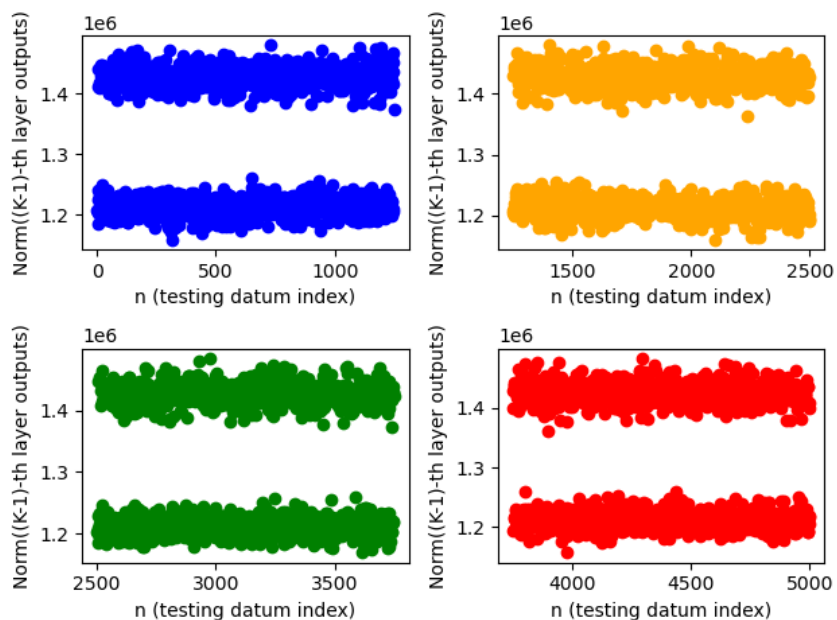


Fig. 20: A scatter plot of  $\|\tilde{\mathbf{y}}_{K-1,n}^{(T)}\|$  versus  $n$  under High-SNR-T,  $(K, H) = (50, 50)$ , and testing at 35 dB: the computed testing  $\check{P}_e$  at 35 dB is  $\check{P}_e = 1.0$ .

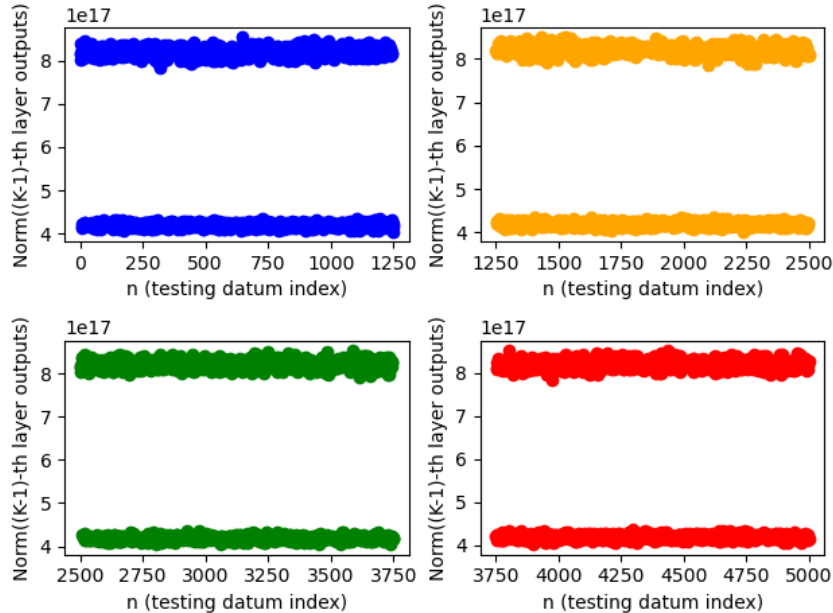


Fig. 21: A scatter plot of  $\|\tilde{\mathbf{y}}_{K-1,n}^{(T)}\|$  versus  $n$  under Low-SNR-T,  $(K, H) = (50, 50)$ , and testing at 35 dB: the computed testing  $\check{P}_e$  at 35 dB is  $\check{P}_e = 1.0$ .

We now move on to our concluding remarks and this work’s research outlook.

## VII. CONCLUDING REMARKS AND RESEARCH OUTLOOK

DL has led to several breakthroughs in many disciplines as diverse as chemistry, computer science, electrical engineering, mathematics, medicine, neuroscience, and physics. Despite it having such broad impacts and successes, a comprehensive understanding of why and how DL is empirically successful in astronomically many AI/ML problems remains fundamentally elusive. To this end, a formidable challenge is devising an interpretable DL-based AI/ML algorithm that is backed by a theory about the fundamental interpretability of deep networks. However, no fundamental work has managed yet to quantify the testing performance limits of DL-based classifiers that are trained with cross-entropy loss or hinge loss. To overcome this limitation and contribute to the fundamental interpretability of deep FNNs trained using hinge loss, we developed a theory – using the tools of probability theory and high-dimensional statistics – for the asymptotic testing performance limits of deep ReLU FNNs and deep FNNs with ReLU and Tanh activation. Our theory is intuitive and successfully interprets some of the results of our extensive

computer experiments. Accordingly, our theory can be used to interpret binary classifiers that are based on deep FNNs trained with hinge loss regardless of the problem domain.

As for this work's research outlook, what will be quite relevant is a fundamental theory on the non-asymptotic performance limits of binary classifiers that are based on deep FNNs. In this vein, the following fundamental research directions are worth pursuing:

- The non-asymptotic testing performance limits of binary classifiers that are based on deep ReLU FNNs.
- The non-asymptotic testing performance limits of binary classifiers that are based on FNNs with ReLU and Tanh activation.

Looking ahead from our theory research, a hugely challenging and very useful fundamental problem that is worth attacking is determining the fundamental testing performance limits of *DL-based multi-level classifiers trained using cross-entropy loss*, which undoubtedly entails more complex decision regions/boundaries.

## APPENDIX A

## BACK-PROPAGATION W.R.T. HINGE LOSS AND SGD FOR FNNs WITH DUAL ACTIVATION FUNCTIONS

The overarching goal of neural network training is to find the (possibly optimal) weights that minimize empirical loss over the training set such that a trained neural network will be able to generalize better when tested with a never-before-seen testing set. In the context of our detection problem, our training process should aim to find the (nearly) optimal weight matrices and vectors that minimize training loss. In such an iterative minimization process, the way to begin updating each network weight is to posit that all neurons contribute to the overall loss. The training loss can then be minimized as a *credit assignment problem* by penalizing or rewarding hidden neurons [111]. In the context of a credit-assignment problem, the back-propagation algorithm was discovered – by the authors of [89] – to operate by back-propagating the local gradients<sup>8</sup> that are deployed to estimate the error contribution of each neuron.

Inspired by the back-propagation algorithm [111, Ch. 4] w.r.t. square loss and online gradient descent, we derive – using matrix calculus [118], [119] – the update rules for back-propagation w.r.t. hinge loss and SGD for FNNs with dual activation functions.

**Theorem 3 (Back-propagation w.r.t. hinge loss and SGD for FNNs with dual activation functions).** *Let  $t \in \mathbb{N}_0$ ,  $i \in \mathbb{N}_{\geq 1}$ , and  $K \in \mathbb{N}_{\geq 2}$ . Let  $B \in \mathbb{N}_{\geq 1}$  and  $N_k, N_{k-1} \in \mathbb{N}_{\geq 1}$  for  $k \in [K]$ . Assume a deep FNN has been trained over  $\mathcal{D} := \{(x_n, y_n)\}_{n=1}^N$ , with  $x_n$  being the  $n$ -th input generated per (27) and  $y_n \in \{-1, 1\}$  being the  $n$ -th label. Consider a deep FNN with dual activation functions (per Definition 12) that has been trained using hinge loss (per Definition 11) and SGD (per Definition 13) as an optimizer. Let  $f_{K,i}^{(t)} := y_i y_{K,i}^{(t)} = y_i \phi(\mathbf{w}_K^{(t)} \mathbf{y}_{K-1,i}^{(t)}) \in \mathbb{R}$  for  $y_{K,i}^{(t)}$  defined in (22c). Then, the underneath weight update rule follows:*

$$(\mathbf{W}_k^{(t+1)})_{p,q} = (\mathbf{W}_k^{(t)})_{p,q} + (\Delta \mathbf{W}_k^{(t)})_{p,q}, \quad (50)$$

where  $p \in [N_k]$ ,  $q \in [N_{k-1}]$ ,  $k \in [K]$ ,  $\mathbf{W}_K^{(t)} := \mathbf{w}_K^{(t)}$ , and

$$(\Delta \mathbf{W}_k^{(t)})_{p,q} = \frac{\eta t}{B} \sum_{i \in \mathcal{B}^{(t)}} (\boldsymbol{\delta}_{k,i}^{(t)})_p (\mathbf{y}_{k-1,i}^{(t)})_q \mathbb{I}\{1 - f_{K,i}^{(t)} > 0\}, \quad (51)$$

<sup>8</sup>Local gradients are often defined as the partial derivative of the error function (empirical loss function) w.r.t. the pre-activation input of each neuron in a neural network [111].

where  $(\delta_{k,i}^{(t)})_p$  is the local gradient of the  $p$ -th neuron in the  $k$ -th ReLU FNN layer given by

$$(\delta_{k,i}^{(t)})_p = \begin{cases} \delta_{K,i}^{(t)} = y_i \phi'(\mathbf{w}_K^{(t)} \mathbf{y}_{K-1,i}^{(t)}) & : k = K \\ \varphi'((\mathbf{v}_{k,i}^{(t)})_p) \sum_{q=1}^{N_{k+1}} (\delta_{k+1,i}^{(t)})_q (\mathbf{W}_{k+1}^{(t)})_{q,p} & : k \neq K. \end{cases} \quad (52)$$

*Proof.* We derive the back-propagation update rules pertaining to all layers of FNNs with dual activation functions (per Definition 12) using the component-wise activation functions  $\varphi(\cdot)$  and  $\phi(\cdot)$ . To this end, employing the  $K$ -th neuron's output given by (22c) in (23) gives

$$\mathbf{w}_K^{(t+1)} = \mathbf{w}_K^{(t)} - \frac{\eta_t}{B} \sum_{i \in \mathcal{B}^{(t)}} \frac{\partial \ell(y_i, \phi(\mathbf{w}_K^{(t)} \mathbf{y}_{K-1,i}^{(t)}))}{\partial \mathbf{w}_K^{(t)}}. \quad (53)$$

Deploying (21) in (53) leads to

$$\mathbf{w}_K^{(t+1)} = \mathbf{w}_K^{(t)} - \frac{\eta_t}{B} \sum_{i \in \mathcal{B}^{(t)}} \frac{\partial \max(0, 1 - f_{K,i}^{(t)})}{\partial \mathbf{w}_K^{(t)}}, \quad (54)$$

where

$$f_{K,i}^{(t)} = y_i \phi(\mathbf{w}_K^{(t)} \mathbf{y}_{K-1,i}^{(t)}). \quad (55)$$

While adopting the *denominator layout notation*<sup>9</sup> from matrix calculus [118] (see also [119]), applying the chain rule to the RHS of (54) produces

$$\frac{\partial \ell(y_i, \mathbf{w}_K^{(t)} \mathbf{y}_{K-1,i}^{(t)})}{\partial \mathbf{w}_K^{(t)}} = \begin{cases} -(y_i \mathbf{y}_{K-1,i}^{(t)})^\top \phi'(\mathbf{w}_K^{(t)} \mathbf{y}_{K-1,i}^{(t)}) & \text{if } f_{K,i}^{(t)} < 1 \\ 0 & \text{if } f_{K,i}^{(t)} \geq 1. \end{cases} \quad (56)$$

Using an indicator function makes it possible to write (56) compactly as

$$\frac{\partial \ell(y_i, \mathbf{w}_K^{(t)} \mathbf{y}_{K-1,i}^{(t)})}{\partial \mathbf{w}_K^{(t)}} = -(y_i \mathbf{y}_{K-1,i}^{(t)})^\top \phi'(\mathbf{w}_K^{(t)} \mathbf{y}_{K-1,i}^{(t)}) \mathbb{I}\{1 - f_{K,i}^{(t)} > 0\}. \quad (57)$$

By substituting (57) into (53), we obtain the  $K$ -th FNN layer's weight update rule, which is given by

$$\mathbf{w}_K^{(t+1)} = \mathbf{w}_K^{(t)} + \frac{\eta_t}{B} \sum_{i \in \mathcal{B}^{(t)}} (y_i \mathbf{y}_{K-1,i}^{(t)})^\top \phi'(\mathbf{w}_K^{(t)} \mathbf{y}_{K-1,i}^{(t)}) \mathbb{I}\{1 - f_{K,i}^{(t)} > 0\}. \quad (58)$$

Eq. (58) can also be written in scalar form for all  $p \in [N_{K-1}]$  as

$$(\mathbf{w}_K^{(t+1)})_p = (\mathbf{w}_K^{(t)})_p + \frac{\eta_t}{B} \sum_{i \in \mathcal{B}^{(t)}} y_i (\mathbf{y}_{K-1,i}^{(t)})_p \phi'(\mathbf{w}_K^{(t)} \mathbf{y}_{K-1,i}^{(t)}) \mathbb{I}\{1 - f_{K,i}^{(t)} > 0\}, \quad (59)$$

<sup>9</sup>The denominator layout notation: for  $\mathbf{y} = [y_1, y_2, \dots, y_m]^\top$  and  $\mathbf{x} = [x_1, x_2, \dots, x_n]^\top$ ,  $\frac{\partial \mathbf{y}}{\partial \mathbf{x}}$  is laid out as an  $n \times m$  matrix according to  $\mathbf{y}^\top$  and  $\mathbf{x}$  [118]. Similarly, for  $\mathbf{X} \in \mathbb{R}^{p \times q}$ ,  $\frac{\partial \mathbf{y}}{\partial \mathbf{X}}$  is laid out as a  $p \times q$  matrix whose  $(i, j)$ -th element is equal to  $\frac{\partial y_i}{\partial (\mathbf{X})_{i,j}}$  [118].

where  $t = 0, 1, \dots, T - 1$ .

In what follows, we derive the error back-propagation rule that is valid for the neurons in the  $k$ -th and  $(k - 1)$ -th layers for  $k \in \{2, \dots, K - 1\}$ . To begin, we rewrite (22b) as

$$\mathbf{y}_{k,n}^{(t)} = \varphi(\mathbf{W}_k^{(t)} \mathbf{y}_{k-1,n}^{(t)}) = \varphi(\mathbf{v}_{k,n}^{(t)}), \quad (60)$$

where  $k \in \{2, \dots, K - 1\}$  and

$$\mathbf{v}_{k,n}^{(t)} = \mathbf{W}_k^{(t)} \mathbf{y}_{k-1,n}^{(t)}. \quad (61)$$

Using (23) to update the weights of the  $k$ -th layer leads to

$$\mathbf{W}_k^{(t+1)} = \mathbf{W}_k^{(t)} - \frac{\eta_t}{B} \sum_{i \in \mathcal{B}^{(t)}} \frac{\partial \ell(y_i, \phi(\mathbf{w}_K^{(t)} \mathbf{y}_{K-1,i}^{(t)}))}{\partial \mathbf{W}_k^{(t)}} \quad (62a)$$

$$= \mathbf{W}_k^{(t)} - \frac{\eta_t}{B} \sum_{i \in \mathcal{B}^{(t)}} \frac{\partial \max(0, 1 - f_{K,i}^{(t)})}{\partial \mathbf{W}_k^{(t)}}, \quad (62b)$$

where it follows from (55) that

$$f_{K,i}^{(t)} = y_i y_{K,i}^{(t)} = y_i \phi(\mathbf{w}_K^{(t)} \mathbf{y}_{K-1,i}^{(t)}) \stackrel{(a)}{=} y_i \phi(\mathbf{w}_K^{(t)} \varphi(\mathbf{v}_{K-1,i}^{(t)})), \quad (63)$$

where (a) follows from (60). It follows from the RHS of (62b) that

$$\frac{\partial \max(0, 1 - f_{K,i}^{(t)})}{\partial \mathbf{W}_k^{(t)}} = -\mathbb{I}\{1 - f_{K,i}^{(t)} > 0\} \frac{\partial f_{K,i}^{(t)}}{\partial \mathbf{W}_k^{(t)}}. \quad (64)$$

According to the denominator layout notation [118],

$$\frac{\partial f_{K,i}^{(t)}}{\partial \mathbf{W}_k^{(t)}} = \begin{bmatrix} \frac{\partial f_{K,i}^{(t)}}{\partial (\mathbf{W}_k^{(t)})_{1,1}} & \dots & \frac{\partial f_{K,i}^{(t)}}{\partial (\mathbf{W}_k^{(t)})_{1,N_{k-1}}} \\ \frac{\partial f_{K,i}^{(t)}}{\partial (\mathbf{W}_k^{(t)})_{2,1}} & \dots & \frac{\partial f_{K,i}^{(t)}}{\partial (\mathbf{W}_k^{(t)})_{2,N_{k-1}}} \\ \vdots & \ddots & \vdots \\ \frac{\partial f_{K,i}^{(t)}}{\partial (\mathbf{W}_k^{(t)})_{N_k,1}} & \dots & \frac{\partial f_{K,i}^{(t)}}{\partial (\mathbf{W}_k^{(t)})_{N_k,N_{k-1}}} \end{bmatrix}. \quad (65)$$

To compute the elements of the matrix in the RHS of (65), we simplify  $\frac{\partial f_{K,i}^{(t)}}{\partial (\mathbf{W}_k^{(t)})_{p,q}}$  for  $p \in [N_k]$  and  $q \in [N_{k-1}]$ . To this end, applying the chain rule leads to

$$\frac{\partial f_{K,i}^{(t)}}{\partial (\mathbf{W}_k^{(t)})_{p,q}} = \frac{\partial f_{K,i}^{(t)}}{\partial (\mathbf{y}_{k,i}^{(t)})^\top} \frac{\partial (\mathbf{y}_{k,i}^{(t)})^\top}{\partial (\mathbf{v}_{k,i}^{(t)})^\top} \frac{\partial (\mathbf{v}_{k,i}^{(t)})^\top}{\partial (\mathbf{W}_k^{(t)})_{p,q}}. \quad (66)$$

To compute the reward or penalty pertaining to all neurons in the  $k$ -th layer, we define  $\delta_{k,i}^{(t)}$  as the local gradient vector of the  $k$ -th layer w.r.t. the  $i$ -th input of the  $t$ -th iteration and

$$\delta_{k,i}^{(t)} = \begin{cases} \delta_{k,i}^{(t)} = \frac{\partial f_{K,i}^{(t)}}{\partial (\mathbf{y}_{k,i}^{(t)})^\top} \frac{\partial (\mathbf{y}_{k,i}^{(t)})^\top}{\partial (\mathbf{v}_{k,i}^{(t)})^\top} & : k \in [K - 1] \\ \delta_{K,i}^{(t)} = \frac{\partial f_{K,i}^{(t)}}{\partial y_{K,i}^{(t)}} \frac{\partial y_{K,i}^{(t)}}{\partial v_{K,i}^{(t)}} & : k = K. \end{cases} \quad (67)$$

Applying the definition in (67) to (66) leads to

$$\frac{\partial f_{K,i}^{(t)}}{\partial (\mathbf{W}_k^{(t)})_{p,q}} = \boldsymbol{\delta}_{k,i}^{(t)} \frac{\partial (\mathbf{v}_{k,i}^{(t)})^\top}{\partial (\mathbf{W}_k^{(t)})_{p,q}}. \quad (68)$$

Following (67), we define the local gradient corresponding to the  $p$ -th neuron of the  $k$ -th FNN layer w.r.t. the  $i$ -th input of the  $t$ -th iteration as

$$(\boldsymbol{\delta}_{k,i}^{(t)})_p = \begin{cases} (\boldsymbol{\delta}_{k,i}^{(t)})_p = \frac{\partial f_{K,i}^{(t)}}{\partial (\mathbf{y}_{k,i}^{(t)})^\top} \frac{\partial (\mathbf{y}_{k,i}^{(t)})^\top}{\partial (\mathbf{v}_{k,i}^{(t)})_p} & : k \in [K-1] \\ \delta_{K,i}^{(t)} = \frac{\partial f_{K,i}^{(t)}}{\partial y_{K,i}^{(t)}} \frac{\partial y_{K,i}^{(t)}}{\partial v_{K,i}^{(t)}} & : k = K, \end{cases} \quad (69)$$

where  $p \in [N_k]$  and

$$v_{K,i}^{(t)} = \mathbf{w}_K^{(t)} \mathbf{y}_{K-1,i}^{(t)} \quad (70a)$$

$$y_{K,i}^{(t)} = \phi(v_{K,i}^{(t)}) = \phi(\mathbf{w}_K^{(t)} \mathbf{y}_{K-1,i}^{(t)}). \quad (70b)$$

Eq. (69) makes it possible to re-cast (68) as

$$\frac{\partial f_{K,i}^{(t)}}{\partial (\mathbf{W}_k^{(t)})_{p,q}} = [(\boldsymbol{\delta}_{k,i}^{(t)})_1 \cdots (\boldsymbol{\delta}_{k,i}^{(t)})_{N_k}] \frac{\partial (\mathbf{v}_{k,i}^{(t)})^\top}{\partial (\mathbf{W}_k^{(t)})_{p,q}}. \quad (71)$$

To simplify the RHS of (71), we recursively derive  $(\boldsymbol{\delta}_{k,i}^{(t)})_p$  for  $k = K, K-1, K-2, \dots, k$  and  $p \in [N_k]$ . To begin, it follows from (69) w.r.t.  $k = K$  that

$$\delta_{K,i}^{(t)} = \frac{\partial f_{K,i}^{(t)}}{\partial y_{K,i}^{(t)}} \frac{\partial y_{K,i}^{(t)}}{\partial v_{K,i}^{(t)}} \stackrel{(a)}{=} \frac{\partial f_{K,i}^{(t)}}{\partial y_{K,i}^{(t)}} \phi'(\mathbf{w}_K^{(t)} \mathbf{y}_{K-1,i}^{(t)}) \stackrel{(b)}{=} y_i \phi'(\mathbf{w}_K^{(t)} \mathbf{y}_{K-1,i}^{(t)}), \quad (72)$$

where (a) is due to (70a) and (70b) that  $\frac{\partial y_{K,i}^{(t)}}{\partial v_{K,i}^{(t)}} = \phi'(\mathbf{w}_K^{(t)} \mathbf{y}_{K-1,i}^{(t)})$  and (b) is due to (63). In the meantime, substituting (72) into (59) gives the update rule

$$(\mathbf{w}_K^{(t+1)})_p = (\mathbf{w}_K^{(t)})_p + \frac{\eta t}{B} \sum_{i \in \mathcal{B}^{(t)}} \delta_{K,i}^{(t)} (\mathbf{y}_{K-1,i}^{(t)})_p \mathbb{I}\{1 - f_{K,i}^{(t)} > 0\}. \quad (73)$$

We continue by employing (69) for  $k = K-1$  as follows:

$$(\boldsymbol{\delta}_{K-1,i}^{(t)})_p = \frac{\partial f_{K,i}^{(t)}}{\partial (\mathbf{y}_{K-1,i}^{(t)})^\top} \frac{\partial (\mathbf{y}_{K-1,i}^{(t)})^\top}{\partial (\mathbf{v}_{K-1,i}^{(t)})_p}, \quad (74)$$

where  $p \in [N_{K-1}]$ . Following the denominator layout notation,

$$\frac{\partial f_{K,i}^{(t)}}{\partial (\mathbf{y}_{k,i}^{(t)})^\top} = \left[ \frac{\partial f_{K,i}^{(t)}}{\partial (\mathbf{y}_{k,i}^{(t)})_1} \quad \frac{\partial f_{K,i}^{(t)}}{\partial (\mathbf{y}_{k,i}^{(t)})_2} \quad \cdots \quad \frac{\partial f_{K,i}^{(t)}}{\partial (\mathbf{y}_{k,i}^{(t)})_{N_k}} \right], \quad (75)$$

where  $k \in [K - 1]$ . Thus, it follows from (75) w.r.t.  $k = K - 1$  that

$$\frac{\partial f_{K,i}^{(t)}}{\partial(\mathbf{y}_{K-1,i}^{(t)})^\top} = \left[ \frac{\partial f_{K,i}^{(t)}}{\partial(\mathbf{y}_{K-1,i}^{(t)})_1} \quad \cdots \quad \frac{\partial f_{K,i}^{(t)}}{\partial(\mathbf{y}_{K-1,i}^{(t)})_{N_{k-1}}} \right] \quad (76a)$$

$$\stackrel{(a)}{=} \left[ y_i \phi'(\mathbf{w}_K^{(t)} \mathbf{y}_{K-1,i}^{(t)}) (\mathbf{w}_K^{(t)})_1 \quad \cdots \quad y_i \phi'(\mathbf{w}_K^{(t)} \mathbf{y}_{K-1,i}^{(t)}) (\mathbf{w}_K^{(t)})_{N_{k-1}} \right] \quad (76b)$$

$$\stackrel{(b)}{=} \left[ \delta_{K,i}^{(t)} (\mathbf{w}_K^{(t)})_1 \quad \cdots \quad \delta_{K,i}^{(t)} (\mathbf{w}_K^{(t)})_{N_{k-1}} \right], \quad (76c)$$

where (a) follows from (63) and (b) is due to (72). Adopting the denominator layout notation leads to

$$\frac{\partial(\mathbf{y}_{k,i}^{(t)})^\top}{\partial(\mathbf{v}_{k,i}^{(t)})_p} = \left[ \frac{\partial(\mathbf{y}_{k,i}^{(t)})_1}{\partial(\mathbf{v}_{k,i}^{(t)})_p} \quad \cdots \quad \frac{\partial(\mathbf{y}_{k,i}^{(t)})_{N_k}}{\partial(\mathbf{v}_{k,i}^{(t)})_p} \right]^\top, \quad (77)$$

where  $k \in [K - 1]$ . Hence, deploying (77) w.r.t.  $k = K - 1$  and exploiting (60) gives

$$\frac{\partial(\mathbf{y}_{K-1,i}^{(t)})^\top}{\partial(\mathbf{v}_{K-1,i}^{(t)})_p} = \left[ 0 \quad \cdots \quad \varphi'((\mathbf{v}_{K-1,i}^{(t)})_p) \cdots 0 \right]^\top, \quad (78)$$

where (78) represents a column vector – of length  $N_{K-1}$  – whose entries are zero except for the  $p$ -th entry. Meanwhile, plugging (78) and (76c) into (74) gives

$$(\boldsymbol{\delta}_{K-1,i}^{(t)})_p = \delta_{K,i}^{(t)} (\mathbf{w}_K^{(t)})_p \varphi'((\mathbf{v}_{K-1,i}^{(t)})_p). \quad (79)$$

Similarly, it follows from (69) w.r.t.  $k = K - 2$  that

$$(\boldsymbol{\delta}_{K-2,i}^{(t)})_p = \frac{\partial f_{K,i}^{(t)}}{\partial(\mathbf{y}_{K-2,i}^{(t)})^\top} \frac{\partial(\mathbf{y}_{K-2,i}^{(t)})^\top}{\partial(\mathbf{v}_{K-2,i}^{(t)})_p}, \quad (80)$$

where  $p \in [N_{K-2}]$ . We simplify (80) by simplifying both partial derivatives. To this end, employing (77) w.r.t.  $k = K - 2$  and exploiting (60) gives

$$\frac{\partial(\mathbf{y}_{K-2,i}^{(t)})^\top}{\partial(\mathbf{v}_{K-2,i}^{(t)})_p} = [0, \cdots, \varphi'((\mathbf{v}_{K-2,i}^{(t)})_p), \cdots, 0]^\top, \quad (81)$$

where the RHS of (81) is a column vector of length  $N_{K-2}$ . We continue by using the chain rule to obtain

$$\frac{\partial f_{K,i}^{(t)}}{\partial(\mathbf{y}_{K-2,i}^{(t)})^\top} = \overbrace{\frac{\partial f_{K,i}^{(t)}}{\partial(\mathbf{y}_{K-1,i}^{(t)})^\top} \frac{\partial(\mathbf{y}_{K-1,i}^{(t)})^\top}{\partial(\mathbf{v}_{K-1,i}^{(t)})^\top} \frac{\partial(\mathbf{v}_{K-1,i}^{(t)})^\top}{\partial(\mathbf{y}_{K-2,i}^{(t)})^\top}}^{=\boldsymbol{\theta}_{K-1,i}^{(t)}}. \quad (82)$$

We simplify (82) by simplifying  $\boldsymbol{\theta}_{K-1,i}^{(t)}$  – which is defined in (82) – as follows in accordance with the denominator layout notation,

$$\frac{\partial(\mathbf{y}_{K-1,i}^{(t)})^\top}{\partial(\mathbf{v}_{K-1,i}^{(t)})^\top} = \left[ \frac{\partial(\mathbf{y}_{K-1,i}^{(t)})_1}{\partial(\mathbf{v}_{K-1,i}^{(t)})_1} \quad \cdots \quad \frac{\partial(\mathbf{y}_{K-1,i}^{(t)})_{N_{K-1}}}{\partial(\mathbf{v}_{K-1,i}^{(t)})_{N_{K-1}}} \right]. \quad (83)$$

$$\boldsymbol{\theta}_{K-1,i}^{(t)} = \left[ \frac{\partial f_{K,i}^{(t)}}{\partial (\mathbf{y}_{K-1,i}^{(t)})^\top} \frac{\partial (\mathbf{y}_{K-1,i}^{(t)})^\top}{\partial (\mathbf{v}_{K-1,i}^{(t)})_1} \cdots \frac{\partial f_{K,i}^{(t)}}{\partial (\mathbf{y}_{K-1,i}^{(t)})^\top} \frac{\partial (\mathbf{y}_{K-1,i}^{(t)})^\top}{\partial (\mathbf{v}_{K-1,i}^{(t)})_{N_{K-1}}} \right] \stackrel{(a)}{=} \left[ (\boldsymbol{\delta}_{K-1,i}^{(t)})_1 \cdots (\boldsymbol{\delta}_{K-1,i}^{(t)})_{N_{K-1}} \right]. \quad (84)$$

Plugging (83) into  $\boldsymbol{\theta}_{K-1,i}^{(t)}$  as defined in (82), (84) follows, while (a) is due to (74).

We further simplify (82) by simplifying  $\frac{\partial (\mathbf{v}_{K-1,i}^{(t)})^\top}{\partial (\mathbf{y}_{K-2,i}^{(t)})^\top}$ . To this end, per the denominator layout notation,

$$\frac{\partial (\mathbf{v}_{k,i}^{(t)})^\top}{\partial (\mathbf{y}_{k-1,i}^{(t)})^\top} = \begin{bmatrix} \frac{\partial (\mathbf{v}_{k,i}^{(t)})_1}{\partial (\mathbf{y}_{k-1,i}^{(t)})_1} & \cdots & \frac{\partial (\mathbf{v}_{k,i}^{(t)})_1}{\partial (\mathbf{y}_{k-1,i}^{(t)})_{N_{k-1}}} \\ \frac{\partial (\mathbf{v}_{k,i}^{(t)})_2}{\partial (\mathbf{y}_{k-1,i}^{(t)})_1} & \cdots & \frac{\partial (\mathbf{v}_{k,i}^{(t)})_2}{\partial (\mathbf{y}_{k-1,i}^{(t)})_{N_{k-1}}} \\ \vdots & \ddots & \vdots \\ \frac{\partial (\mathbf{v}_{k,i}^{(t)})_{N_k}}{\partial (\mathbf{y}_{k-1,i}^{(t)})_1} & \cdots & \frac{\partial (\mathbf{v}_{k,i}^{(t)})_{N_k}}{\partial (\mathbf{y}_{k-1,i}^{(t)})_{N_{k-1}}} \end{bmatrix}. \quad (85)$$

It follows from (61) that  $(\mathbf{v}_{k,i}^{(t)})_p = \sum_{q=1}^{N_k} (\mathbf{W}_k^{(t)})_{p,q} (\mathbf{y}_{k-1,i}^{(t)})_q$ . Thus,

$$\frac{\partial (\mathbf{v}_{k,i}^{(t)})_p}{\partial (\mathbf{y}_{k-1,i}^{(t)})_q} = (\mathbf{W}_k^{(t)})_{p,q}. \quad (86)$$

Consequently, exploiting (86) in (85) w.r.t.  $k = K - 1$  gives

$$\frac{\partial (\mathbf{v}_{K-1,i}^{(t)})^\top}{\partial (\mathbf{y}_{K-2,i}^{(t)})^\top} = \begin{bmatrix} (\mathbf{W}_{K-1}^{(t)})_{1,1} & \cdots & (\mathbf{W}_{K-1}^{(t)})_{1,v} \\ (\mathbf{W}_{K-1}^{(t)})_{2,1} & \cdots & (\mathbf{W}_{K-1}^{(t)})_{2,v} \\ \vdots & \ddots & \vdots \\ (\mathbf{W}_{K-1}^{(t)})_{u,1} & \cdots & (\mathbf{W}_{K-1}^{(t)})_{u,v} \end{bmatrix}, \quad (87)$$

where  $u = N_{K-1}$  and  $v = N_{K-2}$ .

Meanwhile, substituting (87) and (84) into (82) leads to

$$\frac{\partial f_{K,i}^{(t)}}{\partial (\mathbf{y}_{K-2,i}^{(t)})^\top} = [(\mathbf{s}_{K-1,i}^{(t)})_1 \cdots (\mathbf{s}_{K-1,i}^{(t)})_{N_{K-2}}], \quad (88)$$

where  $(\mathbf{s}_{K-1,i}^{(t)})_p = \sum_{q=1}^{N_{K-1}} (\boldsymbol{\delta}_{K-1,i}^{(t)})_q (\mathbf{W}_{K-1}^{(t)})_{q,p}$ . Finally, substituting (88) and (78) into (80) gives

$$(\boldsymbol{\delta}_{K-2,i}^{(t)})_p = \varphi'((\mathbf{v}_{K-1,i}^{(t)})_p) \sum_{q=1}^{N_{K-1}} (\boldsymbol{\delta}_{K-1,i}^{(t)})_q (\mathbf{W}_{K-1}^{(t)})_{q,p}. \quad (89)$$

Similarly, it follows from (69) w.r.t.  $k = K - 3$  that

$$(\boldsymbol{\delta}_{K-3,i}^{(t)})_p = \frac{\partial f_{K,i}^{(t)}}{\partial (\mathbf{y}_{K-3,i}^{(t)})^\top} \frac{\partial (\mathbf{y}_{K-3,i}^{(t)})^\top}{\partial (\mathbf{v}_{K-3,i}^{(t)})_p}. \quad (90)$$

As for (81), it follows from (77) and (60) that

$$\frac{\partial(\mathbf{y}_{K-3,i}^{(t)})^\top}{\partial(\mathbf{v}_{K-3,i}^{(t)})_p} = \left[ 0 \quad \cdots \quad \varphi'((\mathbf{v}_{K-3,i}^{(t)})_p) \quad \cdots \quad 0 \right]^\top, \quad (91)$$

where the RHS of (91) is a column vector of length  $N_{K-3}$ . Using the chain rule similar to (82), we obtain

$$\frac{\partial f_{K,i}^{(t)}}{\partial(\mathbf{y}_{K-3,i}^{(t)})^\top} = \frac{\overbrace{\frac{\partial f_{K,i}^{(t)}}{\partial(\mathbf{y}_{K-2,i}^{(t)})^\top} \frac{\partial(\mathbf{y}_{K-2,i}^{(t)})^\top}{\partial(\mathbf{v}_{K-2,i}^{(t)})^\top}}^{=\boldsymbol{\theta}_{K-2,i}^{(t)}} \frac{\partial(\mathbf{v}_{K-2,i}^{(t)})^\top}{\partial(\mathbf{y}_{K-3,i}^{(t)})^\top}}{\partial(\mathbf{y}_{K-2,i}^{(t)})^\top \frac{\partial(\mathbf{y}_{K-2,i}^{(t)})^\top}{\partial(\mathbf{v}_{K-2,i}^{(t)})^\top} \frac{\partial(\mathbf{v}_{K-2,i}^{(t)})^\top}{\partial(\mathbf{y}_{K-3,i}^{(t)})^\top}}. \quad (92)$$

Per the denominator layout notation,

$$\frac{\partial(\mathbf{y}_{K-2,i}^{(t)})^\top}{\partial(\mathbf{v}_{K-2,i}^{(t)})^\top} = \left[ \frac{\partial(\mathbf{y}_{K-2,i}^{(t)})^\top}{\partial(\mathbf{v}_{K-2,i}^{(t)})_1} \quad \cdots \quad \frac{\partial(\mathbf{y}_{K-2,i}^{(t)})^\top}{\partial(\mathbf{v}_{K-2,i}^{(t)})_{N_{K-2}}} \right]. \quad (93)$$

Plugging (93) into the RHS of (92) – that is equated to  $\boldsymbol{\theta}_{K-2,i}^{(t)}$  – and using (80) give

$$\boldsymbol{\theta}_{K-2,i}^{(t)} = \left[ (\boldsymbol{\delta}_{K-2,i}^{(t)})_1 \quad \cdots \quad (\boldsymbol{\delta}_{K-2,i}^{(t)})_{N_{K-2}} \right]. \quad (94)$$

Similarly, deploying (85) and (86) w.r.t.  $k = K - 2$  leads to

$$\frac{\partial(\mathbf{v}_{K-2,i}^{(t)})^\top}{\partial(\mathbf{y}_{K-3,i}^{(t)})^\top} = \begin{bmatrix} (\mathbf{W}_{K-2}^{(t)})_{1,1} & \cdots & (\mathbf{W}_{K-2}^{(t)})_{1,v} \\ (\mathbf{W}_{K-2}^{(t)})_{2,1} & \cdots & (\mathbf{W}_{K-2}^{(t)})_{2,v} \\ \vdots & \ddots & \vdots \\ (\mathbf{W}_{K-2}^{(t)})_{u,1} & \cdots & (\mathbf{W}_{K-2}^{(t)})_{u,v} \end{bmatrix}, \quad (95)$$

where  $u = N_{K-2}$  and  $v = N_{K-3}$ . In the meantime, substituting (94) and (95) into (92) produces

$$\frac{\partial f_{K,i}^{(t)}}{\partial(\mathbf{y}_{K-3,i}^{(t)})^\top} = \left[ (\mathbf{s}_{K-2,i}^{(t)})_1 \quad \cdots \quad (\mathbf{s}_{K-2,i}^{(t)})_{N_{K-3}} \right], \quad (96)$$

where  $(\mathbf{s}_{K-2,i}^{(t)})_p = \sum_{q=1}^{N_{K-2}} (\boldsymbol{\delta}_{K-2,i}^{(t)})_q (\mathbf{W}_{K-2}^{(t)})_{q,p}$ . Eventually, substituting (96) and (91) into (90) results in

$$(\boldsymbol{\delta}_{K-3,i}^{(t)})_p = \varphi'((\mathbf{v}_{K-3,i}^{(t)})_p) \sum_{q=1}^{N_{K-2}} (\boldsymbol{\delta}_{K-2,i}^{(t)})_q (\mathbf{W}_{K-2}^{(t)})_{q,p}. \quad (97)$$

Therefore, it can be deduced from (97), (89), (79), and (72) that (52) generalizes all local gradients of all FNN layers.

To wrap up the simplification of (71) through (52), we simplify  $\frac{\partial(\mathbf{v}_{k,i}^{(t)})^\top}{\partial(\mathbf{w}_k^{(t)})_{p,q}}$  in accordance with the denominator layout notation as follows:

$$\frac{\partial(\mathbf{v}_{k,i}^{(t)})^\top}{\partial(\mathbf{w}_k^{(t)})_{p,q}} = \left[ \frac{\partial(\mathbf{v}_{k,i}^{(t)})_1}{\partial(\mathbf{w}_k^{(t)})_{p,q}} \quad \cdots \quad \frac{\partial(\mathbf{v}_{k,i}^{(t)})_{N_k}}{\partial(\mathbf{w}_k^{(t)})_{p,q}} \right]^\top, \quad (98)$$

where  $p \in [N_k]$  and  $q \in [N_{k-1}]$ . It follows from (61) that  $(\mathbf{v}_{k,i}^{(t)})_{\tilde{p}} = \sum_{q=1}^{N_{k-1}} (\mathbf{W}_k^{(t)})_{\tilde{p},q} (\mathbf{y}_{k-1,i}^{(t)})_q$ .

Hence,

$$\frac{\partial (\mathbf{v}_{k,i}^{(t)})_{\tilde{p}}}{\partial (\mathbf{W}_k^{(t)})_{p,q}} = \begin{cases} (\mathbf{y}_{k-1,i}^{(t)})_q & : \tilde{p} = p \\ 0 & : \tilde{p} \neq p \end{cases} \quad (99)$$

$$\frac{\partial (\mathbf{v}_{k,i}^{(t)})^\top}{\partial (\mathbf{W}_k^{(t)})_{p,q}} = \begin{bmatrix} 0 & \cdots & (d_{k,i}^{(t)})_p & \cdots & 0 \end{bmatrix}^\top, \quad (100)$$

where  $(d_{k,i}^{(t)})_p = (\mathbf{y}_{k-1,i}^{(t)})_q$ . In the interim, substituting (100) into (71) produces the expression

$$\frac{\partial f_{K,i}^{(t)}}{\partial (\mathbf{W}_k^{(t)})_{p,q}} = (\boldsymbol{\delta}_{k,i}^{(t)})_p (d_{k,i}^{(t)})_p = (\boldsymbol{\delta}_{k,i}^{(t)})_p (\mathbf{y}_{k-1,i}^{(t)})_q. \quad (101)$$

Deploying (101) in (65) leads to

$$\frac{\partial f_{K,i}^{(t)}}{\partial \mathbf{W}_k^{(t)}} = \begin{bmatrix} (\boldsymbol{\delta}_{k,i}^{(t)})_1 (\mathbf{y}_{k-1,i}^{(t)})_1 & \cdots & (\boldsymbol{\delta}_{k,i}^{(t)})_1 (\mathbf{y}_{k-1,i}^{(t)})_v \\ (\boldsymbol{\delta}_{k,i}^{(t)})_2 (\mathbf{y}_{k-1,i}^{(t)})_1 & \cdots & (\boldsymbol{\delta}_{k,i}^{(t)})_2 (\mathbf{y}_{k-1,i}^{(t)})_v \\ \vdots & \ddots & \vdots \\ (\boldsymbol{\delta}_{k,i}^{(t)})_u (\mathbf{y}_{k-1,i}^{(t)})_1 & \cdots & (\boldsymbol{\delta}_{k,i}^{(t)})_u (\mathbf{y}_{k-1,i}^{(t)})_v \end{bmatrix}, \quad (102)$$

where  $u = N_k$  and  $v = N_{k-1}$ .

Finally, substituting (102) into (64) and, in turn, (62b) gives a scalar weight update rule that is expressed as

$$(\mathbf{W}_k^{(t+1)})_{p,q} = (\mathbf{W}_k^{(t)})_{p,q} + \frac{\eta_t}{B} \sum_{i \in \mathcal{B}^{(t)}} (\boldsymbol{\delta}_{k,i}^{(t)})_p (\mathbf{y}_{k-1,i}^{(t)})_q \mathbb{I}\{1 - f_{K,i}^{(t)} > 0\}, \quad (103)$$

where  $k \in [K]$  and  $(\boldsymbol{\delta}_{k,i}^{(t)})_p$  is given by (52). Note that this update rule subsumes (73) when  $\mathbf{W}_K^{(t)} = \mathbf{w}_K^{(t)}$ ,  $\forall t$ . This concludes the proof of Theorem 3.  $\blacksquare$

**Remark 15.**  $\varphi'((\mathbf{v}_{k,i}^{(t)})_p) = \rho((\mathbf{v}_{k,i}^{(t)})_p) / (\mathbf{v}_{k,i}^{(t)})_p$  for ReLU FNNs and  $\varphi(\cdot)$  can be any component-wise activation function. Eq. (51) states the back-propagation algorithm for our classification AI/ML problem and quantifies the penalty/reward pertaining to each neuron subjected to (52), which is the back-propagation of all local gradients of FNNs with dual activation functions.

## APPENDIX B

## PROOF OF LEMMA 1: DERIVATION OF EQUIVALENCE FOR POINT NON-EQUALITY

Let us first recall the sign function [120] w.r.t.  $x \in \mathbb{R}$ :

$$\text{sgn}(x) = \begin{cases} -1 & : \text{for } x < 0 \\ 0 & : \text{for } x = 0 \\ 1 & : \text{for } x > 0. \end{cases} \equiv \begin{cases} \frac{x}{|x|} & : \text{for } x \neq 0 \\ 0 & : \text{for } x = 0, \end{cases} \quad (104)$$

where  $|x|$  is the absolute value of  $x$ . To prove Lemma 1 and (36), we consider two cases:  $\Phi^{(T)}(x_n) = 0$  and  $\Phi^{(T)}(x_n) \neq 0$ . If we begin with the former, i.e.,  $\Phi^{(T)}(x_n) = 0$ ,

$$\mathbb{I}\{y_n \neq \text{sgn}(\Phi^{(T)}(x_n))\} = \mathbb{I}\{y_n \neq \text{sgn}(0)\} = \mathbb{I}\{y_n \neq 0\} = \mathbb{I}\{y_n \Phi^{(T)}(x_n) = 0\} = 1. \quad (105)$$

To proceed to the case  $\Phi^{(T)}(x_n) \neq 0$ , it follows from (104) that  $\text{sgn}(\Phi^{(T)}(x_n)) = \frac{\Phi^{(T)}(x_n)}{|\Phi^{(T)}(x_n)|}$ . Consequently,

$$\mathbb{I}\{y_n \neq \text{sgn}(\Phi^{(T)}(x_n))\} = \mathbb{I}\left\{y_n \neq \frac{\Phi^{(T)}(x_n)}{|\Phi^{(T)}(x_n)|}\right\} \stackrel{(a)}{=} \mathbb{I}\left\{1 \neq \frac{y_n \Phi^{(T)}(x_n)}{|\Phi^{(T)}(x_n)|}\right\} \quad (106a)$$

$$\stackrel{(b)}{=} \mathbb{I}\{|\Phi^{(T)}(x_n)| \neq y_n \Phi^{(T)}(x_n)\}, \quad (106b)$$

where (a) follows from multiplying both sides of the argument by  $y_n$  and from the fact that  $y_n^2 = 1$  for  $y_n \in \{-1, 1\}$ ; and (b) follows from multiplying both sides of the argument by  $|\Phi^{(T)}(x_n)|$ . Since  $|\Phi^{(T)}(x_n)|$  is always non-negative and hence  $|\Phi^{(T)}(x_n)| \geq 0$ , the non-equality in the RHS of (106b) is true if and only if  $y_n \Phi^{(T)}(x_n) < 0$ . As a result, it directly follows from (106b) that

$$\mathbb{I}\{y_n \neq \text{sgn}(\Phi^{(T)}(x_n))\} = \mathbb{I}\{y_n \Phi^{(T)}(x_n) < 0\}, \quad (107)$$

where  $\Phi^{(T)}(x_n) \neq 0$ . Thus, combining (107) and (105) – which correspond to the two cases considered – produces the equivalence in (36). This completes the proof of Lemma 1.  $\blacksquare$

## APPENDIX C

## PROOF OF THEOREM 1

When it comes to the testing performance of a trained deep ReLU FNN  $\Phi^{(T)}$ , it directly follows from (28) that

$$\Phi^{(T)}(x_n) = \mathbf{w}_K^{(T)} \mathbf{y}_{K-1,n}^{(T)} = \sum_{q=1}^{2H} (\mathbf{w}_K^{(T)})_q (\mathbf{y}_{K-1,n}^{(T)})_q \in \mathbb{R}, \quad (108)$$

where  $n \in \{N + 1, \dots, N + \tilde{N}\}$  and it follows from (29) for  $\Sigma_{1,n}^{(T)} = \text{diag}(\mathbb{I}\{\mathbf{w}_1^{(T)} x_n \geq 0\}) \in \{0, 1\}^{2H \times 2H}$  and  $\Sigma_{k,n}^{(T)} = \text{diag}(\mathbb{I}\{\mathbf{W}_k^{(T)} (\prod_{l=1}^{k-2} \Sigma_{k-l,n}^{(T)} \mathbf{W}_{k-l}^{(T)}) \Sigma_{1,n}^{(T)} \mathbf{w}_1^{(T)} x_n \geq 0\}) \in \{0, 1\}^{2H \times 2H}$  that

$$\mathbf{y}_{K-1,n}^{(T)} = \left( \prod_{k=1}^{K-2} \Sigma_{K-k,n}^{(T)} \mathbf{W}_{K-k}^{(T)} \right) \Sigma_{1,n}^{(T)} \mathbf{w}_1^{(T)} x_n \in \mathbb{R}^{2H}. \quad (109)$$

The  $K$ -th FNN layer's weight vector at convergence  $\mathbf{w}_K^{(T)} \in \mathbb{R}^{1 \times 2H}$  can be expressed via (34c) for all  $q \in [2H]$  as

$$(\mathbf{w}_K^{(T)})_q = (\mathbf{w}_K)_q + \sum_{t=0}^{T-1} (\Delta \mathbf{w}_K^{(t)})_q, \quad (110)$$

where  $(\mathbf{w}_K)_q := (\mathbf{w}_K^{(0)})_q$  is initialized with a Gaussian initializer such as LeCun normal or He normal (see Definition 10) and hence  $(\mathbf{w}_K)_q \sim \mathcal{N}(0, \alpha/2H)$  for  $\alpha \in \{1, 2\}$  ( $\alpha = 1$  for LeCun normal and  $\alpha = 2$  for He normal); and  $\Delta \mathbf{w}_K^{(t)}$  is the weight correction during the  $t$ -th iteration of SGD, SGD with momentum, RMSProp, or Adam.

Substituting (110) into the RHS of (108) leads to

$$\Phi^{(T)}(x_n) = \sum_{q=1}^{2H} \left[ (\mathbf{w}_K)_q + \sum_{t=0}^{T-1} (\Delta \mathbf{w}_K^{(t)})_q \right] (\mathbf{y}_{K-1,n}^{(T)})_q \quad (111a)$$

$$= \sum_{q=1}^{2H} (\mathbf{w}_K)_q (\mathbf{y}_{K-1,n}^{(T)})_q + \sum_{q=1}^{2H} \sum_{t=0}^{T-1} (\Delta \mathbf{w}_K^{(t)})_q (\mathbf{y}_{K-1,n}^{(T)})_q \quad (111b)$$

$$= Y + S, \quad (111c)$$

where  $(\mathbf{w}_K)_q \sim \mathcal{N}(0, \frac{\alpha}{2H})$ ;  $n \in \{N + 1, \dots, N + \tilde{N}\}$ ; and  $Y$  and  $S$  are continuous RVs that have already been conditioned on the generated random vector  $\mathbf{y}_{K-1,n}^{(T)}$  and are defined as

$$Y = \sum_{q=1}^{2H} (\mathbf{w}_K)_q (\mathbf{y}_{K-1,n}^{(T)})_q \left\{ \mathbf{y}_{K-1,n}^{(T)} \stackrel{(a)}{=} \left( \prod_{k=1}^{K-2} \Sigma_{K-k,n}^{(T)} \mathbf{W}_{K-k}^{(T)} \right) \Sigma_{1,n}^{(T)} \mathbf{w}_1^{(T)} x_n \right\} \quad (112a)$$

$$S = \sum_{q=1}^{2H} \sum_{t=0}^{T-1} (\Delta \mathbf{w}_K^{(t)})_q (\mathbf{y}_{K-1,n}^{(T)})_q \left\{ \mathbf{y}_{K-1,n}^{(T)} \stackrel{(a)}{=} \left( \prod_{k=1}^{K-2} \Sigma_{K-k,n}^{(T)} \mathbf{W}_{K-k}^{(T)} \right) \Sigma_{1,n}^{(T)} \mathbf{w}_1^{(T)} x_n \right\}, \quad (112b)$$

where (a) follows from (29). For a given  $\mathbf{y}_{K-1,n}^{(T)} = [(\mathbf{y}_{K-1,n}^{(T)})_1, \dots, (\mathbf{y}_{K-1,n}^{(T)})_{2H}]^\top \in \mathbb{R}^{2H}$  previously delivered by the deep ReLU FNN's  $(K - 1)$ -th layer,  $Y$  would be the sum of  $2H$  zero mean Gaussian RVs and hence a Gaussian RV distributed as  $Y \sim \mathcal{N}(0, \sigma^2)$ , where

$$\sigma^2 = \frac{\alpha}{2H} \sum_{q=1}^{2H} [(\mathbf{y}_{K-1,n}^{(T)})_q]^2 = \frac{\alpha}{2H} \|\mathbf{y}_{K-1,n}^{(T)}\|^2. \quad (113)$$

Meanwhile, by substituting (111c) into the RHS of (41), the probability of point misclassification error  $P_e$  manifested by  $\Phi^{(T)}$  becomes

$$P_e = \frac{1}{2}(P_e|\mathcal{H}_{-1} + P_e|\mathcal{H}_1), \quad (114)$$

where for  $Y|\mathcal{H}_{-1} \sim \mathcal{N}(0, \sigma^2|\mathcal{H}_{-1})$  and  $Y|\mathcal{H}_1 \sim \mathcal{N}(0, \sigma^2|\mathcal{H}_1)$

$$P_e|\mathcal{H}_{-1} = \mathbb{P}(Y + S > 0|\mathcal{H}_{-1}) = \mathbb{P}(Y|\mathcal{H}_{-1} > -S|\mathcal{H}_{-1}) \quad (115a)$$

$$P_e|\mathcal{H}_1 = \mathbb{P}(Y + S < 0|\mathcal{H}_1) = \mathbb{P}(Y|\mathcal{H}_1 < -S|\mathcal{H}_1). \quad (115b)$$

Moreover, it follows from (113) that

$$\sigma^2|\mathcal{H}_{-1} = \frac{\alpha}{2H} \|\mathbf{y}_{K-1,n}^{(T)}\|^2|\mathcal{H}_{-1} \quad \text{and} \quad \sigma^2|\mathcal{H}_1 = \frac{\alpha}{2H} \|\mathbf{y}_{K-1,n}^{(T)}\|^2|\mathcal{H}_1. \quad (116)$$

We use (115a) and (115b) to derive below closed-form expressions for  $P_e|\mathcal{H}_{-1}$  and  $P_e|\mathcal{H}_1$ .

To derive  $P_e|\mathcal{H}_{-1}$  from the RHS of (115a), we first underscore that  $S|\mathcal{H}_{-1}$ , which is defined in (112b), is a continuous RV that can take values in  $(-\infty, \infty)$  with some probability. Thus, we can condition on the continuous random values of  $S|\mathcal{H}_{-1}$  while employing the law of total probability for a continuous case (see Law 2) to simplify the RHS of (115a) as follows:

$$P_e|\mathcal{H}_{-1} = \mathbb{P}(Y|\mathcal{H}_{-1} > -S|\mathcal{H}_{-1}) \stackrel{(a)}{=} \int_{-\infty}^{\infty} \mathbb{P}(Y|\mathcal{H}_{-1} > -S_{-1}|S_{-1} = s) f_{S_{-1}}(s) ds \quad (117a)$$

$$= \int_{-\infty}^{\infty} \mathbb{P}(Y|\mathcal{H}_{-1} > -s) f_{S_{-1}}(s) ds, \quad (117b)$$

where  $S_{-1} := S|\mathcal{H}_{-1}$ ; (a) follows from (19) w.r.t. an event  $\mathcal{A} = \{Y|\mathcal{H}_{-1} > -S|\mathcal{H}_{-1}\}$ ; and  $f_{S_{-1}}$  is the PDF of  $S_{-1} := S|\mathcal{H}_{-1}$ . We simplify the RHS of (117b) by simplifying  $\mathbb{P}(Y|\mathcal{H}_{-1} > -s)$  w.r.t. the Gaussian RV  $Y|\mathcal{H}_{-1} \sim \mathcal{N}(0, \sigma^2|\mathcal{H}_{-1})$  for  $\sigma^2 = \sigma^2|\mathcal{H}_{-1}$  as follows:

$$\mathbb{P}(Y|\mathcal{H}_{-1} > -s) = \frac{1}{\sigma\sqrt{2\pi}} \int_{-s}^{\infty} e^{-y^2/2\sigma^2} dy \stackrel{(a)}{=} \frac{1}{\sqrt{2\pi}} \int_{-s/\sigma}^{\infty} e^{-t^2/2} dt \quad (118a)$$

$$\stackrel{(b)}{=} \mathcal{Q}(-s/\sigma) \quad (118b)$$

$$\stackrel{(c)}{=} \mathcal{Q}\left(\frac{-s\sqrt{2H/\alpha}}{\|\mathbf{y}_{K-1,n}^{(T)}\||\mathcal{H}_{-1}}\right), \quad (118c)$$

where  $\sigma^2 = \sigma^2|\mathcal{H}_{-1}$  as defined in (116); (a) follows from integration by substitution w.r.t.  $t = y/\sigma$  and hence  $dt = dy/\sigma$ ; (b) follows directly from (1); and (c) follows from (116) w.r.t.  $\sigma^2 = \sigma^2|\mathcal{H}_{-1}$ . Substituting (118c) into the RHS of (117b) then produces the expression

$$P_e|\mathcal{H}_{-1} = \int_{-\infty}^{\infty} \mathcal{Q}\left(\frac{-s\sqrt{2H/\alpha}}{\|\mathbf{y}_{K-1,n}^{(T)}\||\mathcal{H}_{-1}}\right) f_{S_{-1}}(s) ds. \quad (119)$$

Similarly, it follows from the RHS of (115b) and the law of total probability for a continuous case (see Law 2) that

$$P_e|\mathcal{H}_1 = \mathbb{P}(Y|\mathcal{H}_1 < -S|\mathcal{H}_1) \stackrel{(a)}{=} \int_{-\infty}^{\infty} \mathbb{P}(Y|\mathcal{H}_1 < -S_1|S_1 = s) f_{S_1}(s) ds \quad (120a)$$

$$= \int_{-\infty}^{\infty} \mathbb{P}(Y|\mathcal{H}_1 < -s) f_{S_1}(s) ds, \quad (120b)$$

where  $S_1 := S|\mathcal{H}_1$ ; (a) follows from (19) w.r.t. an event  $\mathcal{A} = \{Y|\mathcal{H}_1 < -S|\mathcal{H}_1\}$ ; and  $f_{S_1}$  is the PDF of  $S_1 := S|\mathcal{H}_1$ . We simplify the RHS of (120b) by simplifying  $\mathbb{P}(Y|\mathcal{H}_1 < -s)$  w.r.t. the Gaussian RV  $Y|\mathcal{H}_1 \sim \mathcal{N}(0, \sigma^2|\mathcal{H}_1)$  for  $\sigma^2 = \sigma^2|\mathcal{H}_1$  as follows:

$$\mathbb{P}(Y|\mathcal{H}_1 < -s) = \frac{1}{\sigma\sqrt{2\pi}} \int_{-\infty}^{-s} e^{-y^2/2\sigma^2} dy \stackrel{(a)}{=} \frac{1}{\sqrt{2\pi}} \int_{s/\sigma}^{\infty} e^{-t^2/2} dt \quad (121a)$$

$$\stackrel{(b)}{=} \mathcal{Q}(s/\sigma) \quad (121b)$$

$$\stackrel{(c)}{=} \mathcal{Q}\left(\frac{s\sqrt{2H/\alpha}}{\|\mathbf{y}_{K-1,n}^{(T)}\||\mathcal{H}_1}\right), \quad (121c)$$

where (a) follows from integration by substitution w.r.t.  $t = -y/\sigma$  and hence  $dt = -dy/\sigma$ ; (b) follows directly from (1); and (c) follows from (116) since we let  $\sigma^2 = \sigma^2|\mathcal{H}_1$ . Substituting (121c) into the RHS of (120b) then gives

$$P_e|\mathcal{H}_1 = \int_{-\infty}^{\infty} \mathcal{Q}\left(\frac{s\sqrt{2H/\alpha}}{\|\mathbf{y}_{K-1,n}^{(T)}\||\mathcal{H}_1}\right) f_{S_1}(s) ds. \quad (122)$$

Accordingly, substituting (122) and (119) into the RHS of (114) gives

$$P_e = \frac{1}{2} \left[ \int_{-\infty}^{\infty} \mathcal{Q}\left(\frac{-s\sqrt{2H/\alpha}}{\|\mathbf{y}_{K-1,n}^{(T)}\||\mathcal{H}_{-1}}\right) f_{S_{-1}}(s) ds + \int_{-\infty}^{\infty} \mathcal{Q}\left(\frac{s\sqrt{2H/\alpha}}{\|\mathbf{y}_{K-1,n}^{(T)}\||\mathcal{H}_1}\right) f_{S_1}(s) ds \right]. \quad (123)$$

This is a closed-form expression of the exhibited probability – manifested by  $\Phi^{(T)}$  – of point misclassification error whose RHS is impacted by the norm of the output of the deep ReLU FNN's penultimate layer under  $\mathcal{H}_{-1}$  and  $\mathcal{H}_1$ . Setting asymptotic limits on this norm makes it possible to characterize the exhibited asymptotic  $P_e$  by deriving the bounds of the RHS of (123).

To this end, if  $\|\mathbf{y}_{K-1,n}^{(T)}\|_{\mathcal{H}_{-1}}, \|\mathbf{y}_{K-1,n}^{(T)}\|_{\mathcal{H}_1} \rightarrow \infty$  for  $\alpha \in \{1, 2\}$  and  $H < \infty$ , applying the limit and its properties to (123) then leads to

$$\begin{aligned} \lim_{\|\mathbf{y}_{K-1,n}^{(T)}\|_{\mathcal{H}_{-1}}, \|\mathbf{y}_{K-1,n}^{(T)}\|_{\mathcal{H}_1} \rightarrow \infty} P_e &= \frac{1}{2} \left[ \int_{-\infty}^{\infty} \lim_{\|\mathbf{y}_{K-1,n}^{(T)}\|_{\mathcal{H}_{-1}}, \|\mathbf{y}_{K-1,n}^{(T)}\|_{\mathcal{H}_1} \rightarrow \infty} \mathcal{Q} \left( \frac{-s\sqrt{2H/\alpha}}{\|\mathbf{y}_{K-1,n}^{(T)}\|_{\mathcal{H}_{-1}}} \right) \times \right. \\ &\quad \lim_{\|\mathbf{y}_{K-1,n}^{(T)}\|_{\mathcal{H}_{-1}}, \|\mathbf{y}_{K-1,n}^{(T)}\|_{\mathcal{H}_1} \rightarrow \infty} f_{S_{-1}}(s) ds + \int_{-\infty}^{\infty} \lim_{\|\mathbf{y}_{K-1,n}^{(T)}\|_{\mathcal{H}_{-1}}, \|\mathbf{y}_{K-1,n}^{(T)}\|_{\mathcal{H}_1} \rightarrow \infty} \mathcal{Q} \left( \frac{s\sqrt{2H/\alpha}}{\|\mathbf{y}_{K-1,n}^{(T)}\|_{\mathcal{H}_1}} \right) \times \\ &\quad \left. \lim_{\|\mathbf{y}_{K-1,n}^{(T)}\|_{\mathcal{H}_{-1}}, \|\mathbf{y}_{K-1,n}^{(T)}\|_{\mathcal{H}_1} \rightarrow \infty} f_{S_1}(s) ds \right]. \quad (124) \end{aligned}$$

Thus, it follows from the properties of the  $Q$ -function and limit that

$$\lim_{\|\mathbf{y}_{K-1,n}^{(T)}\|_{\mathcal{H}_{-1}}, \|\mathbf{y}_{K-1,n}^{(T)}\|_{\mathcal{H}_1} \rightarrow \infty} \mathcal{Q} \left( \frac{-s\sqrt{2H/\alpha}}{\|\mathbf{y}_{K-1,n}^{(T)}\|_{\mathcal{H}_{-1}}} \right) \stackrel{(a)}{=} \mathcal{Q}(0) \stackrel{(b)}{=} \frac{1}{\sqrt{2\pi}} \int_0^{\infty} \exp\left(-\frac{t^2}{2}\right) dt = \frac{1}{2} \quad (125a)$$

$$\lim_{\|\mathbf{y}_{K-1,n}^{(T)}\|_{\mathcal{H}_{-1}}, \|\mathbf{y}_{K-1,n}^{(T)}\|_{\mathcal{H}_1} \rightarrow \infty} \mathcal{Q} \left( \frac{s\sqrt{2H/\alpha}}{\|\mathbf{y}_{K-1,n}^{(T)}\|_{\mathcal{H}_1}} \right) \stackrel{(a)}{=} \mathcal{Q}(0) \stackrel{(b)}{=} \frac{1}{\sqrt{2\pi}} \int_0^{\infty} \exp\left(-\frac{t^2}{2}\right) dt = \frac{1}{2}, \quad (125b)$$

where (a) is valid for any  $s \in (-\infty, \infty)$  and (b) follows from (1). Plugging (125a) and (125b) into the RHS of (124) gives

$$\begin{aligned} \lim_{\|\mathbf{y}_{K-1,n}^{(T)}\|_{\mathcal{H}_{-1}}, \|\mathbf{y}_{K-1,n}^{(T)}\|_{\mathcal{H}_1} \rightarrow \infty} P_e &= \lim_{\|\mathbf{y}_{K-1,n}^{(T)}\|_{\mathcal{H}_{-1}}, \|\mathbf{y}_{K-1,n}^{(T)}\|_{\mathcal{H}_1} \rightarrow \infty} \left[ \int_{-\infty}^{\infty} f_{S_{-1}}(s) ds + \int_{-\infty}^{\infty} f_{S_1}(s) ds \right] \frac{1}{4} \\ &\stackrel{(a)}{=} \frac{1}{2}, \quad (126) \end{aligned}$$

where (a) is due to a PDF property (see Definition 7) that  $\int_{-\infty}^{\infty} f_{S_{-1}}(s) ds = \int_{-\infty}^{\infty} f_{S_1}(s) ds = 1$ .

This proves (47a).  $\square$

To prove (47b), we first decompose the RHS of (123) into the sum of four summands that constitute a closed-form expression given by

$$\begin{aligned} P_e &= \frac{1}{2} \left[ \int_{-\infty}^0 \mathcal{Q} \left( \frac{-s\sqrt{2H/\alpha}}{\|\mathbf{y}_{K-1,n}^{(T)}\|_{\mathcal{H}_{-1}}} \right) f_{S_{-1}}(s) ds + \int_0^{\infty} \mathcal{Q} \left( \frac{-s\sqrt{2H/\alpha}}{\|\mathbf{y}_{K-1,n}^{(T)}\|_{\mathcal{H}_{-1}}} \right) f_{S_{-1}}(s) ds \right. \\ &\quad \left. + \int_{-\infty}^0 \mathcal{Q} \left( \frac{s\sqrt{2H/\alpha}}{\|\mathbf{y}_{K-1,n}^{(T)}\|_{\mathcal{H}_1}} \right) f_{S_1}(s) ds + \int_0^{\infty} \mathcal{Q} \left( \frac{s\sqrt{2H/\alpha}}{\|\mathbf{y}_{K-1,n}^{(T)}\|_{\mathcal{H}_1}} \right) f_{S_1}(s) ds \right]. \quad (127) \end{aligned}$$

As a result, (127) can also be expressed as

$$\begin{aligned} P_e &= \frac{1}{2} \left[ \int_{-\infty}^0 \mathcal{Q} \left( \frac{-s\sqrt{2H/\alpha}}{\|\mathbf{y}_{K-1,n}^{(T)}\|_{\mathcal{H}_{-1}}} \middle| s < 0 \right) f_{S_{-1}}(s) ds + \int_0^{\infty} \mathcal{Q} \left( \frac{-s\sqrt{2H/\alpha}}{\|\mathbf{y}_{K-1,n}^{(T)}\|_{\mathcal{H}_{-1}}} \middle| s > 0 \right) f_{S_{-1}}(s) ds \right. \\ &\quad \left. + \int_{-\infty}^0 \mathcal{Q} \left( \frac{s\sqrt{2H/\alpha}}{\|\mathbf{y}_{K-1,n}^{(T)}\|_{\mathcal{H}_1}} \middle| s < 0 \right) f_{S_1}(s) ds + \int_0^{\infty} \mathcal{Q} \left( \frac{s\sqrt{2H/\alpha}}{\|\mathbf{y}_{K-1,n}^{(T)}\|_{\mathcal{H}_1}} \middle| s > 0 \right) f_{S_1}(s) ds \right]. \quad (128) \end{aligned}$$

If we now proceed to the condition from (47b) that  $\|\mathbf{y}_{K-1,n}^{(T)}\|_{\mathcal{H}_{-1}}, \|\mathbf{y}_{K-1,n}^{(T)}\|_{\mathcal{H}_1} \rightarrow 0$ , applying the limit and its properties to (128) yields

$$\begin{aligned}
\lim_{\|\mathbf{y}_{K-1,n}^{(T)}\|_{\mathcal{H}_{-1}}, \|\mathbf{y}_{K-1,n}^{(T)}\|_{\mathcal{H}_1} \rightarrow 0} P_e &= \frac{1}{2} \left[ \int_{-\infty}^0 \lim_{\|\mathbf{y}_{K-1,n}^{(T)}\|_{\mathcal{H}_{-1}}, \|\mathbf{y}_{K-1,n}^{(T)}\|_{\mathcal{H}_1} \rightarrow 0} \mathcal{Q} \left( \frac{-s\sqrt{2H/\alpha}}{\|\mathbf{y}_{K-1,n}^{(T)}\|_{\mathcal{H}_{-1}}} \middle| s < 0 \right) \times \lim_{\|\mathbf{y}_{K-1,n}^{(T)}\|_{\mathcal{H}_{-1}}, \|\mathbf{y}_{K-1,n}^{(T)}\|_{\mathcal{H}_1} \rightarrow 0} f_{S_{-1}}(s) ds + \right. \\
&\int_0^{\infty} \lim_{\|\mathbf{y}_{K-1,n}^{(T)}\|_{\mathcal{H}_{-1}}, \|\mathbf{y}_{K-1,n}^{(T)}\|_{\mathcal{H}_1} \rightarrow 0} \mathcal{Q} \left( \frac{-s\sqrt{2H/\alpha}}{\|\mathbf{y}_{K-1,n}^{(T)}\|_{\mathcal{H}_{-1}}} \middle| s > 0 \right) \times \lim_{\|\mathbf{y}_{K-1,n}^{(T)}\|_{\mathcal{H}_{-1}}, \|\mathbf{y}_{K-1,n}^{(T)}\|_{\mathcal{H}_1} \rightarrow 0} f_{S_{-1}}(s) ds + \\
&\int_{-\infty}^0 \lim_{\|\mathbf{y}_{K-1,n}^{(T)}\|_{\mathcal{H}_{-1}}, \|\mathbf{y}_{K-1,n}^{(T)}\|_{\mathcal{H}_1} \rightarrow 0} \mathcal{Q} \left( \frac{s\sqrt{2H/\alpha}}{\|\mathbf{y}_{K-1,n}^{(T)}\|_{\mathcal{H}_1}} \middle| s < 0 \right) \times \lim_{\|\mathbf{y}_{K-1,n}^{(T)}\|_{\mathcal{H}_{-1}}, \|\mathbf{y}_{K-1,n}^{(T)}\|_{\mathcal{H}_1} \rightarrow 0} f_{S_1}(s) ds + \\
&\left. \int_0^{\infty} \lim_{\|\mathbf{y}_{K-1,n}^{(T)}\|_{\mathcal{H}_{-1}}, \|\mathbf{y}_{K-1,n}^{(T)}\|_{\mathcal{H}_1} \rightarrow 0} \mathcal{Q} \left( \frac{s\sqrt{2H/\alpha}}{\|\mathbf{y}_{K-1,n}^{(T)}\|_{\mathcal{H}_1}} \middle| s > 0 \right) \times \lim_{\|\mathbf{y}_{K-1,n}^{(T)}\|_{\mathcal{H}_{-1}}, \|\mathbf{y}_{K-1,n}^{(T)}\|_{\mathcal{H}_1} \rightarrow 0} f_{S_1}(s) ds \right]. \tag{129}
\end{aligned}$$

Hence, it follows from the  $\mathcal{Q}$ -function and limit properties w.r.t.  $\alpha \in \{1, 2\}$  and  $H < \infty$  that

$$\lim_{\|\mathbf{y}_{K-1,n}^{(T)}\|_{\mathcal{H}_{-1}}, \|\mathbf{y}_{K-1,n}^{(T)}\|_{\mathcal{H}_1} \rightarrow 0} \mathcal{Q} \left( \frac{-s\sqrt{2H/\alpha}}{\|\mathbf{y}_{K-1,n}^{(T)}\|_{\mathcal{H}_{-1}}} \middle| s < 0 \right) = \mathcal{Q}(\infty) \stackrel{(a)}{=} \frac{1}{\sqrt{2\pi}} \int_{\infty}^{\infty} \exp(-t^2/2) dt = 0 \tag{130a}$$

$$\lim_{\|\mathbf{y}_{K-1,n}^{(T)}\|_{\mathcal{H}_{-1}}, \|\mathbf{y}_{K-1,n}^{(T)}\|_{\mathcal{H}_1} \rightarrow 0} \mathcal{Q} \left( \frac{-s\sqrt{2H/\alpha}}{\|\mathbf{y}_{K-1,n}^{(T)}\|_{\mathcal{H}_{-1}}} \middle| s > 0 \right) = \mathcal{Q}(-\infty) \stackrel{(a)}{=} \frac{1}{\sqrt{2\pi}} \int_{-\infty}^{\infty} \exp(-t^2/2) dt = 1 \tag{130b}$$

$$\lim_{\|\mathbf{y}_{K-1,n}^{(T)}\|_{\mathcal{H}_{-1}}, \|\mathbf{y}_{K-1,n}^{(T)}\|_{\mathcal{H}_1} \rightarrow 0} \mathcal{Q} \left( \frac{s\sqrt{2H/\alpha}}{\|\mathbf{y}_{K-1,n}^{(T)}\|_{\mathcal{H}_1}} \middle| s < 0 \right) = \mathcal{Q}(-\infty) \stackrel{(a)}{=} \frac{1}{\sqrt{2\pi}} \int_{-\infty}^{\infty} \exp(-t^2/2) dt = 1 \tag{130c}$$

$$\lim_{\|\mathbf{y}_{K-1,n}^{(T)}\|_{\mathcal{H}_{-1}}, \|\mathbf{y}_{K-1,n}^{(T)}\|_{\mathcal{H}_1} \rightarrow 0} \mathcal{Q} \left( \frac{s\sqrt{2H/\alpha}}{\|\mathbf{y}_{K-1,n}^{(T)}\|_{\mathcal{H}_1}} \middle| s > 0 \right) = \mathcal{Q}(\infty) \stackrel{(a)}{=} \frac{1}{\sqrt{2\pi}} \int_{\infty}^{\infty} \exp(-t^2/2) dt = 0, \tag{130d}$$

where (a) follows from (1). Consequently, employing (130a)-(130d) in the RHS of (129) gives

$$\begin{aligned}
\lim_{\|\mathbf{y}_{K-1,n}^{(T)}\|_{\mathcal{H}_{-1}}, \|\mathbf{y}_{K-1,n}^{(T)}\|_{\mathcal{H}_1} \rightarrow 0} P_e &= \frac{1}{2} \left[ \int_0^{\infty} \lim_{\|\mathbf{y}_{K-1,n}^{(T)}\|_{\mathcal{H}_{-1}}, \|\mathbf{y}_{K-1,n}^{(T)}\|_{\mathcal{H}_1} \rightarrow 0} f_{S_{-1}}(s) ds + \right. \\
&\left. \int_{-\infty}^0 \lim_{\|\mathbf{y}_{K-1,n}^{(T)}\|_{\mathcal{H}_{-1}}, \|\mathbf{y}_{K-1,n}^{(T)}\|_{\mathcal{H}_1} \rightarrow 0} f_{S_1}(s) ds \right], \tag{131}
\end{aligned}$$

where it follows from (112b) that

$$S_{-1} := S|\mathcal{H}_{-1} = \sum_{q=1}^{2H} \sum_{t=0}^{T-1} (\Delta \mathbf{w}_K^{(t)})_q [(\mathbf{y}_{K-1,n}^{(T)})_q | \mathcal{H}_{-1}] \quad (132a)$$

$$S_1 := S|\mathcal{H}_1 = \sum_{q=1}^{2H} \sum_{t=0}^{T-1} (\Delta \mathbf{w}_K^{(t)})_q [(\mathbf{y}_{K-1,n}^{(T)})_q | \mathcal{H}_1]. \quad (132b)$$

Since  $\|\mathbf{y}_{K-1,n}^{(T)}\|_{\mathcal{H}_{-1}}, \|\mathbf{y}_{K-1,n}^{(T)}\|_{\mathcal{H}_1} \rightarrow 0$ ,  $(\mathbf{y}_{K-1,n}^{(T)})_q | \mathcal{H}_{-1}, (\mathbf{y}_{K-1,n}^{(T)})_q | \mathcal{H}_1 \rightarrow 0$  for all  $q \in [2H]$ . Consequently,  $\lim_{\|\mathbf{y}_{K-1,n}^{(T)}\|_{\mathcal{H}_{-1}}, \|\mathbf{y}_{K-1,n}^{(T)}\|_{\mathcal{H}_1} \rightarrow 0} f_{S_{-1}}(s)$  and  $\lim_{\|\mathbf{y}_{K-1,n}^{(T)}\|_{\mathcal{H}_{-1}}, \|\mathbf{y}_{K-1,n}^{(T)}\|_{\mathcal{H}_1} \rightarrow 0} f_{S_1}(s)$  precisely become the Dirac delta function  $\delta(s)$ . Plugging  $\delta(s)$  into the RHS (131) thus produces

$$\lim_{\|\mathbf{y}_{K-1,n}^{(T)}\|_{\mathcal{H}_{-1}}, \|\mathbf{y}_{K-1,n}^{(T)}\|_{\mathcal{H}_1} \rightarrow 0} P_e = \frac{1}{2} \left[ \int_0^\infty \delta(s) ds + \int_{-\infty}^0 \delta(s) ds \right] \stackrel{(a)}{=} 1, \quad (133)$$

where (a) is due to the fact that  $\int_0^\infty \delta(s) ds = \int_{-\infty}^0 \delta(s) ds = 1$ . This proves (47b).  $\square$

Therefore, (47a) and (47b) are now proven. This concludes the proof of Theorem 1.  $\blacksquare$

## APPENDIX D

### PROOF OF THEOREM 2

It follows from (46) and (30) that

$$\check{P}_e = \frac{1}{2} [\mathbb{P}(\check{\Phi}^{(T)}(x_n) > 0 | \mathcal{H}_{-1}) + \mathbb{P}(\check{\Phi}^{(T)}(x_n) < 0 | \mathcal{H}_1)], \quad (134)$$

where  $\check{\Phi}^{(T)}(x_n) = \tanh(\check{\mathbf{w}}_K^{(T)} \check{\mathbf{y}}_{K-1,n}^{(T)})$ . Let us now consider

$$\theta = \check{\mathbf{w}}_K^{(T)} \check{\mathbf{y}}_{K-1,n}^{(T)} = \sum_{q=1}^{2H} (\check{\mathbf{w}}_K^{(T)})_q (\check{\mathbf{y}}_{K-1,n}^{(T)})_q, \quad (135)$$

where  $n \in \{N+1, \dots, N+\tilde{N}\}$  and it follows from (31) for  $\check{\Sigma}_{1,n}^{(T)} = \text{diag}(\mathbb{I}\{\check{\mathbf{w}}_1^{(T)} x_n \geq 0\}) \in \{0, 1\}^{2H \times 2H}$  and  $\check{\Sigma}_{k,n}^{(T)} = \text{diag}(\mathbb{I}\{\check{\mathbf{W}}_k^{(T)} (\prod_{l=1}^{k-2} \check{\Sigma}_{k-l,n}^{(T)} \check{\mathbf{W}}_{k-l}^{(T)}) \check{\Sigma}_{1,n}^{(T)} \check{\mathbf{w}}_1^{(T)} x_n \geq 0\}) \in \{0, 1\}^{2H \times 2H}$  that

$$\check{\mathbf{y}}_{K-1,n}^{(T)} = \left( \prod_{k=1}^{K-2} \check{\Sigma}_{K-k,n}^{(T)} \check{\mathbf{W}}_{K-k}^{(T)} \right) \check{\Sigma}_{1,n}^{(T)} \check{\mathbf{w}}_1^{(T)} x_n \in \mathbb{R}^{2H}. \quad (136)$$

It then follows from (135) and the definition of the hyperbolic tangent function  $\tanh(\cdot)$  [112] that

$$\check{\Phi}^{(T)}(x_n) = \tanh(\theta) = \frac{e^\theta - e^{-\theta}}{e^\theta + e^{-\theta}} = \frac{e^{2\theta} - 1}{e^{2\theta} + 1}, \quad (137)$$

where  $\theta$  is given by (135). Employing (137) in the RHS of (134) leads to

$$\check{P}_e = \frac{1}{2} [\mathbb{P}(\tanh(\theta) > 0 | \mathcal{H}_{-1}) + \mathbb{P}(\tanh(\theta) < 0 | \mathcal{H}_1)]. \quad (138)$$

Using the equivalences in (137), the underlying probabilities can be simplified as follows

$$\mathbb{P}(\tanh(\theta) > 0) = \mathbb{P}\left(\frac{e^{2\theta} - 1}{e^{2\theta} + 1} > 0\right) = \mathbb{P}(e^{2\theta} > 1) \stackrel{(a)}{=} \mathbb{P}(\ln(e^{2\theta}) > \ln(1)) \stackrel{(b)}{=} \mathbb{P}(\theta > 0) \quad (139a)$$

$$\mathbb{P}(\tanh(\theta) < 0) = \mathbb{P}\left(\frac{e^{2\theta} - 1}{e^{2\theta} + 1} < 0\right) = \mathbb{P}(e^{2\theta} < 1) \stackrel{(a)}{=} \mathbb{P}(\ln(e^{2\theta}) < \ln(1)) \stackrel{(b)}{=} \mathbb{P}(\theta < 0), \quad (139b)$$

where (a) follows from applying the monotonically increasing function  $\ln(x)$  to both sides; (b) is due to the fact that  $\ln(e^{2\theta}) = 2\theta$  and  $\ln(1) = 1$ . Accordingly, it follows directly from (139a) and (139b) that

$$\mathbb{P}(\tanh(\theta) > 0 | \mathcal{H}_{-1}) = \mathbb{P}(\theta > 0 | \mathcal{H}_{-1}) \quad (140a)$$

$$\mathbb{P}(\tanh(\theta) < 0 | \mathcal{H}_1) = \mathbb{P}(\theta < 0 | \mathcal{H}_1). \quad (140b)$$

Meanwhile, substituting (140a) and (140b) into the RHS of (138) leads to the expression

$$\check{P}_e = \frac{1}{2} [\mathbb{P}(\theta > 0 | \mathcal{H}_{-1}) + \mathbb{P}(\theta < 0 | \mathcal{H}_1)], \quad (141)$$

where  $\theta$  is defined in (135). We now simplify  $\theta$  so as to simplify the RHS of (141).

The  $K$ -th FNN layer's weight vector at convergence  $\check{\mathbf{w}}_K^{(T)} \in \mathbb{R}^{1 \times 2H}$  can be expressed via (42c) for all  $q \in [2H]$  as

$$(\check{\mathbf{w}}_K^{(T)})_q = (\check{\mathbf{w}}_K)_q + \sum_{t=0}^{T-1} (\Delta \check{\mathbf{w}}_K^{(t)})_q, \quad (142)$$

where  $(\check{\mathbf{w}}_K)_q := (\check{\mathbf{w}}_K^{(0)})_q$  is initialized with a Gaussian initializer such as LeCun normal or He normal (see Definition 10) and hence  $(\check{\mathbf{w}}_K)_q \sim \mathcal{N}(0, \alpha/2H)$  for  $\alpha \in \{1, 2\}$  ( $\alpha = 1$  for LeCun normal and  $\alpha = 2$  for He normal); and  $\Delta \check{\mathbf{w}}_K^{(t)}$  is the weight correction during the  $t$ -th iteration of SGD, SGD with momentum, RMSProp, or Adam. Meanwhile, substituting (142) into the RHS of (135) gives

$$\theta = \sum_{q=1}^{2H} \left[ (\check{\mathbf{w}}_K)_q + \sum_{t=0}^{T-1} (\Delta \check{\mathbf{w}}_K^{(t)})_q \right] (\check{\mathbf{y}}_{K-1,n}^{(T)})_q \quad (143a)$$

$$= \sum_{q=1}^{2H} (\check{\mathbf{w}}_K)_q (\check{\mathbf{y}}_{K-1,n}^{(T)})_q + \sum_{q=1}^{2H} \sum_{t=0}^{T-1} (\Delta \check{\mathbf{w}}_K^{(t)})_q (\check{\mathbf{y}}_{K-1,n}^{(T)})_q \quad (143b)$$

$$= \check{Y} + \check{S}, \quad (143c)$$

where  $(\check{\mathbf{w}}_K)_q \sim \mathcal{N}(0, \frac{\alpha}{2H})$ ;  $n \in \{N+1, \dots, N+\tilde{N}\}$ ; and  $\check{Y}$  and  $\check{S}$  are continuous RVs that have already been conditioned on a previously computed random vector  $\check{\mathbf{y}}_{K-1,n}^{(T)}$  and are defined as

$$\check{Y} = \sum_{q=1}^{2H} (\check{\mathbf{w}}_K)_q (\check{\mathbf{y}}_{K-1,n}^{(T)})_q \left| \left\{ \check{\mathbf{y}}_{K-1,n}^{(T)} \stackrel{(a)}{=} \left( \prod_{k=1}^{K-2} \check{\Sigma}_{K-k,n}^{(T)} \check{\mathbf{W}}_{K-k}^{(T)} \check{\Sigma}_{1,n}^{(T)} \check{\mathbf{w}}_1^{(T)} x_n \right) \right\} \right. \quad (144a)$$

$$\check{S} = \sum_{q=1}^{2H} \sum_{t=0}^{T-1} (\Delta \check{\mathbf{w}}_K^{(t)})_q (\check{\mathbf{y}}_{K-1,n}^{(T)})_q \left| \left\{ \check{\mathbf{y}}_{K-1,n}^{(T)} \stackrel{(a)}{=} \left( \prod_{k=1}^{K-2} \check{\Sigma}_{K-k,n}^{(T)} \check{\mathbf{W}}_{K-k}^{(T)} \check{\Sigma}_{1,n}^{(T)} \check{\mathbf{w}}_1^{(T)} x_n \right) \right\}, \quad (144b)$$

where (a) follows from (31). For a given  $\check{\mathbf{y}}_{K-1,n}^{(T)} = [(\check{\mathbf{y}}_{K-1,n}^{(T)})_1, \dots, (\check{\mathbf{y}}_{K-1,n}^{(T)})_{2H}]^\top \in \mathbb{R}^{2H}$  previously produced by the deep FNN's  $(K-1)$ -th layer,  $\check{Y}$  would be the sum of  $2H$  zero mean Gaussian RVs and hence  $\check{Y} \sim \mathcal{N}(0, \check{\sigma}^2)$ , where

$$\check{\sigma}^2 = \frac{\alpha}{2H} \sum_{q=1}^{2H} [(\check{\mathbf{y}}_{K-1,n}^{(T)})_q]^2 = \frac{\alpha}{2H} \|\check{\mathbf{y}}_{K-1,n}^{(T)}\|^2. \quad (145)$$

By substituting (143c) into the RHS of (141), the probability of point misclassification error  $\check{P}_e$  manifested by  $\check{\Phi}^{(T)}$  can be equivalently expressed as

$$\check{P}_e = \frac{1}{2} (\check{P}_e | \mathcal{H}_{-1} + \check{P}_e | \mathcal{H}_1), \quad (146)$$

where for  $\check{Y} | \mathcal{H}_{-1} \sim \mathcal{N}(0, \check{\sigma}^2 | \mathcal{H}_{-1})$  and  $\check{Y} | \mathcal{H}_1 \sim \mathcal{N}(0, \check{\sigma}^2 | \mathcal{H}_1)$

$$\check{P}_e | \mathcal{H}_{-1} = \mathbb{P}(\check{Y} + \check{S} > 0 | \mathcal{H}_{-1}) = \mathbb{P}(\check{Y} | \mathcal{H}_{-1} > -\check{S} | \mathcal{H}_{-1}) \quad (147a)$$

$$\check{P}_e | \mathcal{H}_1 = \mathbb{P}(\check{Y} + \check{S} < 0 | \mathcal{H}_1) = \mathbb{P}(\check{Y} | \mathcal{H}_1 < -\check{S} | \mathcal{H}_1). \quad (147b)$$

Furthermore, it follows from (145) that

$$\check{\sigma}^2 | \mathcal{H}_{-1} = \frac{\alpha}{2H} \|\check{\mathbf{y}}_{K-1,n}^{(T)}\|^2 | \mathcal{H}_{-1} \quad \text{and} \quad \check{\sigma}^2 | \mathcal{H}_1 = \frac{\alpha}{2H} \|\check{\mathbf{y}}_{K-1,n}^{(T)}\|^2 | \mathcal{H}_1. \quad (148)$$

We use (147a)-(147b) to derive the below closed-form expressions for  $\check{P}_e | \mathcal{H}_{-1}$  and  $\check{P}_e | \mathcal{H}_1$ .

To derive  $\check{P}_e | \mathcal{H}_{-1}$  from the RHS of (147a), we first highlight that  $\check{S} | \mathcal{H}_{-1}$  is a continuous RV that can take values in  $(-\infty, \infty)$  per (144b). Hence, we can condition on the continuous random values of  $\check{S} | \mathcal{H}_{-1}$  while employing the law of total probability for a continuous case (see Law 2) to simplify the RHS of (147a) as follows:

$$\check{P}_e | \mathcal{H}_{-1} = \mathbb{P}(\check{Y} | \mathcal{H}_{-1} > -\check{S} | \mathcal{H}_{-1}) \stackrel{(a)}{=} \int_{-\infty}^{\infty} \mathbb{P}(\check{Y} | \mathcal{H}_{-1} > -\check{S}_{-1} | \check{S}_{-1} = s) f_{\check{S}_{-1}}(s) ds \quad (149a)$$

$$= \int_{-\infty}^{\infty} \mathbb{P}(\check{Y} | \mathcal{H}_{-1} > -s) f_{\check{S}_{-1}}(s) ds, \quad (149b)$$

where  $\check{S}_{-1} := \check{S}|\mathcal{H}_{-1}$ ; (a) follows from (19) w.r.t. an event  $\mathcal{A} = \{\check{Y}|\mathcal{H}_{-1} > -\check{S}|\mathcal{H}_{-1}\}$ ; and  $f_{\check{S}_{-1}}$  is the PDF of  $\check{S}_{-1} := \check{S}|\mathcal{H}_{-1}$ . We simplify the RHS of (149b) by simplifying  $\mathbb{P}(\check{Y}|\mathcal{H}_{-1} > -s)$  w.r.t. the Gaussian RV  $\check{Y}|\mathcal{H}_{-1} \sim \mathcal{N}(0, \check{\sigma}^2|\mathcal{H}_{-1})$  for  $\check{\sigma}^2 = \check{\sigma}^2|\mathcal{H}_{-1}$  as follows:

$$\mathbb{P}(\check{Y}|\mathcal{H}_{-1} > -s) = \frac{1}{\check{\sigma}\sqrt{2\pi}} \int_{-s}^{\infty} e^{-y^2/2\check{\sigma}^2} dy \stackrel{(a)}{=} \frac{1}{\sqrt{2\pi}} \int_{-s/\check{\sigma}}^{\infty} e^{-t^2/2} dt \quad (150a)$$

$$\stackrel{(b)}{=} \mathcal{Q}(-s/\check{\sigma}) \quad (150b)$$

$$\stackrel{(c)}{=} \mathcal{Q}\left(\frac{-s\sqrt{2H/\alpha}}{\|\check{\mathbf{y}}_{K-1,n}^{(T)}\|\mathcal{H}_{-1}}\right), \quad (150c)$$

where  $\check{\sigma}^2 = \check{\sigma}^2|\mathcal{H}_{-1}$  as defined in (148); (a) follows from integration by substitution w.r.t.  $t = y/\check{\sigma}$  and thus  $dt = dy/\check{\sigma}$ ; (b) follows directly from (1); and (c) follows from (148) w.r.t.  $\check{\sigma}^2 = \check{\sigma}^2|\mathcal{H}_{-1}$ . Substituting (150c) into the RHS of (149b) then gives

$$\check{P}_e|\mathcal{H}_{-1} = \int_{-\infty}^{\infty} \mathcal{Q}\left(\frac{-s\sqrt{2H/\alpha}}{\|\check{\mathbf{y}}_{K-1,n}^{(T)}\|\mathcal{H}_{-1}}\right) f_{\check{S}_{-1}}(s) ds. \quad (151)$$

Similarly, it follows from the RHS of (147b) and the law of total probability for a continuous case (see Law 2) that

$$\check{P}_e|\mathcal{H}_1 = \mathbb{P}(\check{Y}|\mathcal{H}_1 < -\check{S}|\mathcal{H}_1) \stackrel{(a)}{=} \int_{-\infty}^{\infty} \mathbb{P}(\check{Y}|\mathcal{H}_1 < -\check{S}|\check{S}_1 = s) f_{\check{S}_1}(s) ds \quad (152a)$$

$$= \int_{-\infty}^{\infty} \mathbb{P}(\check{Y}|\mathcal{H}_1 < -s) f_{\check{S}_1}(s) ds, \quad (152b)$$

where  $\check{S}_1 := \check{S}|\mathcal{H}_1$ ; (a) follows from (19) w.r.t. an event  $\mathcal{A} = \{\check{Y}|\mathcal{H}_1 < -\check{S}|\mathcal{H}_1\}$ ; and  $f_{\check{S}_1}$  is the PDF of  $\check{S}_1 = \check{S}|\mathcal{H}_1$ . We simplify the RHS of (152b) by simplifying  $\mathbb{P}(\check{Y}|\mathcal{H}_1 < -s)$  w.r.t. the Gaussian RV  $\check{Y}|\mathcal{H}_1 \sim \mathcal{N}(0, \check{\sigma}^2|\mathcal{H}_1)$  for  $\check{\sigma}^2 = \check{\sigma}^2|\mathcal{H}_1$  as follows:

$$\mathbb{P}(\check{Y}|\mathcal{H}_1 < -s) = \frac{1}{\check{\sigma}\sqrt{2\pi}} \int_{-\infty}^{-s} e^{-y^2/2\check{\sigma}^2} dy \stackrel{(a)}{=} \frac{1}{\sqrt{2\pi}} \int_{s/\check{\sigma}}^{\infty} e^{-t^2/2} dt \quad (153a)$$

$$\stackrel{(b)}{=} \mathcal{Q}(s/\check{\sigma}) \quad (153b)$$

$$\stackrel{(c)}{=} \mathcal{Q}\left(\frac{s\sqrt{2H/\alpha}}{\|\check{\mathbf{y}}_{K-1,n}^{(T)}\|\mathcal{H}_1}\right), \quad (153c)$$

where (a) follows from integration by substitution w.r.t.  $t = -y/\check{\sigma}$  and thus  $dt = -dy/\check{\sigma}$ ; (b) follows directly from (1); and (c) follows from (148) since we let  $\check{\sigma}^2 = \check{\sigma}^2|\mathcal{H}_1$ . Thus, substituting (153c) into the RHS of (152b) leads to

$$\check{P}_e|\mathcal{H}_1 = \int_{-\infty}^{\infty} \mathcal{Q}\left(\frac{s\sqrt{2H/\alpha}}{\|\check{\mathbf{y}}_{K-1,n}^{(T)}\|\mathcal{H}_1}\right) f_{\check{S}_1}(s) ds. \quad (154)$$

Accordingly, substituting (154) and (151) into the RHS of (146) gives

$$\check{P}_e = \frac{1}{2} \left[ \int_{-\infty}^{\infty} \mathcal{Q} \left( \frac{-s\sqrt{2H/\alpha}}{\|\check{\mathbf{y}}_{K-1,n}^{(T)}\|_{\mathcal{H}_{-1}}} \right) f_{\check{S}_{-1}}(s) ds + \int_{-\infty}^{\infty} \mathcal{Q} \left( \frac{s\sqrt{2H/\alpha}}{\|\check{\mathbf{y}}_{K-1,n}^{(T)}\|_{\mathcal{H}_1}} \right) f_{\check{S}_1}(s) ds \right], \quad (155)$$

where it follows from (144b) that

$$\check{S}_{-1} := \check{S}|\mathcal{H}_{-1} = \sum_{q=1}^{2H} \sum_{t=0}^{T-1} (\Delta \check{\mathbf{w}}_K^{(t)})_q [(\check{\mathbf{y}}_{K-1,n}^{(T)})_q | \mathcal{H}_{-1}] \quad (156a)$$

$$\check{S}_1 := \check{S}|\mathcal{H}_1 = \sum_{q=1}^{2H} \sum_{t=0}^{T-1} (\Delta \check{\mathbf{w}}_K^{(t)})_q [(\check{\mathbf{y}}_{K-1,n}^{(T)})_q | \mathcal{H}_1]. \quad (156b)$$

Setting asymptotic limits on  $\|\check{\mathbf{y}}_{K-1,n}^{(T)}\|_{\mathcal{H}_{-1}}$ ,  $\|\check{\mathbf{y}}_{K-1,n}^{(T)}\|_{\mathcal{H}_1}$  makes it possible to quantify the exhibited asymptotic  $\check{P}_e$  by bounding the RHS of (155). To this end, if  $\|\check{\mathbf{y}}_{K-1,n}^{(T)}\|_{\mathcal{H}_{-1}}$ ,  $\|\check{\mathbf{y}}_{K-1,n}^{(T)}\|_{\mathcal{H}_1} \rightarrow \infty$  for  $\alpha \in \{1, 2\}$  and  $H < \infty$ , applying the limit and its properties to (155) then produces

$$\begin{aligned} \lim_{\|\check{\mathbf{y}}_{K-1,n}^{(T)}\|_{\mathcal{H}_{-1}}, \|\check{\mathbf{y}}_{K-1,n}^{(T)}\|_{\mathcal{H}_1} \rightarrow \infty} \check{P}_e &= \frac{1}{2} \left[ \int_{-\infty}^{\infty} \lim_{\|\check{\mathbf{y}}_{K-1,n}^{(T)}\|_{\mathcal{H}_{-1}}, \|\check{\mathbf{y}}_{K-1,n}^{(T)}\|_{\mathcal{H}_1} \rightarrow \infty} \mathcal{Q} \left( \frac{-s\sqrt{2H/\alpha}}{\|\check{\mathbf{y}}_{K-1,n}^{(T)}\|_{\mathcal{H}_{-1}}} \right) \times \right. \\ &\quad \lim_{\|\check{\mathbf{y}}_{K-1,n}^{(T)}\|_{\mathcal{H}_{-1}}, \|\check{\mathbf{y}}_{K-1,n}^{(T)}\|_{\mathcal{H}_1} \rightarrow \infty} f_{\check{S}_{-1}}(s) ds + \int_{-\infty}^{\infty} \lim_{\|\check{\mathbf{y}}_{K-1,n}^{(T)}\|_{\mathcal{H}_{-1}}, \|\check{\mathbf{y}}_{K-1,n}^{(T)}\|_{\mathcal{H}_1} \rightarrow \infty} \mathcal{Q} \left( \frac{s\sqrt{2H/\alpha}}{\|\check{\mathbf{y}}_{K-1,n}^{(T)}\|_{\mathcal{H}_1}} \right) \times \\ &\quad \left. \lim_{\|\check{\mathbf{y}}_{K-1,n}^{(T)}\|_{\mathcal{H}_{-1}}, \|\check{\mathbf{y}}_{K-1,n}^{(T)}\|_{\mathcal{H}_1} \rightarrow \infty} f_{\check{S}_1}(s) ds \right]. \quad (157) \end{aligned}$$

Meanwhile, it follows from the properties of limit and the  $Q$ -function that

$$\lim_{\|\check{\mathbf{y}}_{K-1,n}^{(T)}\|_{\mathcal{H}_{-1}}, \|\check{\mathbf{y}}_{K-1,n}^{(T)}\|_{\mathcal{H}_1} \rightarrow \infty} \mathcal{Q} \left( \frac{-s\sqrt{2H/\alpha}}{\|\check{\mathbf{y}}_{K-1,n}^{(T)}\|_{\mathcal{H}_{-1}}} \right) \stackrel{(a)}{=} \mathcal{Q}(0) \stackrel{(b)}{=} \frac{1}{\sqrt{2\pi}} \int_0^{\infty} \exp \left( -\frac{t^2}{2} \right) dt = \frac{1}{2} \quad (158a)$$

$$\lim_{\|\check{\mathbf{y}}_{K-1,n}^{(T)}\|_{\mathcal{H}_{-1}}, \|\check{\mathbf{y}}_{K-1,n}^{(T)}\|_{\mathcal{H}_1} \rightarrow \infty} \mathcal{Q} \left( \frac{s\sqrt{2H/\alpha}}{\|\check{\mathbf{y}}_{K-1,n}^{(T)}\|_{\mathcal{H}_1}} \right) \stackrel{(a)}{=} \mathcal{Q}(0) \stackrel{(b)}{=} \frac{1}{\sqrt{2\pi}} \int_0^{\infty} \exp \left( -\frac{t^2}{2} \right) dt = \frac{1}{2}, \quad (158b)$$

where (a) is valid for any  $s \in (-\infty, \infty)$  and (b) follows from (1). Plugging (158a) and (158b) into the RHS of (157) gives

$$\begin{aligned} \lim_{\|\check{\mathbf{y}}_{K-1,n}^{(T)}\|_{\mathcal{H}_{-1}}, \|\check{\mathbf{y}}_{K-1,n}^{(T)}\|_{\mathcal{H}_1} \rightarrow \infty} \check{P}_e &= \lim_{\|\check{\mathbf{y}}_{K-1,n}^{(T)}\|_{\mathcal{H}_{-1}}, \|\check{\mathbf{y}}_{K-1,n}^{(T)}\|_{\mathcal{H}_1} \rightarrow \infty} \left[ \int_{-\infty}^{\infty} f_{\check{S}_{-1}}(s) ds + \int_{-\infty}^{\infty} f_{\check{S}_1}(s) ds \right] \\ &\quad \times 1/4 \stackrel{(a)}{=} 1/2, \quad (159) \end{aligned}$$

where (a) is due to a PDF property (per Definition 7) that  $\int_{-\infty}^{\infty} f_{\check{S}_{-1}}(s) ds = \int_{-\infty}^{\infty} f_{\check{S}_1}(s) ds = 1$ . This proves (48a).  $\square$

To prove (48b), we first break down the RHS of (155) as follows:

$$\begin{aligned} \check{P}_e = & \frac{1}{2} \left[ \int_{-\infty}^0 \mathcal{Q} \left( \frac{-s\sqrt{2H/\alpha}}{\|\check{\mathbf{y}}_{K-1,n}^{(T)}\|_{\mathcal{H}_{-1}}} \right) f_{\check{s}_{-1}}(s) ds + \int_0^{\infty} \mathcal{Q} \left( \frac{-s\sqrt{2H/\alpha}}{\|\check{\mathbf{y}}_{K-1,n}^{(T)}\|_{\mathcal{H}_{-1}}} \right) f_{\check{s}_{-1}}(s) ds \right. \\ & \left. + \int_{-\infty}^0 \mathcal{Q} \left( \frac{s\sqrt{2H/\alpha}}{\|\check{\mathbf{y}}_{K-1,n}^{(T)}\|_{\mathcal{H}_1}} \right) f_{\check{s}_1}(s) ds \right] + \int_0^{\infty} \mathcal{Q} \left( \frac{s\sqrt{2H/\alpha}}{\|\check{\mathbf{y}}_{K-1,n}^{(T)}\|_{\mathcal{H}_1}} \right) f_{\check{s}_1}(s) ds \Big]. \quad (160) \end{aligned}$$

Consequently, (160) can also be expressed as

$$\begin{aligned} \check{P}_e = & \frac{1}{2} \left[ \int_{-\infty}^0 \mathcal{Q} \left( \frac{-s\sqrt{2H/\alpha}}{\|\check{\mathbf{y}}_{K-1,n}^{(T)}\|_{\mathcal{H}_{-1}}} \Big|_{s < 0} \right) f_{\check{s}_{-1}}(s) ds + \int_0^{\infty} \mathcal{Q} \left( \frac{-s\sqrt{2H/\alpha}}{\|\check{\mathbf{y}}_{K-1,n}^{(T)}\|_{\mathcal{H}_{-1}}} \Big|_{s > 0} \right) f_{\check{s}_{-1}}(s) ds \right. \\ & \left. + \int_{-\infty}^0 \mathcal{Q} \left( \frac{s\sqrt{2H/\alpha}}{\|\check{\mathbf{y}}_{K-1,n}^{(T)}\|_{\mathcal{H}_1}} \Big|_{s < 0} \right) f_{\check{s}_1}(s) ds \right] + \int_0^{\infty} \mathcal{Q} \left( \frac{s\sqrt{2H/\alpha}}{\|\check{\mathbf{y}}_{K-1,n}^{(T)}\|_{\mathcal{H}_1}} \Big|_{s > 0} \right) f_{\check{s}_1}(s) ds \Big]. \quad (161) \end{aligned}$$

If we now consider the condition from (48b) that  $\|\check{\mathbf{y}}_{K-1,n}^{(T)}\|_{\mathcal{H}_{-1}}, \|\check{\mathbf{y}}_{K-1,n}^{(T)}\|_{\mathcal{H}_1} \rightarrow 0$ , applying the limit and its properties to (161) leads to the expression

$$\begin{aligned} \lim_{\|\check{\mathbf{y}}_{K-1,n}^{(T)}\|_{\mathcal{H}_{-1}}, \|\check{\mathbf{y}}_{K-1,n}^{(T)}\|_{\mathcal{H}_1} \rightarrow 0} \check{P}_e = & \frac{1}{2} \left[ \int_{-\infty}^0 \lim_{\|\check{\mathbf{y}}_{K-1,n}^{(T)}\|_{\mathcal{H}_{-1}}, \|\check{\mathbf{y}}_{K-1,n}^{(T)}\|_{\mathcal{H}_1} \rightarrow 0} \mathcal{Q} \left( \frac{-s\sqrt{2H/\alpha}}{\|\check{\mathbf{y}}_{K-1,n}^{(T)}\|_{\mathcal{H}_{-1}}} \Big|_{s < 0} \right) \times \lim_{\|\check{\mathbf{y}}_{K-1,n}^{(T)}\|_{\mathcal{H}_{-1}}, \|\check{\mathbf{y}}_{K-1,n}^{(T)}\|_{\mathcal{H}_1} \rightarrow 0} f_{\check{s}_{-1}}(s) ds + \right. \\ & \int_0^{\infty} \lim_{\|\check{\mathbf{y}}_{K-1,n}^{(T)}\|_{\mathcal{H}_{-1}}, \|\check{\mathbf{y}}_{K-1,n}^{(T)}\|_{\mathcal{H}_1} \rightarrow 0} \mathcal{Q} \left( \frac{-s\sqrt{2H/\alpha}}{\|\check{\mathbf{y}}_{K-1,n}^{(T)}\|_{\mathcal{H}_{-1}}} \Big|_{s > 0} \right) \times \lim_{\|\check{\mathbf{y}}_{K-1,n}^{(T)}\|_{\mathcal{H}_{-1}}, \|\check{\mathbf{y}}_{K-1,n}^{(T)}\|_{\mathcal{H}_1} \rightarrow 0} f_{\check{s}_{-1}}(s) ds + \\ & \int_{-\infty}^0 \lim_{\|\check{\mathbf{y}}_{K-1,n}^{(T)}\|_{\mathcal{H}_{-1}}, \|\check{\mathbf{y}}_{K-1,n}^{(T)}\|_{\mathcal{H}_1} \rightarrow 0} \mathcal{Q} \left( \frac{s\sqrt{2H/\alpha}}{\|\check{\mathbf{y}}_{K-1,n}^{(T)}\|_{\mathcal{H}_1}} \Big|_{s < 0} \right) \times \lim_{\|\check{\mathbf{y}}_{K-1,n}^{(T)}\|_{\mathcal{H}_{-1}}, \|\check{\mathbf{y}}_{K-1,n}^{(T)}\|_{\mathcal{H}_1} \rightarrow 0} f_{\check{s}_1}(s) ds + \\ & \left. \int_0^{\infty} \lim_{\|\check{\mathbf{y}}_{K-1,n}^{(T)}\|_{\mathcal{H}_{-1}}, \|\check{\mathbf{y}}_{K-1,n}^{(T)}\|_{\mathcal{H}_1} \rightarrow 0} \mathcal{Q} \left( \frac{s\sqrt{2H/\alpha}}{\|\check{\mathbf{y}}_{K-1,n}^{(T)}\|_{\mathcal{H}_1}} \Big|_{s > 0} \right) \times \lim_{\|\check{\mathbf{y}}_{K-1,n}^{(T)}\|_{\mathcal{H}_{-1}}, \|\check{\mathbf{y}}_{K-1,n}^{(T)}\|_{\mathcal{H}_1} \rightarrow 0} f_{\check{s}_1}(s) ds \right]. \quad (162) \end{aligned}$$

Meanwhile, it follows from the properties of the  $Q$ -function and limit w.r.t.  $\alpha \in \{1, 2\}$  and

$H < \infty$  that

$$\lim_{\|\check{\mathbf{y}}_{K-1,n}^{(T)}\|\big|\mathcal{H}_{-1},\|\check{\mathbf{y}}_{K-1,n}^{(T)}\|\big|\mathcal{H}_1 \rightarrow 0} \mathcal{Q}\left(\frac{-s\sqrt{2H/\alpha}}{\|\check{\mathbf{y}}_{K-1,n}^{(T)}\|\big|\mathcal{H}_{-1}} \middle| s < 0\right) = \mathcal{Q}(\infty) \stackrel{(a)}{=} \frac{1}{\sqrt{2\pi}} \int_{-\infty}^{\infty} \exp(-t^2/2) dt = 0 \quad (163a)$$

$$\lim_{\|\check{\mathbf{y}}_{K-1,n}^{(T)}\|\big|\mathcal{H}_{-1},\|\check{\mathbf{y}}_{K-1,n}^{(T)}\|\big|\mathcal{H}_1 \rightarrow 0} \mathcal{Q}\left(\frac{-s\sqrt{2H/\alpha}}{\|\check{\mathbf{y}}_{K-1,n}^{(T)}\|\big|\mathcal{H}_{-1}} \middle| s > 0\right) = \mathcal{Q}(-\infty) \stackrel{(a)}{=} \frac{1}{\sqrt{2\pi}} \int_{-\infty}^{\infty} \exp(-t^2/2) dt = 1 \quad (163b)$$

$$\lim_{\|\check{\mathbf{y}}_{K-1,n}^{(T)}\|\big|\mathcal{H}_{-1},\|\check{\mathbf{y}}_{K-1,n}^{(T)}\|\big|\mathcal{H}_1 \rightarrow 0} \mathcal{Q}\left(\frac{s\sqrt{2H/\alpha}}{\|\check{\mathbf{y}}_{K-1,n}^{(T)}\|\big|\mathcal{H}_1} \middle| s < 0\right) = \mathcal{Q}(-\infty) \stackrel{(a)}{=} \frac{1}{\sqrt{2\pi}} \int_{-\infty}^{\infty} \exp(-t^2/2) dt = 1 \quad (163c)$$

$$\lim_{\|\check{\mathbf{y}}_{K-1,n}^{(T)}\|\big|\mathcal{H}_{-1},\|\check{\mathbf{y}}_{K-1,n}^{(T)}\|\big|\mathcal{H}_1 \rightarrow 0} \mathcal{Q}\left(\frac{s\sqrt{2H/\alpha}}{\|\check{\mathbf{y}}_{K-1,n}^{(T)}\|\big|\mathcal{H}_1} \middle| s > 0\right) = \mathcal{Q}(\infty) \stackrel{(a)}{=} \frac{1}{\sqrt{2\pi}} \int_{-\infty}^{\infty} \exp(-t^2/2) dt = 0, \quad (163d)$$

where (a) is due to (1). As a result, plugging (163a)-(163d) into the RHS of (162) leads to

$$\lim_{\|\check{\mathbf{y}}_{K-1,n}^{(T)}\|\big|\mathcal{H}_{-1},\|\check{\mathbf{y}}_{K-1,n}^{(T)}\|\big|\mathcal{H}_1 \rightarrow 0} \check{P}_e = \frac{1}{2} \left[ \int_0^{\infty} \lim_{\|\check{\mathbf{y}}_{K-1,n}^{(T)}\|\big|\mathcal{H}_{-1},\|\check{\mathbf{y}}_{K-1,n}^{(T)}\|\big|\mathcal{H}_1 \rightarrow 0} f_{\check{S}_{-1}}(s) ds + \int_{-\infty}^0 \lim_{\|\check{\mathbf{y}}_{K-1,n}^{(T)}\|\big|\mathcal{H}_{-1},\|\check{\mathbf{y}}_{K-1,n}^{(T)}\|\big|\mathcal{H}_1 \rightarrow 0} f_{\check{S}_1}(s) ds \right], \quad (164)$$

where  $\check{S}_{-1}$  and  $\check{S}_1$  are given by (156a) and (156b), respectively.

Since  $\|\check{\mathbf{y}}_{K-1,n}^{(T)}\|\big|\mathcal{H}_{-1}, \|\check{\mathbf{y}}_{K-1,n}^{(T)}\|\big|\mathcal{H}_1 \rightarrow 0$ ,  $(\check{\mathbf{y}}_{K-1,n}^{(T)})_q\big|\mathcal{H}_{-1}, (\check{\mathbf{y}}_{K-1,n}^{(T)})_q\big|\mathcal{H}_1 \rightarrow 0$  for all  $q \in [2H]$ . As a consequence,  $\lim_{\|\check{\mathbf{y}}_{K-1,n}^{(T)}\|\big|\mathcal{H}_{-1},\|\check{\mathbf{y}}_{K-1,n}^{(T)}\|\big|\mathcal{H}_1 \rightarrow 0} f_{\check{S}_{-1}}(s)$  and  $\lim_{\|\check{\mathbf{y}}_{K-1,n}^{(T)}\|\big|\mathcal{H}_{-1},\|\check{\mathbf{y}}_{K-1,n}^{(T)}\|\big|\mathcal{H}_1 \rightarrow 0} f_{\check{S}_1}(s)$  accurately become the Dirac delta function  $\delta(s)$ . Substituting  $\delta(s)$  into the RHS of (164) gives

$$\lim_{\|\check{\mathbf{y}}_{K-1,n}^{(T)}\|\big|\mathcal{H}_{-1},\|\check{\mathbf{y}}_{K-1,n}^{(T)}\|\big|\mathcal{H}_1 \rightarrow 0} \check{P}_e = \frac{1}{2} \left[ \int_0^{\infty} \delta(s) ds + \int_{-\infty}^0 \delta(s) ds \right] \stackrel{(a)}{=} 1, \quad (165)$$

where (a) is due to the fact that  $\int_0^{\infty} \delta(s) ds = \int_{-\infty}^0 \delta(s) ds = 1$ . This proves (48b).  $\square$

Therefore, both (48a) and (48b) are now proven. This ends the proof of Theorem 2.  $\blacksquare$

## APPENDIX E

### DERIVATION OF THE OPTIMUM BPSK DETECTOR AND ITS DETECTION PERFORMANCE

For the sake of clarity and completeness, we hereinafter provide the derivation of the optimum BPSK detector and its closed-form performance expression in this section. If we concatenate  $\tilde{\mathbf{N}}$

received signal samples vertically, to begin with, it follows from (49) for  $\tilde{N} \in \mathbb{N}_3$  that

$$\mathbf{r} = \mathbf{s}_m + \mathbf{z}, \quad (166)$$

where  $\mathbf{r} := [r[1], r[2], \dots, r[\tilde{N}]]^\top \in \mathbb{R}^{\tilde{N}}$ ;  $\mathbf{z} := [z[1], z[2], \dots, z[\tilde{N}]]^\top \in \mathbb{R}^{\tilde{N}}$ ; and  $\mathbf{s}_m$  denotes the  $m$ -th message made of  $\tilde{N}$  samples of the transmitted BPSK signal for  $m \in [2^{\tilde{N}}]$ . Since there exist  $2^{\tilde{N}}$  message sequences that can possibly satisfy (166),  $\mathbf{s}_m$  can take one of the following forms:  $\mathbf{s}_0 = [s_0, s_0, \dots, s_0, s_0]$ ;  $\mathbf{s}_1 = [s_0, s_0, \dots, s_0, s_1]$ ;  $\dots$ ;  $\mathbf{s}_{2^{\tilde{N}}-2} = [s_1, s_1, \dots, s_1, s_0]$ ; or  $\mathbf{s}_{2^{\tilde{N}}-1} = [s_1, s_1, \dots, s_1, s_1]$ . The optimum detector maximizes the probability that a message  $\mathbf{s}_m$  is correct by observing  $\mathbf{r}$ . Thus [96, eq. (4.1–8)],

$$\hat{\mathbf{s}}_m = \arg \max_{1 \leq m \leq 2^{\tilde{N}}} \mathbb{P}(\mathbf{s}_m | \mathbf{r}), \quad (167)$$

where  $\hat{\mathbf{s}}_m$  is a sequence resulting from optimum detection. The optimum detection rule given by (167) is known as the *maximum a posteriori probability* (MAP) rule [96]. This rule is employed by a MAP receiver – which is an optimum detector – and can be simplified using Bayes' rule [99], [100] as follows:

$$\hat{\mathbf{s}}_m = \arg \max_{1 \leq m \leq 2^{\tilde{N}}} \frac{\mathbb{P}(\mathbf{r} | \mathbf{s}_m) \mathbb{P}(\mathbf{s}_m)}{\mathbb{P}(\mathbf{r})} \stackrel{(a)}{=} \arg \max_{1 \leq m \leq 2^{\tilde{N}}} \mathbb{P}(\mathbf{r} | \mathbf{s}_m) \mathbb{P}(\mathbf{s}_m) \stackrel{(b)}{=} \arg \max_{1 \leq m \leq 2^{\tilde{N}}} \mathbb{P}(\mathbf{r} | \mathbf{s}_m), \quad (168)$$

where  $\mathbb{P}(\mathbf{s}_m)$  and  $\mathbb{P}(\mathbf{r})$  are the probability of the  $m$ -th sequence and the sampled received baseband signal  $\mathbf{r}$ , respectively; (a) is due to the fact that  $\mathbb{P}(\mathbf{r})$  is the same for all possible messages and independent of  $m$ ; and (b) is for  $\mathbb{P}(\mathbf{s}_m) = 1/2^{\tilde{N}}$  irrespective of  $m$  since we consider equally likely samples of the transmitted BPSK signal.

The optimum detection rule given by (168) is known as the *maximum-likelihood rule*. When this rule is employed by an optimum receiver<sup>10</sup>, it can also be expressed as [96]

$$\hat{\mathbf{s}}_m = \arg \max_{1 \leq m \leq 2^{\tilde{N}}} \mathbb{P}_{\mathbf{z}}(\mathbf{r} - \mathbf{s}_m), \quad (169)$$

where  $\mathbb{P}_{\mathbf{z}}$  denotes probability w.r.t. a Gaussian random vector  $\mathbf{z} := [z[1], z[2], \dots, z[\tilde{N}]]^\top \in \mathbb{R}^{\tilde{N}}$  and  $z[n] \sim \mathcal{N}(0, N_0/2)$  for all  $n \in [\tilde{N}]$ . Because each Gaussian sample  $z[n] \sim \mathcal{N}(0, N_0/2)$  are

<sup>10</sup>The maximum-likelihood receiver (detector) is not an optimum detector unless the messages are equiprobable [96].

sampled independently and  $\mathbb{P}(z[n]) = \frac{1}{\sqrt{\pi N_0}} e^{-\frac{((\mathbf{r})_n - (\mathbf{s}_m)_n)^2}{N_0}}$ , the RHS of (169) can be simplified as follows [96], [121]:

$$\hat{\mathbf{s}}_m = \arg \max_{1 \leq m \leq 2^{\tilde{N}}} \left[ \prod_{n=1}^{\tilde{N}} \mathbb{P}(z[n]) \right] = \arg \max_{1 \leq m \leq 2^{\tilde{N}}} \left[ \left( \frac{1}{\sqrt{\pi N_0}} \right)^{\tilde{N}} e^{-\frac{\|\mathbf{r} - \mathbf{s}_m\|^2}{N_0}} \right] \stackrel{(a)}{=} \arg \max_{1 \leq m \leq 2^{\tilde{N}}} \left[ e^{-\frac{\|\mathbf{r} - \mathbf{s}_m\|^2}{N_0}} \right] \quad (170a)$$

$$\stackrel{(b)}{=} \arg \min_{1 \leq m \leq 2^{\tilde{N}}} \frac{\|\mathbf{r} - \mathbf{s}_m\|^2}{N_0} \stackrel{(c)}{=} \arg \min_{1 \leq m \leq 2^{\tilde{N}}} \|\mathbf{r} - \mathbf{s}_m\|^2, \quad (170b)$$

where (a) is due to the fact that the dropped constant does not contribute to the maximization stated in the RHS of (170a); (b) is due to the fact that the monotonically decreasing function  $e^{-x}$  achieves its optimum value with the smallest value of  $x$ ; and (c) follows from discarding the constant  $N_0$ , as it doesn't contribute to the optimization specified in the RHS of (170b).

Note that  $\|\mathbf{r} - \mathbf{s}_m\|^2 = \|\mathbf{r}\|^2 + \|\mathbf{s}_m\|^2 - 2\langle \mathbf{r}, \mathbf{s}_m \rangle$  and  $\|\mathbf{r}\|^2 + \|\mathbf{s}_m\|^2$  is an identical constant for all  $2^{\tilde{N}}$  message sequences, since all the possible sequences have the same total energy. Accordingly, the RHS of (170b) can be simplified to

$$\hat{\mathbf{s}}_m = \arg \min_{1 \leq m \leq 2^{\tilde{N}}} -2\langle \mathbf{r}, \mathbf{s}_m \rangle = \arg \max_{1 \leq m \leq 2^{\tilde{N}}} \langle \mathbf{r}, \mathbf{s}_m \rangle. \quad (171)$$

The simplified optimum detection rule (maximum-likelihood rule) that applies to our BPSK signal detection problem is given by (171). Per this rule, the optimum decision region can be expressed as [96]

$$D_m = \left\{ \mathbf{r} \in \mathbb{R}^{\tilde{N}} : \langle \mathbf{r}, \mathbf{s}_m \rangle > \langle \mathbf{r}, \mathbf{s}_{\tilde{m}} \rangle \text{ for all } 1 \leq \tilde{m} \leq 2^{\tilde{N}} \text{ and } \tilde{m} \neq m \right\}. \quad (172)$$

If we now consider the special case of  $\tilde{N} = 1$  and  $n \in \mathbb{N}$ , it follows directly from (172) that

$$D_1 = \{r[n] \in \mathbb{R} : r[n]s_1 > r[n]s_0\} = \{r[n] \in \mathbb{R} : r[n]\sqrt{\mathcal{E}_b} > -r[n]\sqrt{\mathcal{E}_b}\} \quad (173a)$$

$$= \{r[n] \in \mathbb{R} : 2r[n]\sqrt{\mathcal{E}_b} > 0\} \quad (173b)$$

$$= \{r[n] \in \mathbb{R} : r[n] > 0\}. \quad (173c)$$

Therefore, the optimum decision threshold of the optimum BPSK detector would be  $r_{\text{th}} = 0$ . This corresponds to the optimum BPSK detector depicted in Fig. 22.

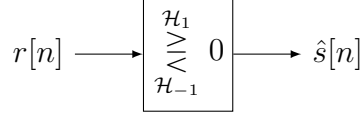


Fig. 22: Optimum detector for a BPSK signal received through an AWGN channel,  $n \in \mathbb{N}$ .

The manifested probability of bit error  $P_e$  of the detector depicted in Fig. 22 is computed as

$$P_e = \frac{1}{2} [\mathbb{P}(r[n] > 0 | \mathcal{H}_{-1}) + \mathbb{P}(r[n] < 0 | \mathcal{H}_1)], \quad (174)$$

where it follows from (49) that  $r[n] | \mathcal{H}_{-1} \sim \mathcal{N}(-\sqrt{\mathcal{E}_b}, N_0/2)$ ;  $r[n] | \mathcal{H}_1 \sim \mathcal{N}(\sqrt{\mathcal{E}_b}, N_0/2)$ ; and  $\sigma^2 = N_0/2$ . Using the Gaussian PDF given by  $f_R(r) = \frac{1}{\sigma\sqrt{2\pi}} e^{-(r-\mu)^2/(2\sigma^2)}$  for  $R \sim \mathcal{N}(\mu, \sigma^2)$  [96], it follows that

$$\mathbb{P}(r[n] < 0 | \mathcal{H}_1) = \frac{1}{\sqrt{2\pi}(N_0/2)} \int_{-\infty}^0 e^{-(r-\sqrt{\mathcal{E}_b})^2/(2 \times N_0/2)} dr. \quad (175)$$

If we now let  $t = -\frac{r-\sqrt{\mathcal{E}_b}}{\sqrt{N_0/2}}$ ,  $dt = -\frac{dr}{\sqrt{N_0/2}}$ , and  $t^2 = \frac{(r-\sqrt{\mathcal{E}_b})^2}{N_0/2}$ . Plugging these values into the RHS of (175), we obtain

$$\mathbb{P}(r[n] < 0 | \mathcal{H}_1) = -\frac{1}{\sqrt{2\pi}} \int_{\infty}^{\sqrt{2\gamma_b}} e^{-t^2/2} dt = \frac{1}{\sqrt{2\pi}} \int_{\sqrt{2\gamma_b}}^{\infty} e^{-t^2/2} dt, \quad (176)$$

where  $\gamma_b := \mathcal{E}_b/N_0$  is the SNR per bit for  $\mathcal{E}_b$  and  $N_0$  are the energy per bit and the PSD of the AWGN, respectively. Thus, by employing the definition of the  $\mathcal{Q}$ -function, the RHS of (176) can be simplified to

$$\mathbb{P}(r[n] < 0 | \mathcal{H}_1) = \mathcal{Q}(\sqrt{2\gamma_b}). \quad (177)$$

Similarly,

$$\mathbb{P}(r[n] > 0 | \mathcal{H}_{-1}) = \frac{1}{\sqrt{2\pi}(N_0/2)} \int_0^{\infty} e^{-\frac{(r+\sqrt{\mathcal{E}_b})^2}{2 \times N_0/2}} dr. \quad (178)$$

If we now let  $t = \frac{r+\sqrt{\mathcal{E}_b}}{\sqrt{N_0/2}}$ ,  $dt = \frac{dr}{\sqrt{N_0/2}}$ , and  $t^2 = \frac{(r+\sqrt{\mathcal{E}_b})^2}{N_0/2}$ . Plugging these values into the RHS of (178), it follows that

$$\mathbb{P}(r[n] > 0 | \mathcal{H}_{-1}) = \frac{1}{\sqrt{2\pi}} \int_{\sqrt{2\gamma_b}}^{\infty} e^{-t^2/2} dt \stackrel{(a)}{=} \mathcal{Q}(\sqrt{2\gamma_b}), \quad (179)$$

where (a) follows from the definition of the  $\mathcal{Q}$ -function.

Finally, substituting (177) and (179) into the RHS of (174) gives the closed-form expression

$$P_e = \mathcal{Q}(\sqrt{2\gamma_b}). \quad (180)$$

This ends the proof. ■

## APPENDIX F

## SUPPLEMENTARY RESULTS FROM THE TRAINING OF ReLU FNNs OF VARIOUS DEPTHS

The results set out in this appendix were generated using the materials and methods detailed in Section VI-B and the (hyper)parameters set out in Table VI, and are our best supplementary computer experiment results regarding the low SNR training, high SNR training, and all SNR training of ReLU FNNs of various depths. More specifically, Figs. 23-28 show the training and validation loss experienced by a shallow ReLU FNN-based BPSK detector when subject to the three training schemes; Figs. 29-34 illustrate the loss experienced by a deep ReLU FNN-based BPSK detector when subject to the three schemes; and Figs. 35-40 show the loss experienced by a deeper ReLU FNN-based BPSK detector when subject to the three schemes. Meanwhile, as can be seen in Figs. 24, 27, 30, 33, 36, and 39, at a high SNR, training stagnates after the second epoch regardless of  $K$  or  $H$ . Similar stagnation was also observed with the normalized inputs (of ReLU FNNs), though we initially wondered whether the large positive or negative samples – of the received BPSK signal – causes the stagnation in learning.

TABLE VI: (Hyper)parameters of computer experiments – unless otherwise mentioned – concerning binary classifiers based on ReLU FNNs.

(Hyper)parameters	Type/Value	Remark(s)
$(K, H)$	$\{(3, 3), (3, 9), (7, 7)\}$ $\{(7, 14), (9, 9), (9, 18)\}$	Shallow/deep depth dimensions and narrow/wide width dimensions
Training-validation split	80% to 20%	Chosen value
Learning rate	0.01	Experimented value that led to optimum testing performance
Epoch size	200	Maximum epoch size.
Batch size	80	Experimented value that led to optimum testing performance
Optimizer	Adam [122]	Adam produced minimum loss and converged fast.
Activation function (for ReLU FNNs)	ReLU	For ReLU FNNs, all layers of the respective network have a ReLU activation except the output layer which is linear.
Loss function (for all layers)	hinge	The focus of this work has been ReLU FNNs trained with the hinge loss.
Metrics	accuracy	Training measure of our ReLU FNN-based BPSK detector.
Kernel initializer (for all layers)	he_normal [108]	$\mathbf{W}_k(i, :) \sim \mathcal{N}(\mathbf{0}, \sigma^2 \mathbf{I}_{N_{k-1}})$ , $\sigma^2 = 2/N_{k-1}$ and $i \in [N_k]$ .
Kernel constraint (for all layers)	min_max_norm(1, 5)	Experimented value that led to optimum testing performance
Bias (for all layers)	0	We investigated ReLU FNNs with no biases. ReLU FNNs with biases can be inferred from ReLU FNNs with no biases.

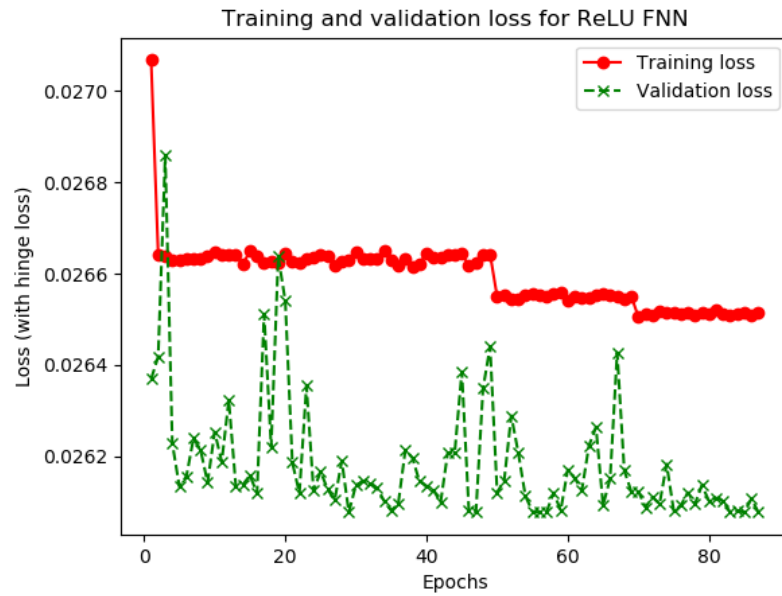


Fig. 23: Training and validation loss of a ReLU FNN-based BPSK detector under an all SNR training scheme:  $(K, H) = (3, 3)$ .

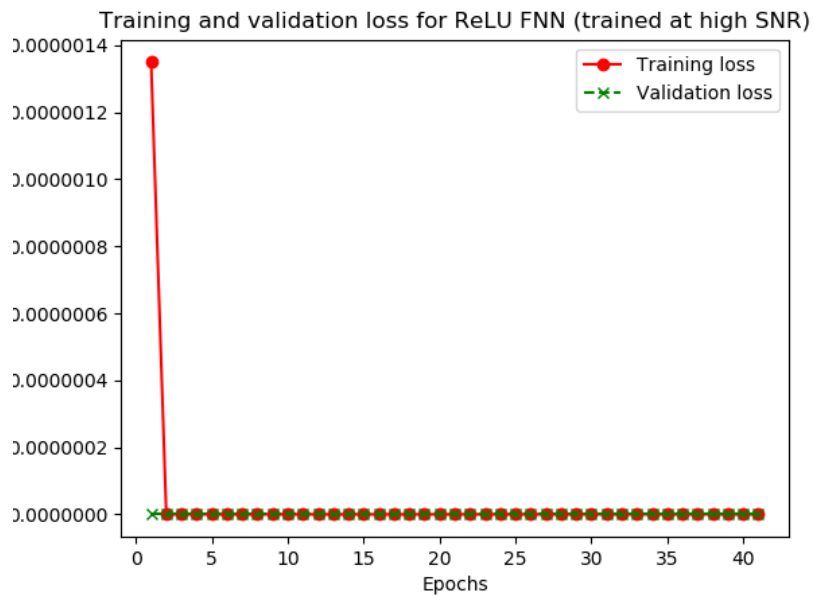


Fig. 24: Training and validation loss of a ReLU FNN-based BPSK detector under a high SNR training scheme:  $(K, H) = (3, 3)$ .

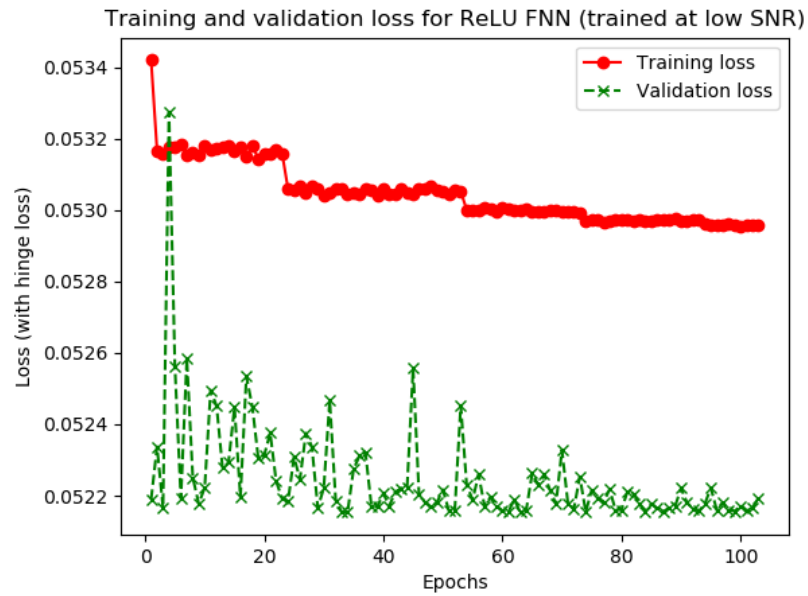


Fig. 25: Training and validation loss of a ReLU FNN-based BPSK detector under a low SNR training scheme:  $(K, H) = (3, 3)$ .

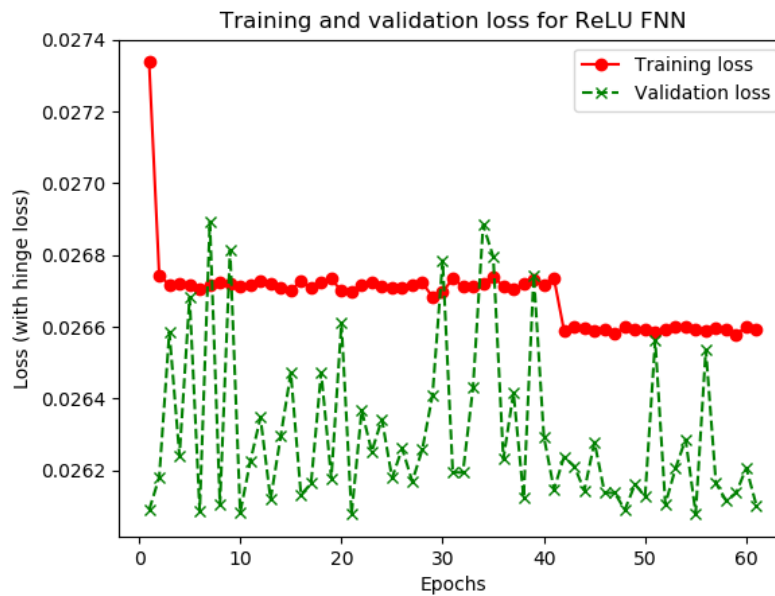


Fig. 26: Training and validation loss of a ReLU FNN-based BPSK detector under an all SNR training scheme:  $(K, H) = (3, 9)$ .

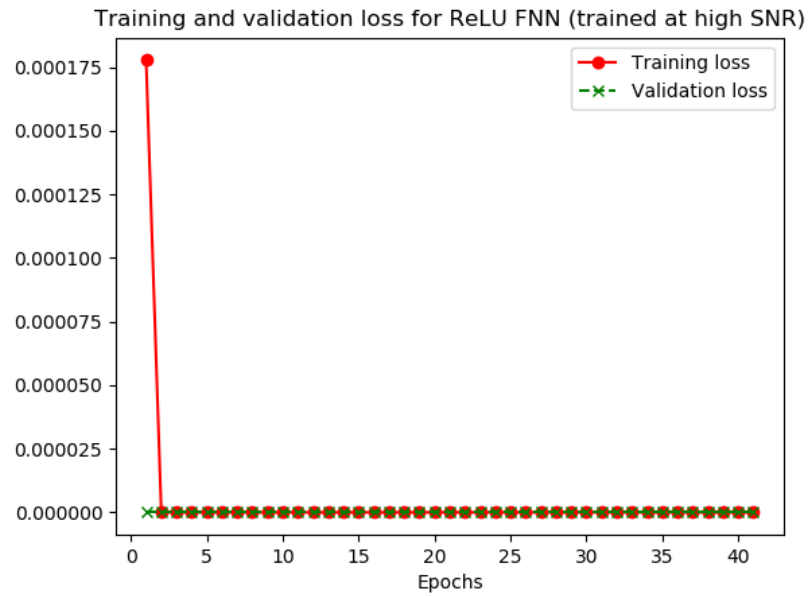


Fig. 27: Training and validation loss of a ReLU FNN-based BPSK detector under a high SNR training scheme:  $(K, H) = (3, 9)$ .

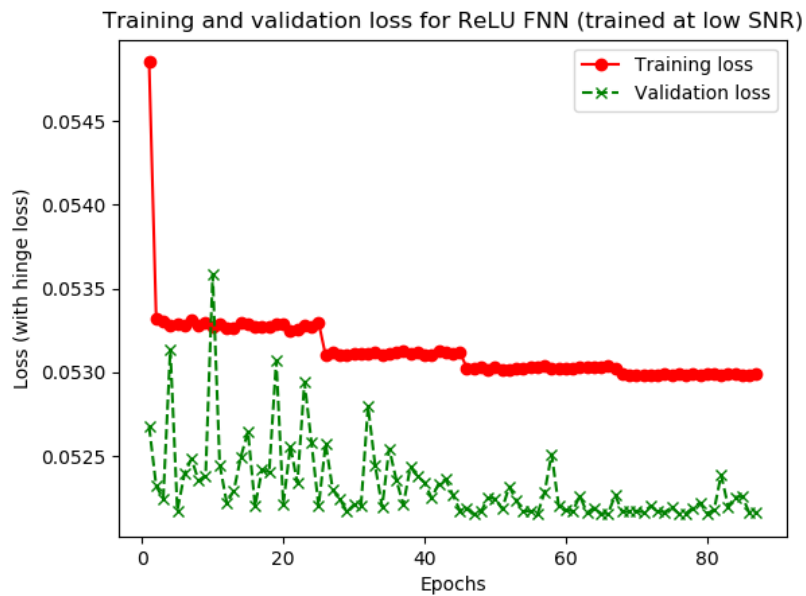


Fig. 28: Training and validation loss of a ReLU FNN-based BPSK detector under a low SNR training scheme:  $(K, H) = (3, 9)$ .

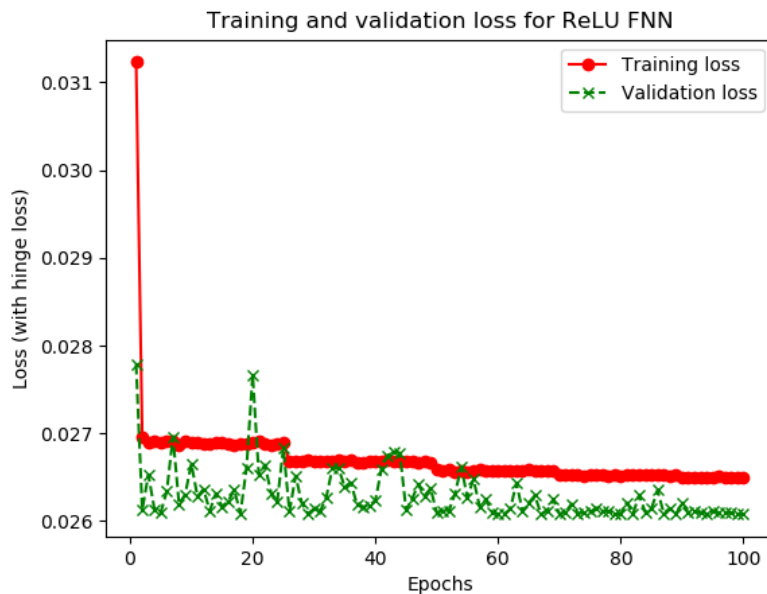


Fig. 29: Training and validation loss of a ReLU FNN-based BPSK detector under an all SNR training scheme:  $(K, H) = (7, 7)$ .

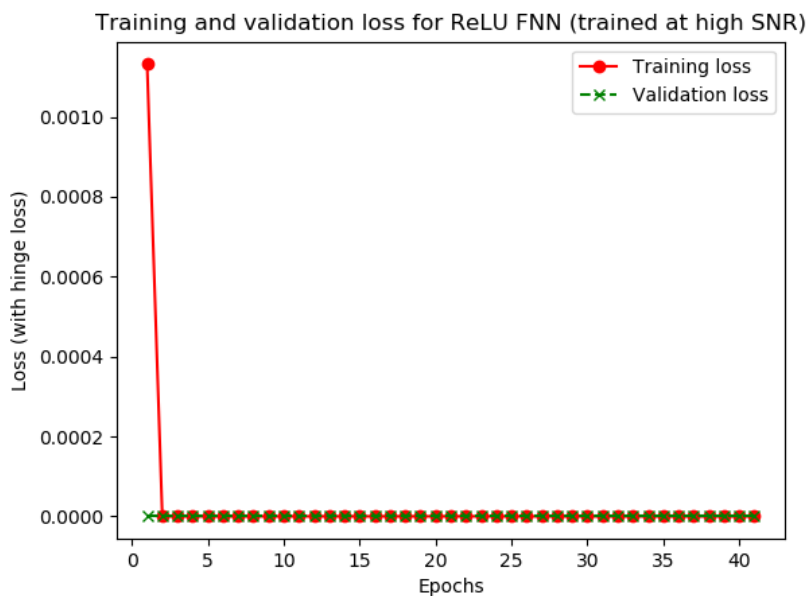


Fig. 30: Training and validation loss of a ReLU FNN-based BPSK detector under a high SNR training scheme:  $(K, H) = (7, 7)$ .

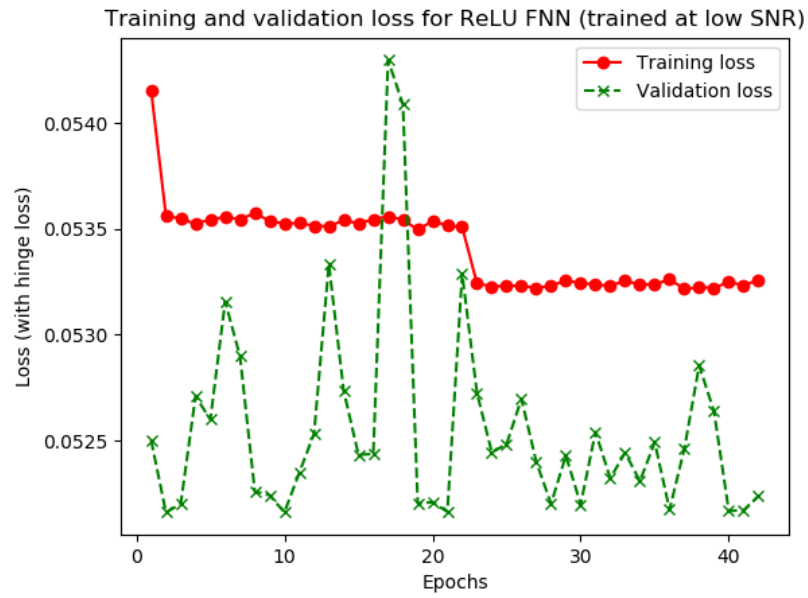


Fig. 31: Training and validation loss of a ReLU FNN-based BPSK detector under a low SNR training scheme:  $(K, H) = (7, 7)$ .

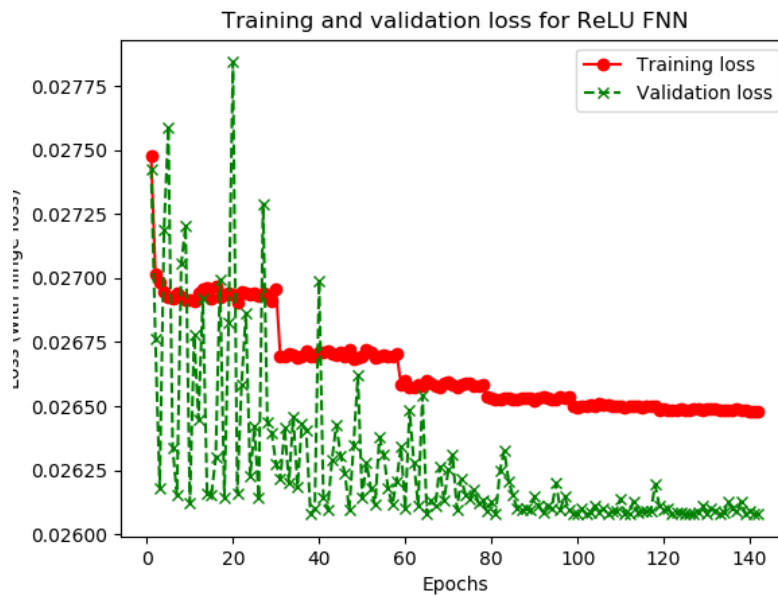


Fig. 32: Training and validation loss of a ReLU FNN-based BPSK detector under an all SNR training scheme:  $(K, H) = (7, 14)$ .

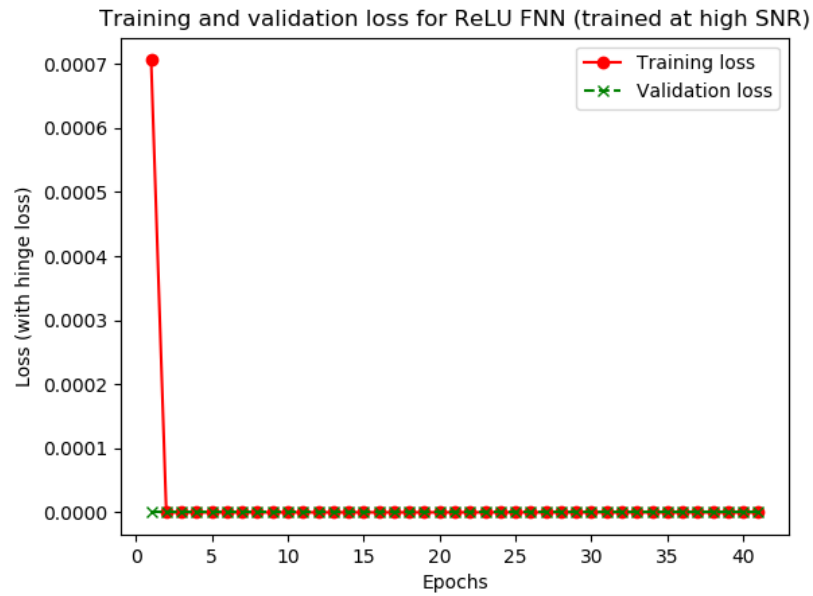


Fig. 33: Training and validation loss of a ReLU FNN-based BPSK detector under a high SNR training scheme:  $(K, H) = (7, 14)$ .

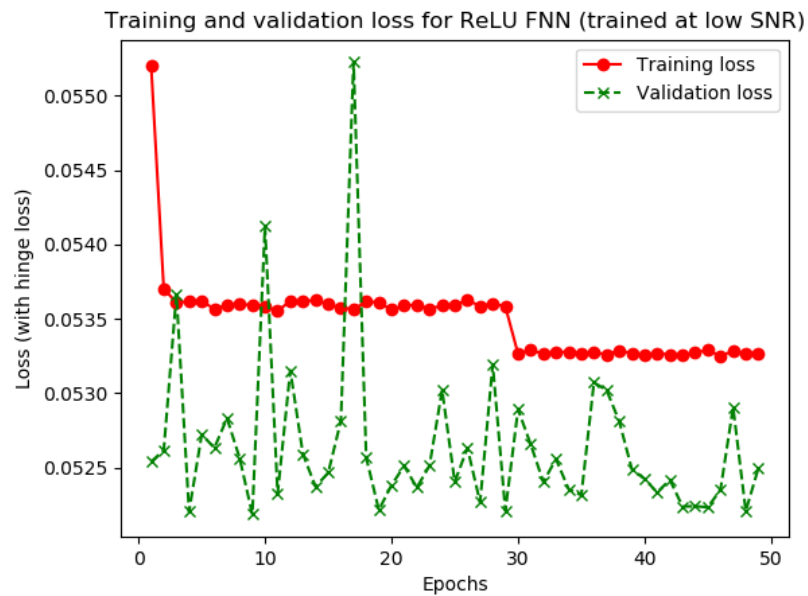


Fig. 34: Training and validation loss of a ReLU FNN-based BPSK detector under a low SNR training scheme:  $(K, H) = (7, 14)$ .

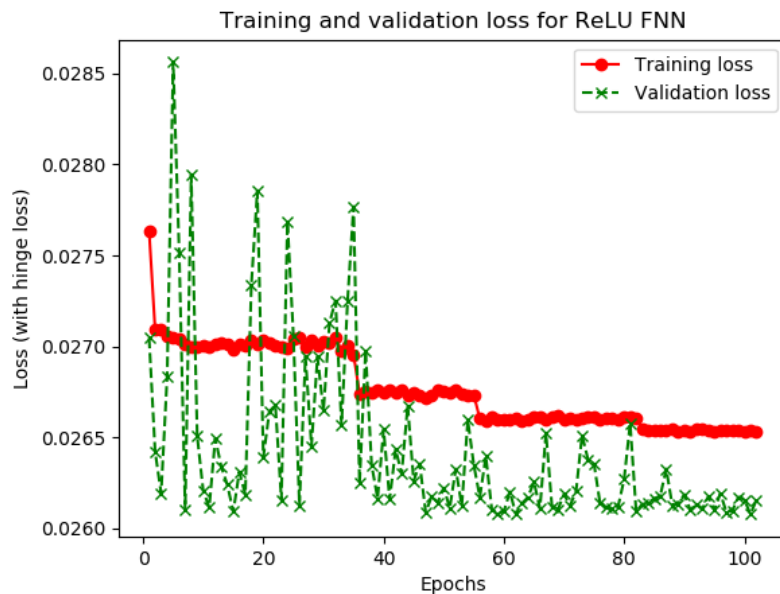


Fig. 35: Training and validation loss of a ReLU FNN-based BPSK detector under an all SNR training scheme:  $(K, H) = (9, 9)$ .

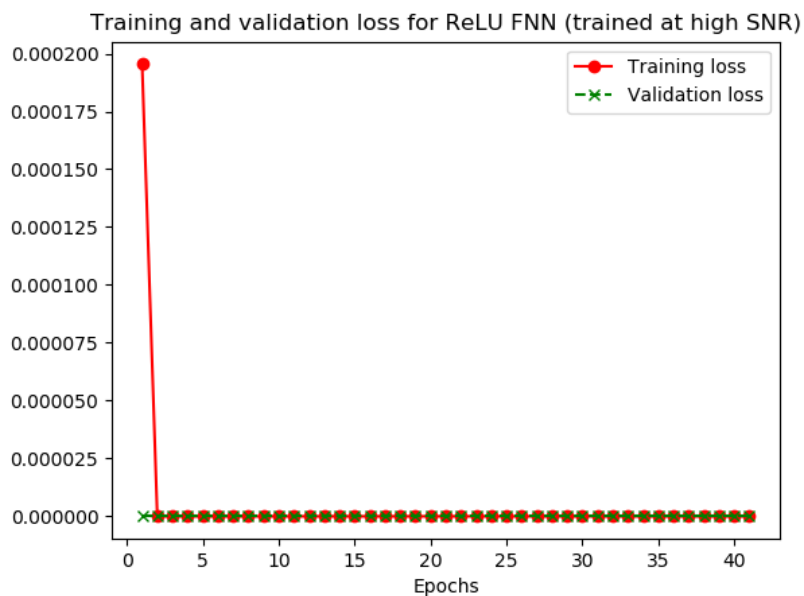


Fig. 36: Training and validation loss of a ReLU FNN-based BPSK detector under a high SNR training scheme:  $(K, H) = (9, 9)$ .

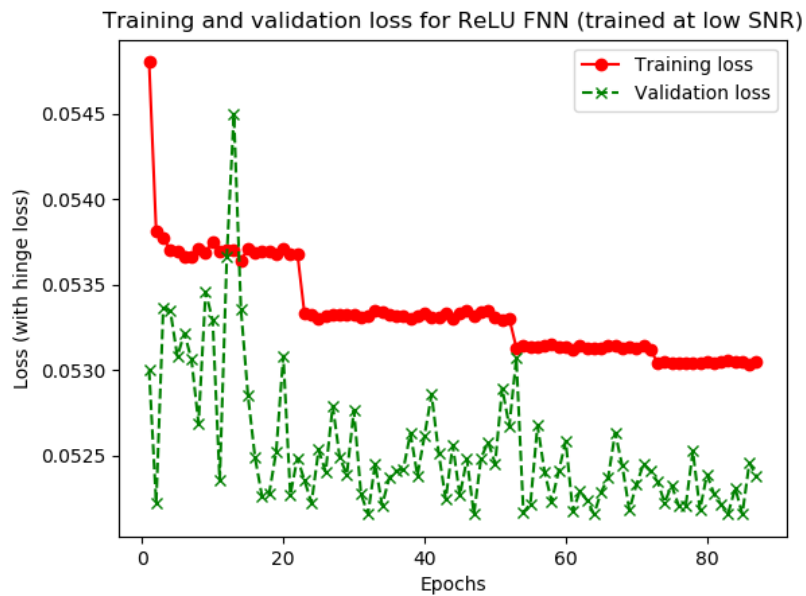


Fig. 37: Training and validation loss of a ReLU FNN-based BPSK detector under a low SNR training scheme:  $(K, H) = (9, 9)$ .

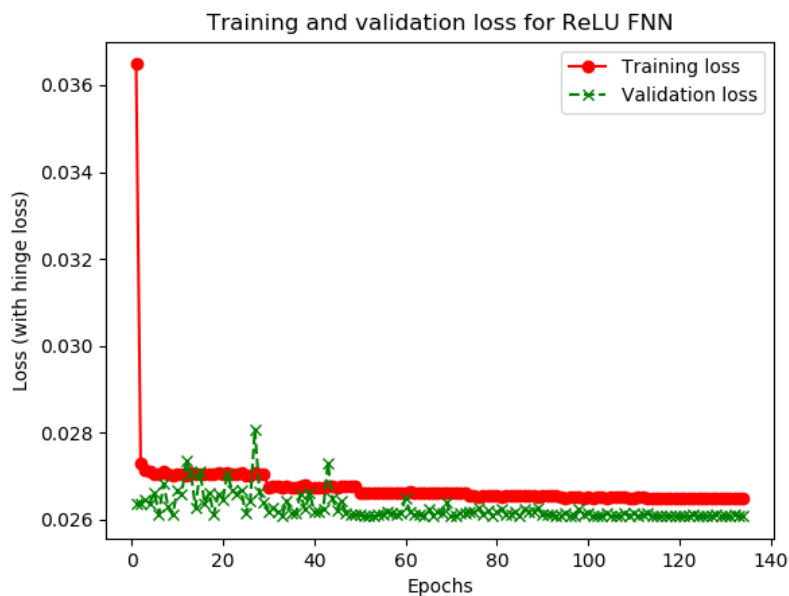


Fig. 38: Training and validation loss of a ReLU FNN-based BPSK detector under an all SNR training scheme:  $(K, H) = (9, 18)$ .

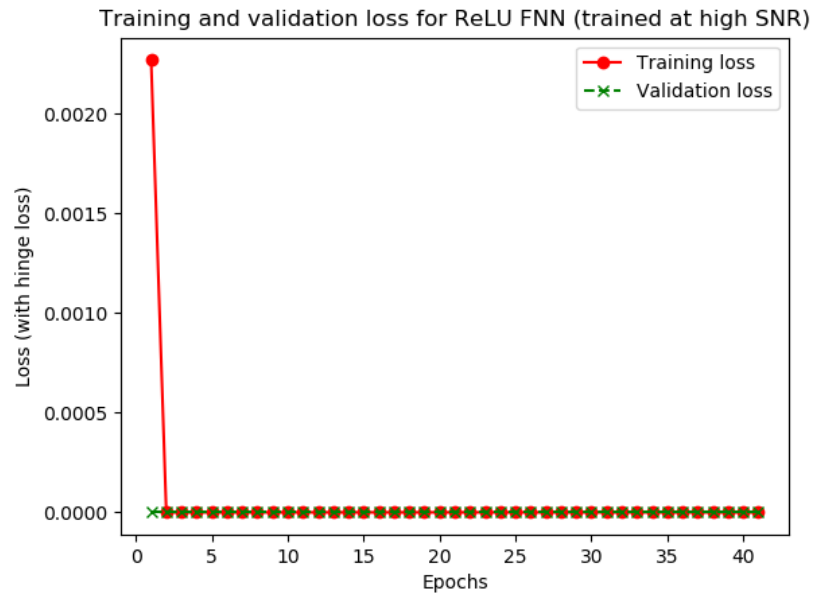


Fig. 39: Training and validation loss of a ReLU FNN-based BPSK detector under a high SNR training scheme:  $(K, H) = (9, 18)$ .

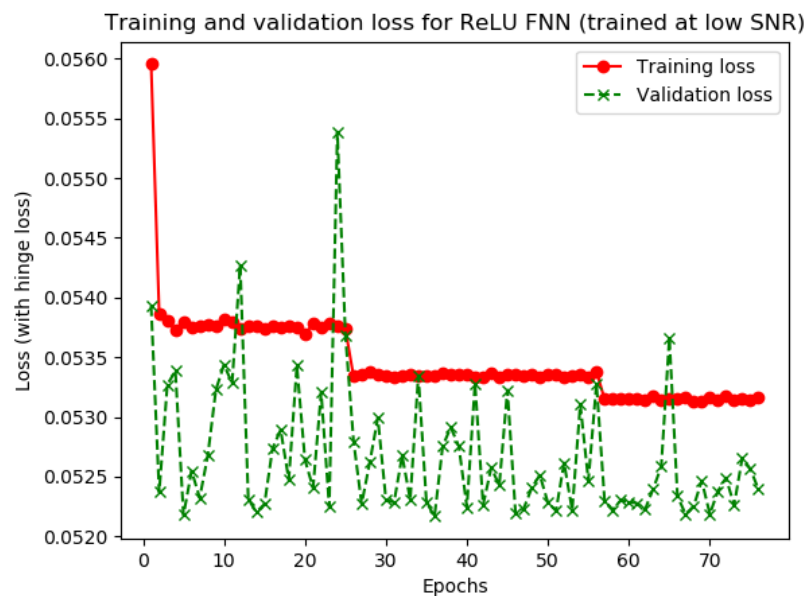


Fig. 40: Training and validation loss of a ReLU FNN-based BPSK detector under a low SNR training scheme:  $(K, H) = (9, 18)$ .

TABLE VII: (Hyper)parameters of our computer experiments – unless otherwise mentioned – regarding binary classifiers based on FNNs with ReLU and Tanh activation.

(Hyper)parameters	Type/Value	Remark(s)
$(K, H)$	$\{(3, 3), (3, 9)\}$ $\{(4, 8), (7, 7)\}$	Shallow/deep depth dimensions and narrow/wide width dimensions
Training-validation split	80% to 20%	Chosen value
Learning rate	0.01	Experimented value that led to optimum testing performance
Epoch size	200	Maximum epoch size.
Batch size	40	Experimented value that led to optimum testing performance
Optimizer	Adam [122]	Adam produced minimum loss and converged fast.
Activation function (for FNNs with ReLU and Tanh activations)	ReLU and Tanh	For FNNs with ReLU and Tanh activations, all layers of the respective network have a ReLU activation except the output layer which has a Tanh activation.
Loss function (for all layers)	hinge	The focus of this work has been ReLU FNNs trained with the hinge loss.
Metrics	accuracy	Training measure of our ReLU FNN-based BPSK detector.
Kernel initializer (for all layers)	he_normal [108]	$\mathbf{W}_k(i, :) \sim \mathcal{N}(\mathbf{0}, \sigma^2 \mathbf{I}_{N_{k-1}})$ , $\sigma^2 = 2/N_{k-1}$ and $i \in [N_k]$ .
Kernel constraint (for all layers)	min_max_norm(1, 5)	Experimented value that led to optimum testing performance
Bias (for all layers)	0	We investigated ReLU FNNs with no biases. ReLU FNNs with biases can be inferred from ReLU FNNs with no biases.

## APPENDIX G

### SUPPLEMENTARY RESULTS FROM THE TRAINING OF FNNs WITH RELU AND TANH ACTIVATION

The results reported in this appendix were produced using the materials and methods detailed in Section VI-B and the (hyper)parameters set out in Table VII, and are our best supplementary computer experiment results regarding the low SNR training, high SNR training, and all SNR training of FNNs with ReLU and Tanh activation. More specifically, Figs. 41-49 show the loss experienced by a BPSK detector that is based on a shallow FNN with ReLU and Tanh activation when subject to the three training schemes, and Figs. 50-52 illustrate the loss experienced by a BPSK detector that is based on a deep FNN with ReLU and Tanh activation when subject to the three training schemes. Meanwhile, as can be seen in Figs. 42, 45, 48, and 51, at a high SNR, training stagnates after the second epoch irrespective of  $K$  or  $H$ .

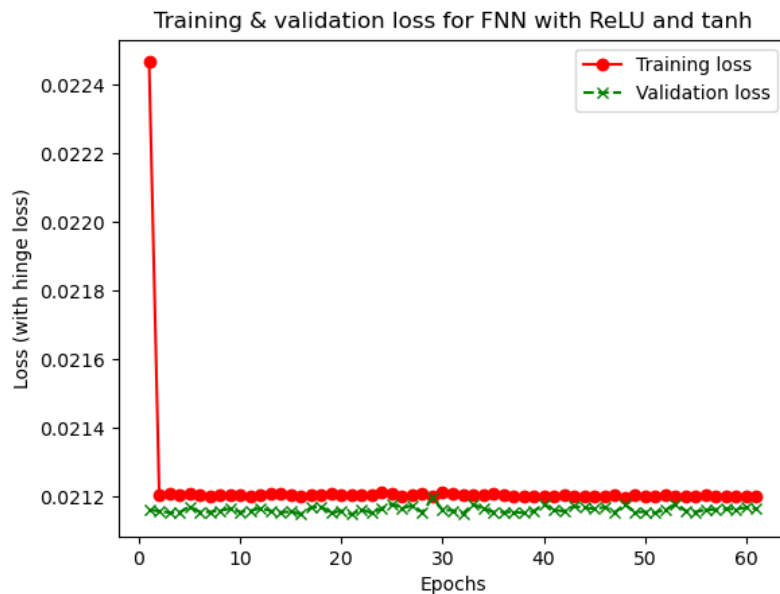


Fig. 41: Training and validation loss of an FNN-based BPSK detector under an all SNR training scheme:  $(K, H) = (3, 3)$ .

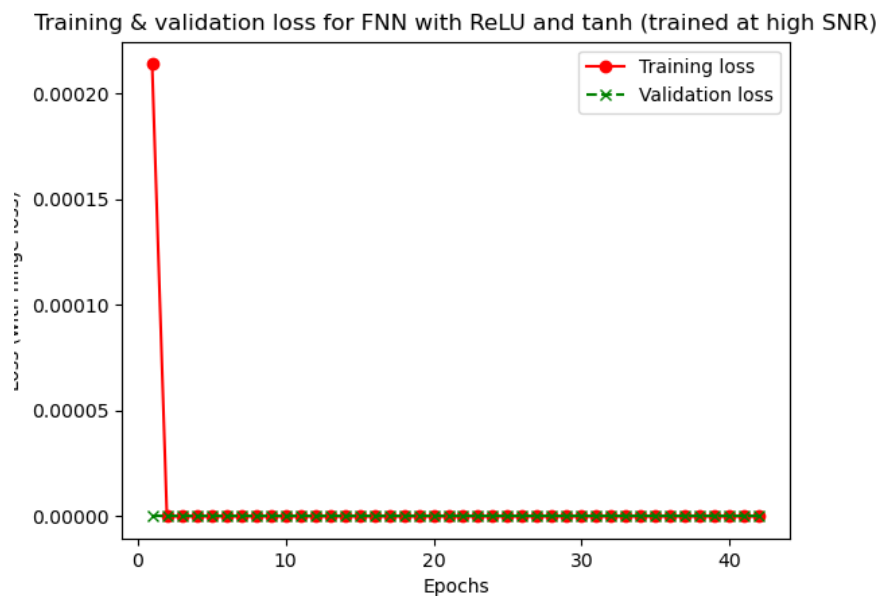


Fig. 42: Training and validation loss of an FNN-based BPSK detector under a high SNR training scheme:  $(K, H) = (3, 3)$ .

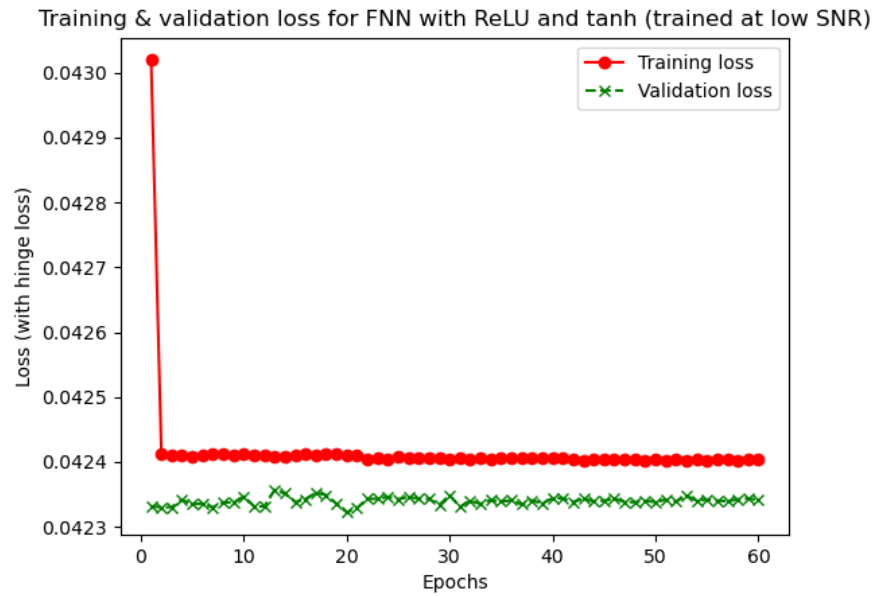


Fig. 43: Training and validation loss of an FNN-based BPSK detector under a low SNR training scheme:  $(K, H) = (3, 3)$ .

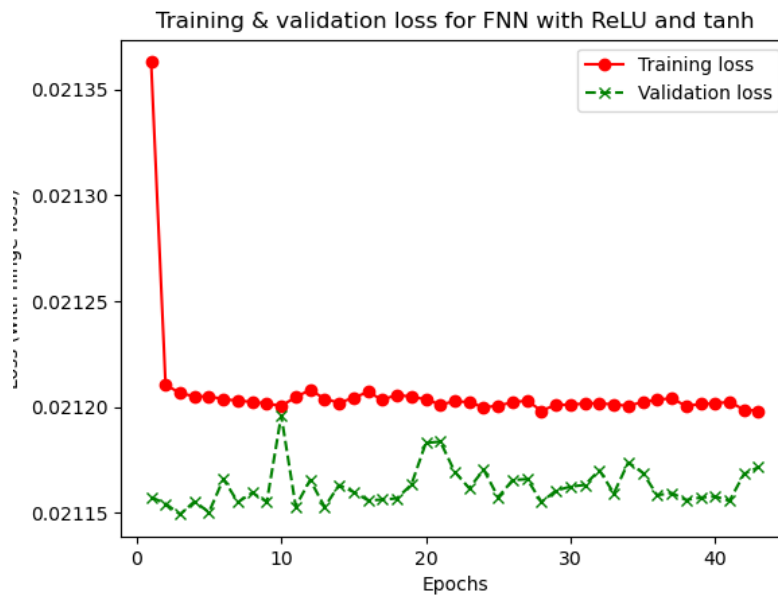


Fig. 44: Training and validation loss of an FNN-based BPSK detector under an all SNR training scheme:  $(K, H) = (3, 9)$ .

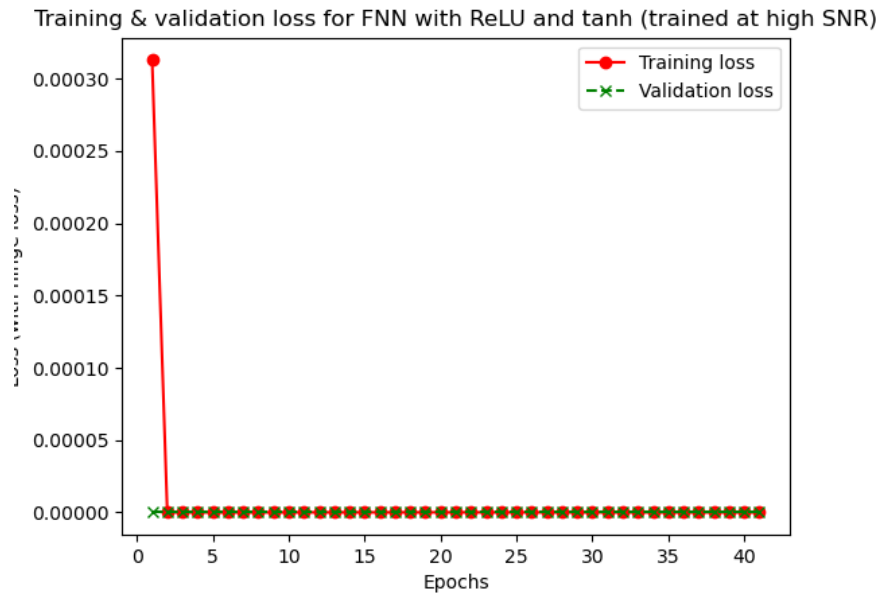


Fig. 45: Training and validation loss of an FNN-based BPSK detector under a high SNR training scheme:  $(K, H) = (3, 9)$ .

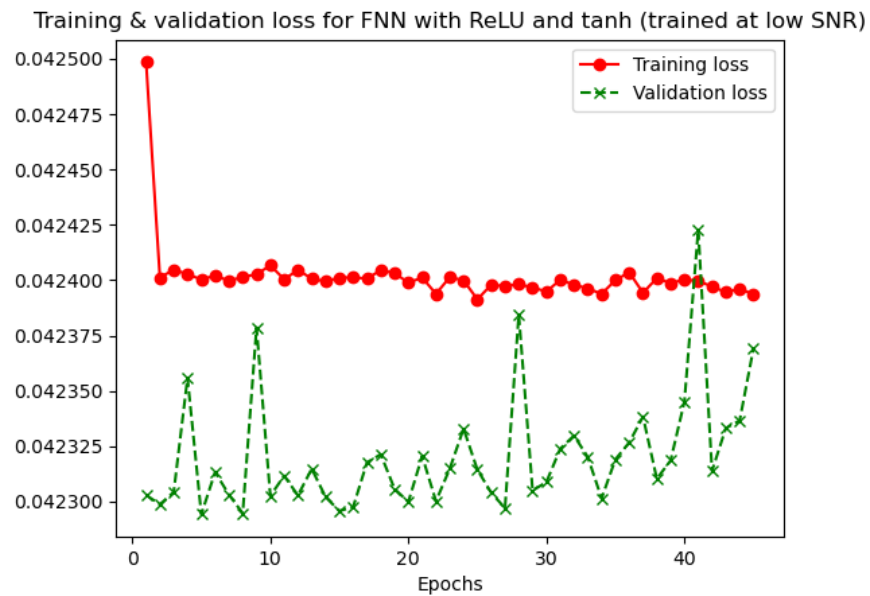


Fig. 46: Training and validation loss of an FNN-based BPSK detector under a low SNR training scheme:  $(K, H) = (3, 9)$ .

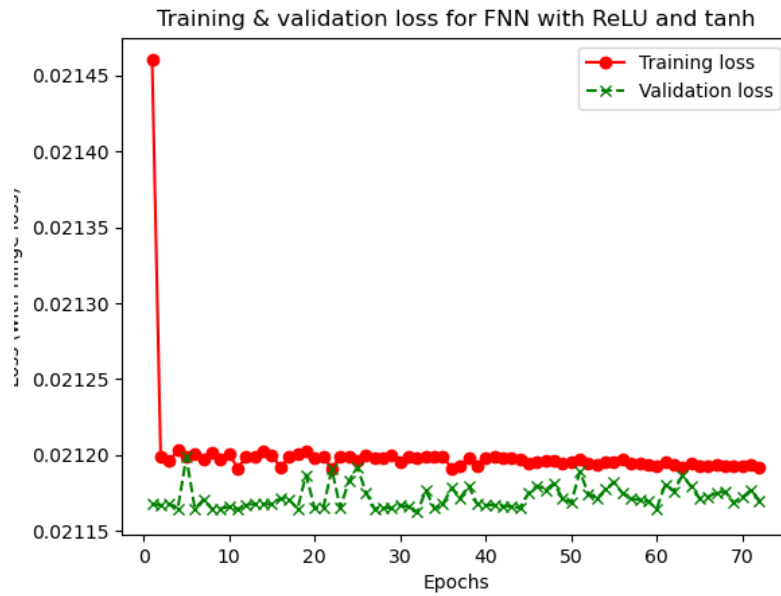


Fig. 47: Training and validation loss of an FNN-based BPSK detector under an all SNR training scheme:  $(K, H) = (4, 8)$ .

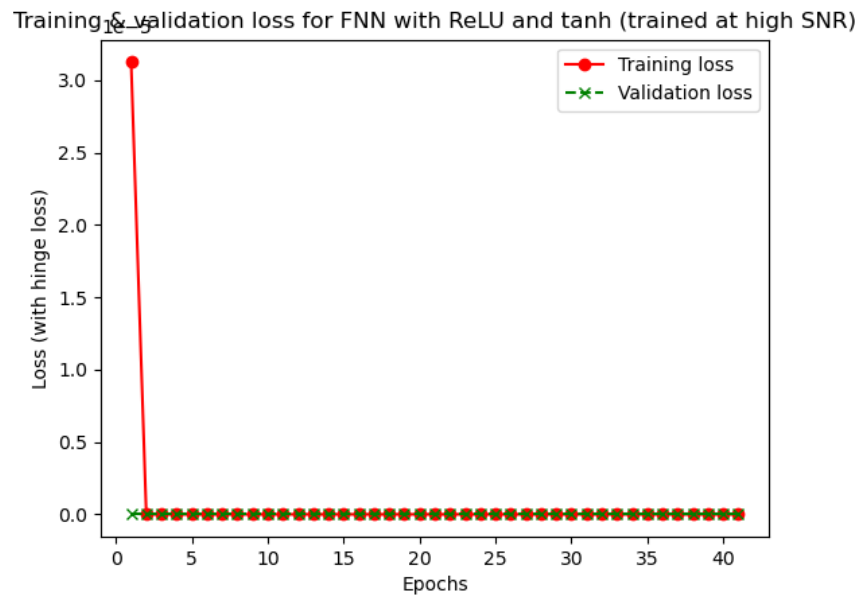


Fig. 48: Training and validation loss of an FNN-based BPSK detector under a high SNR training scheme:  $(K, H) = (4, 8)$ .

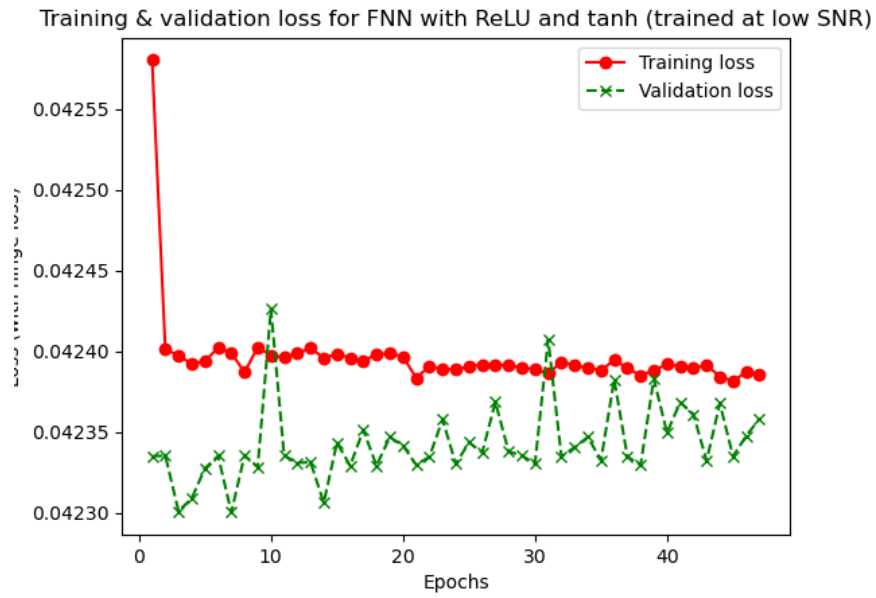


Fig. 49: Training and validation loss of an FNN-based BPSK detector under a low SNR training scheme:  $(K, H) = (4, 8)$ .

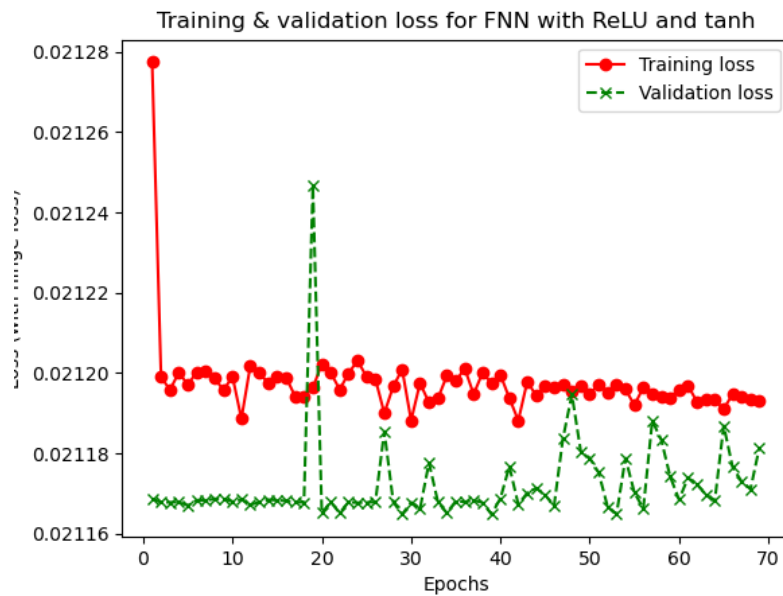


Fig. 50: Training and validation loss of an FNN-based BPSK detector under an all SNR training scheme:  $(K, H) = (7, 7)$ .

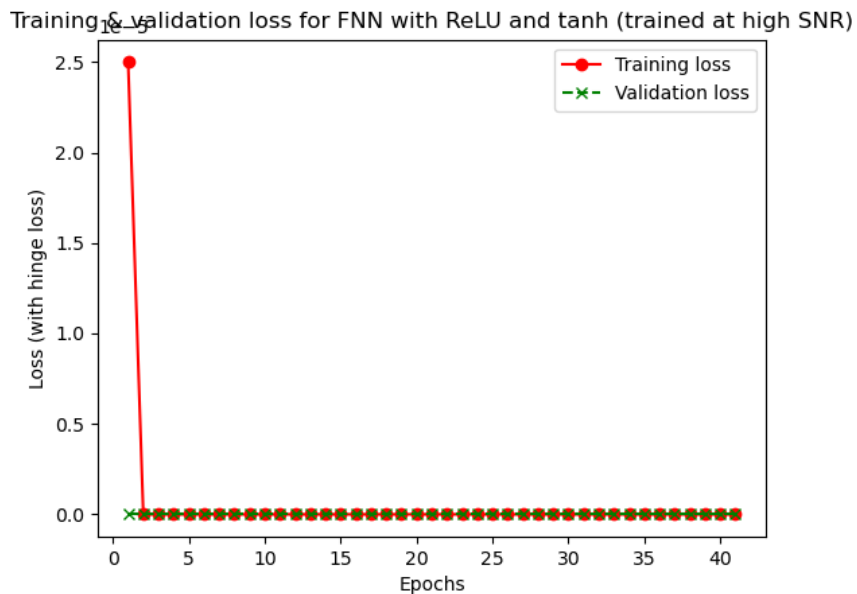


Fig. 51: Training and validation loss of an FNN-based BPSK detector under a high SNR training scheme:  $(K, H) = (7, 7)$ .

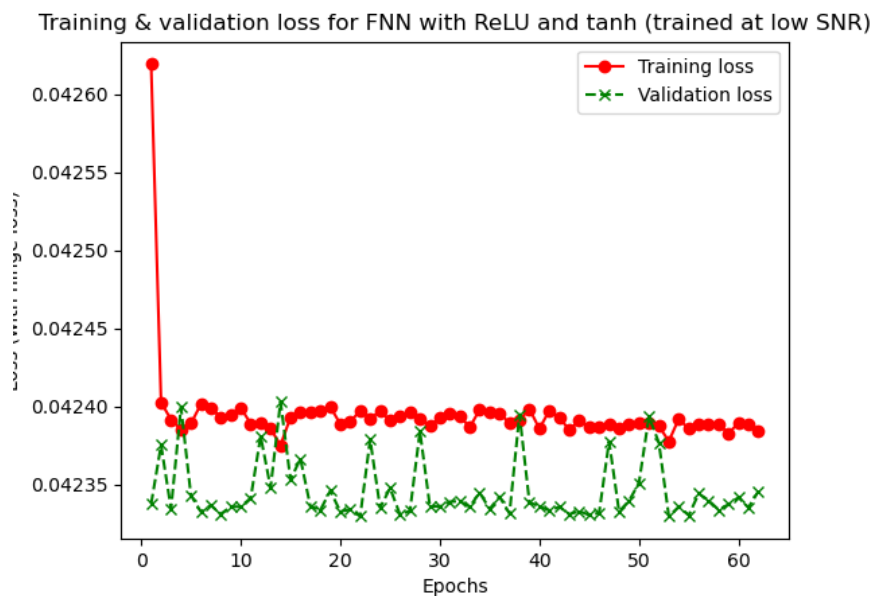


Fig. 52: Training and validation loss of an FNN-based BPSK detector under a low SNR training scheme:  $(K, H) = (7, 7)$ .

## ACKNOWLEDGMENTS

The first author acknowledges Prof. Ali H. Sayed (EPFL, Switzerland) for a fruitful discussion and expert criticisms, which have inspired this work; the U.S. Department of Commerce and its agency NIST for a prior funding support that helped to lay the foundation for this work.

## DISCLAIMER

The identification of any commercial product or trade name does not imply endorsement or recommendation by the National Institute of Standards and Technology, nor is it intended to imply that the materials or equipment identified are necessarily the best available for the purpose.

## REFERENCES

- [1] Y. Lecun, Y. Bengio, and G. Hinton, "Deep learning," *Nature*, vol. 521, pp. 436–444, May 2015.
- [2] L. Deng and D. Yu, "Deep learning: Methods and applications," *Found. Trends Signal Process.*, vol. 7, no. 3–4, pp. 197–387, 2014.
- [3] I. Goodfellow, Y. Bengio, and A. Courville, *Deep Learning*. The MIT Press, 2016.
- [4] A. W. Senior *et al.*, "Improved protein structure prediction using potentials from deep learning," *Nature*, vol. 577, pp. 706–710, 2020.
- [5] V. Mnih *et al.*, "Human-level control through deep reinforcement learning," *Nature*, vol. 518, no. 7540, pp. 529–533, 2015.
- [6] David Silver *et al.*, "Mastering the game of Go with deep neural networks and tree search," *Nature*, vol. 529, pp. 484–489, 2016.
- [7] Q. Mao, F. Hu, and Q. Hao, "Deep learning for intelligent wireless networks: A comprehensive survey," *IEEE Commun. Surveys Tuts.*, vol. 20, no. 4, pp. 2595–2621, 4th Quart. 2018.
- [8] N. C. Luong, D. T. Hoang, S. Gong, D. Niyato, P. Wang, Y.-C. Liang, and D. I. Kim, "Applications of deep reinforcement learning in communications and networking: A survey," *IEEE Commun. Surveys Tuts.*, vol. 21, no. 4, pp. 3133–3174, 2019.
- [9] C. Zhang, P. Patras, and H. Haddadi, "Deep learning in mobile and wireless networking: A survey," *IEEE Commun. Surveys Tuts.*, vol. 21, no. 3, pp. 2224–2287, 3rd Quart. 2019.
- [10] M. Chen, U. Challita, W. Saad, C. Yin, and M. Debbah, "Artificial neural networks-based machine learning for wireless networks: A tutorial," *IEEE Commun. Surveys Tuts.*, vol. 21, no. 4, pp. 3039–3071, 2019.
- [11] D. Gündüz, P. de Kerret, N. D. Sidiropoulos, D. Gesbert, C. R. Murthy, and M. van der Schaar, "Machine learning in the air," *IEEE J. Sel. Areas Commun.*, vol. 37, no. 10, pp. 2184–2199, 2019.
- [12] H. Huang, S. Guo, G. Gui, Z. Yang, J. Zhang, H. Sari, and F. Adachi, "Deep learning for physical-layer 5G wireless techniques: Opportunities, challenges and solutions," *IEEE Wireless Commun.*, vol. 27, no. 1, pp. 214–222, 2020.
- [13] T. O'Shea and J. Hoydis, "An introduction to deep learning for the physical layer," *IEEE Trans. Cogn. Commun. Netw.*, vol. 3, no. 4, pp. 563–575, 2017.
- [14] H. He, C. Wen, S. Jin, and G. Y. Li, "Model-driven deep learning for MIMO detection," *IEEE Trans. Signal Process.*, vol. 68, pp. 1702–1715, 2020.

- [15] J. Han, A. Jentzen, and W. E, “Solving high-dimensional partial differential equations using deep learning,” *Proc. Natl. Acad. Sci. U.S.A.*, vol. 115, no. 34, pp. 8505–8510, 2018. [Online]. Available: <https://www.pnas.org/content/115/34/8505>
- [16] B. Adcock and N. Dexter, “The gap between theory and practice in function approximation with deep neural networks,” *SIAM J. Math Data Sci.*, vol. 3, pp. 624–655, Jan. 2021.
- [17] A. Esteva, B. Kuprel, R. A. Novoa, J. M. Ko, S. M. Swetter, H. M. Blau, and S. Thrun, “Dermatologist-level classification of skin cancer with deep neural networks,” *Nature*, vol. 542, pp. 115–118, 2017.
- [18] J. De Fauw *et al.*, “Clinically applicable deep learning for diagnosis and referral in retinal disease,” *Nat. Med.*, vol. 24, pp. 1342–1350, 2018.
- [19] A. M. Saxe, J. L. McClelland, and S. Ganguli, “A mathematical theory of semantic development in deep neural networks,” *Proc. Natl. Acad. Sci. U.S.A.*, vol. 116, no. 23, pp. 11 537–11 546, 2019. [Online]. Available: <https://www.pnas.org/content/116/23/11537>
- [20] A. Radhakrishnan, M. Belkin, and C. Uhler, “Overparameterized neural networks implement associative memory,” *Proc. Natl. Acad. Sci. U.S.A.*, vol. 117, no. 44, pp. 27 162–27 170, 2020. [Online]. Available: <https://www.pnas.org/content/117/44/27162>
- [21] A. H. Marblestone, G. Wayne, and K. P. Kording, “Toward an integration of deep learning and neuroscience,” *Front. Comput. Neurosci.*, vol. 10, 2016.
- [22] G. Carleo and M. Troyer, “Solving the quantum many-body problem with artificial neural networks,” *Science*, vol. 355, no. 6325, pp. 602–606, 2017.
- [23] Y. Levine, O. Sharir, N. Cohen, and A. Shashua, “Quantum entanglement in deep learning architectures,” *Phys. Rev. Lett.*, vol. 122, p. 065301, Feb. 2019.
- [24] P. Baldi, P. Sadowski, and D. Whiteson, “Searching for exotic particles in high-energy physics with deep learning.” *Nat. Commun.*, vol. 5, Jul. 2014.
- [25] J. Ma, R. P. Sheridan, A. Liaw, G. E. Dahl, and V. Svetnik, “Deep neural nets as a method for quantitative structure-activity relationships,” *J. Chem. Inf. Model.*, vol. 55 2, pp. 263–74, 2015.
- [26] L. Liu, W. Ouyang, X. Wang, P. Fieguth, J. Chen, X. Liu, and M. P. äinen, “Deep learning for generic object detection: A survey,” 2019. [Online]. Available: <https://arxiv.org/pdf/1809.02165.pdf>
- [27] T. Young, D. Hazarika, S. Poria, and E. Cambria, “Recent trends in deep learning based natural language processing,” *IEEE Comput. Intell. Mag.*, vol. 13, no. 3, pp. 55–75, 2018.
- [28] A. Torfi, R. A. Shirvani, Y. Keneshloo, N. Tavaf, and E. A. Fox, “Natural language processing advancements by deep learning: A survey,” 2020. [Online]. Available: <https://arxiv.org/pdf/2003.01200.pdf>
- [29] G. Hinton, L. Deng, D. Yu, G. E. Dahl, A.-r. Mohamed, N. Jaitly, A. Senior, V. Vanhoucke, P. Nguyen, T. N. Sainath, and B. Kingsbury, “Deep neural networks for acoustic modeling in speech recognition: The shared views of four research groups,” *IEEE Signal Process. Mag.*, vol. 29, no. 6, pp. 82–97, 2012.
- [30] V. Monga, Y. Li, and Y. C. Eldar, “Algorithm unrolling: Interpretable, efficient deep learning for signal and image processing,” *IEEE Signal Process. Mag.*, vol. 38, no. 2, pp. 18–44, 2021.
- [31] V. Pappayan, Y. Romano, J. Sulam, and M. Elad, “Theoretical foundations of deep learning via sparse representations: A multilayer sparse model and its connection to convolutional neural networks,” *IEEE Signal Process. Mag.*, vol. 35, no. 4, pp. 72–89, 2018.
- [32] Y. Li, “Deep reinforcement learning,” 15 Oct. 2018. [Online]. Available: <https://arxiv.org/pdf/1810.06339.pdf>
- [33] Y. Bengio, A. Courville, and P. Vincent, “Representation learning: A review and new perspectives,” *IEEE Trans. Pattern Anal. Mach. Intell.*, vol. 35, no. 8, pp. 1798–1828, Aug. 2013.
- [34] D. Castellevecchi, “The Black Box of AI,” *Nature*, vol. 538, pp. 20–23, Oct. 2016.

- [35] Y. Bahri, J. Kadmon, J. Pennington, S. S. Schoenholz, J. Sohl-Dickstein, and S. Ganguli, “Statistical mechanics of deep learning,” *Annu. Rev. Condens. Matter Phys.*, vol. 11, no. 1, pp. 501–528, 2020. [Online]. Available: <https://doi.org/10.1146/annurev-conmatphys-031119-050745>
- [36] T. Poggio, A. Banburski, and Q. Liao, “Theoretical issues in deep networks,” *Proc. Natl. Acad. Sci. U.S.A.*, Jun. 2020.
- [37] B. Zhu, J. Jiao, and D. Tse, “Deconstructing generative adversarial networks,” *IEEE Trans. Inf. Theory*, vol. 66, no. 11, pp. 7155–7179, 2020.
- [38] J. Berner, P. Grohs, G. Kutyniok, and P. Petersen, “The modern mathematics of deep learning,” 2021. [Online]. Available: <https://arxiv.org/pdf/2105.04026.pdf>
- [39] P. L. Bartlett, A. Montanari, and A. Rakhlin, “Deep learning: a statistical viewpoint,” *Acta Numer.*, vol. 30, pp. 87 – 201, 2021.
- [40] G. Cybenko, “Approximation by superpositions of a sigmoidal function,” *Mathematics of Control, Signals, and Systems*, 1989.
- [41] K. Hornik, M. Stinchcombe, and H. White, “Multilayer feedforward networks are universal approximators,” *Neural Netw.*, vol. 2, no. 5, pp. 359–366, Jul. 1989.
- [42] K. Funahashi, “On the approximate realization of continuous mappings by neural networks,” *Neural Netw.*, vol. 2, no. 3, p. 183–192, May 1989.
- [43] A. R. Barron, “Approximation and estimation bounds for artificial neural networks,” *Mach. Learn.*, vol. 14, no. 1, p. 115–133, Jan 1994.
- [44] H. N. Mhaskar, “Neural networks for optimal approximation of smooth and analytic functions,” *Neural Comput.*, vol. 8, pp. 164–177, 1996.
- [45] A. Pinkus, “Approximation theory of the MLP model in neural networks,” *Acta Numerica*, vol. 8, pp. 143–195, 1999.
- [46] D. Rolnick and M. Tegmark, “The power of deeper networks for expressing natural functions,” in *Proc. ICLR*, 2018.
- [47] B. Poole, S. Lahiri, M. Raghu, J. Sohl-Dickstein, and S. Ganguli, “Exponential expressivity in deep neural networks through transient chaos,” in *Proc. NIPS*, 2016, pp. 3368–3376.
- [48] H. W. Lin, M. Tegmark, and D. Rolnick, “Why does deep and cheap learning work so well?” *J. Stat. Phys.*, vol. 168, no. 6, pp. 1223–1247, Jul. 2017.
- [49] R. Eldan and O. Shamir, “The power of depth for feedforward neural networks,” in *Proc. COLT*, 2016, pp. 907–940.
- [50] H. Mhaskar and T. Poggio, “Deep vs. shallow networks : An approximation theory perspective.” [Online]. Available: <https://arxiv.org/pdf/1608.03287.pdf>
- [51] T. Poggio, H. Mhaskar, L. Rosasco, B. Miranda, and Q. Liao, “Why and when can deep-but not shallow-networks avoid the curse of dimensionality: A review,” *Int. J. Autom. Comput.*, vol. 14, pp. 503–519, Dec. 2017.
- [52] Z. Lu, H. Pu, F. Wang, Z. Hu, and L. Wang, “The expressive power of neural networks: A view from the width,” in *Proc. NIPS*, 2017, pp. 6232–6240.
- [53] F.-L. Fan and G. Wang, “Duality of width and depth of neural networks.” [Online]. Available: <https://arxiv.org/pdf/2002.02515.pdf>
- [54] F. Fan, D. Wang, H. Guo, Q. Zhu, P. Yan, G. Wang, and H. Yu, “Slim, sparse, and shortcut networks,” 2018. [Online]. Available: <https://arxiv.org/pdf/1811.09003v2.pdf>
- [55] H. Lin and S. Jegelka, “ResNet with one-neuron hidden layers is a universal approximator.” [Online]. Available: <https://arxiv.org/pdf/1806.10909.pdf>
- [56] I. Daubechies, R. DeVore, S. Foucart, B. Hanin, and G. Petrova, “Nonlinear approximation and (deep) ReLU networks,” 2019.

- [57] W. Hwang and A. Heinecke, “Un-rectifying non-linear networks for signal representation,” *IEEE Trans. Signal Process.*, vol. 68, 2020.
- [58] A. R. Barron and J. M. Klusowski, “Approximation and estimation for high-dimensional deep learning networks,” 2018. [Online]. Available: <https://arxiv.org/pdf/1809.03090.pdf>
- [59] K. Kawaguchi, J. Huang, and L. P. Kaelbling, “Effect of depth and width on local minima in deep learning,” *Neural Comput.*, vol. 31, no. 7, pp. 1462–1498, 2019.
- [60] T. M. Getu, “Error bounds for a matrix-vector product approximation with deep ReLU neural networks,” 2021. [Online]. Available: <https://arxiv.org/pdf/2111.12963.pdf>
- [61] B. Hanin, “Universal function approximation by deep neural nets with bounded width and ReLU activations,” *Mathematics*, vol. 7, 2019.
- [62] P. Grohs, D. Perekrestenko, D. Elbrächter, and H. Boelskei, “Deep neural network approximation theory,” Jan. 2019. [Online]. Available: <https://arxiv.org/pdf/1901.02220.pdf>
- [63] H. Bölcskei, P. Grohs, G. Kutyniok, and P. Petersen, “Optimal approximation with sparsely connected deep neural networks,” *SIAM J. Math Data Sci.*, vol. 1, no. 1, pp. 8–45, 2019.
- [64] I. Gühring, G. Kutyniok, and P. Petersen, “Error bounds for approximations with deep ReLU neural networks in  $\mathbf{W}^{s,p}$  norms,” *Anal. Appl.*, vol. 18, Aug. 2019.
- [65] P. Petersen and F. Voigtlaender, “Optimal approximation of piecewise smooth functions using deep ReLU neural networks,” *Neural Netw.*, vol. 108, pp. 296–330, Dec. 2018.
- [66] M. Geiger, L. Petrini, and M. Wyart, “Landscape and training regimes in deep learning,” *Phys. Rep.*, vol. 924, pp. 1–18, 2021.
- [67] R. Sun, D. Li, S. Liang, T. Ding, and R. Srikant, “The global landscape of neural networks: An overview,” *IEEE Signal Process. Mag.*, vol. 37, no. 5, pp. 95–108, 2020.
- [68] R. Sun, “Optimization for deep learning: theory and algorithms,” 19 Dec. 2019. [Online]. Available: <https://arxiv.org/pdf/1912.08957.pdf>
- [69] C. Baldassi, C. Borgs, J. T. Chayes, A. Ingrosso, C. Lucibello, L. Saglietti, and R. Zecchina, “Unreasonable effectiveness of learning neural networks: From accessible states and robust ensembles to basic algorithmic schemes,” *Proc. Natl. Acad. Sci. U.S.A.*, vol. 113, no. 48, pp. E7655–E7662, 2016.
- [70] C. Baldassi, F. Pittorino, and R. Zecchina, “Shaping the learning landscape in neural networks around wide flat minima,” *Proc. Natl. Acad. Sci. U.S.A.*, vol. 117, no. 1, pp. 161–170, 2020.
- [71] M. Belkin, D. J. Hsu, S. Ma, and S. Mandal, “Reconciling modern machine-learning practice and the classical bias–variance trade-off,” *Proc. Natl. Acad. Sci. U.S.A.*, vol. 116, pp. 15 849–15 854, 2019.
- [72] R. Livni, S. Shalev-Shwartz, and O. Shamir, “On the computational efficiency of training neural networks,” in *Proc. NIPS*, vol. 27, 2014.
- [73] A. Jacot, F. Gabriel, and C. Hongler, “Neural tangent kernel: Convergence and generalization in neural networks,” in *Proc. NIPS*, 2018, pp. 8571–8580.
- [74] L. Chizat, E. Oyallon, and F. Bach, “On lazy training in differentiable programming,” Jan. 2020. [Online]. Available: <https://arxiv.org/pdf/1812.07956.pdf>
- [75] Z. Allen-Zhu, Y. Li, and Z. Song, “A convergence theory for deep learning via over-parameterization,” 2018. [Online]. Available: <https://arxiv.org/pdf/1811.03962.pdf>
- [76] D. Zou, Y. Cao, D. Zhou, and Q. Gu, “Stochastic gradient descent optimizes over-parameterized deep ReLU networks,” 2018. [Online]. Available: <https://arxiv.org/pdf/1811.08888.pdf>

- [77] H. Zhang, D. Yu, M. Yi, W. Chen, and T.-Y. Liu, “Convergence theory of learning over-parameterized ResNet: A full characterization,” 2019. [Online]. Available: <https://arxiv.org/pdf/1903.07120v2.pdf>
- [78] M. Soltanolkotabi, A. Javanmard, and J. D. Lee, “Theoretical insights into the optimization landscape of over-parameterized shallow neural networks,” *IEEE Trans. Inf. Theory*, vol. 65, no. 2, pp. 742–769, 2019.
- [79] S. Oymak and M. Soltanolkotabi, “Toward moderate overparameterization: Global convergence guarantees for training shallow neural networks,” *IEEE J. Sel. Areas Inf. Theory*, vol. 1, no. 1, pp. 84–105, 2020.
- [80] Z. Chen, Y. Cao, D. Zou, and Q. Gu, “How much over-parameterization is sufficient to learn deep ReLU networks?” 2020. [Online]. Available: <https://arxiv.org/pdf/1911.12360.pdf>
- [81] Z. Allen-Zhu, Y. Li, and Y. Liang, “Learning and generalization in overparameterized neural networks, going beyond two layers,” 2020. [Online]. Available: <https://arxiv.org/pdf/1811.04918.pdf>
- [82] Y. Cao and Q. Gu, “Generalization error bounds of gradient descent for learning over-parameterized deep ReLU networks,” 2019. [Online]. Available: <https://arxiv.org/pdf/1902.01384.pdf>
- [83] C. Zhang, S. Bengio, M. Hardt, B. Recht, and O. Vinyals, “Understanding deep learning requires rethinking generalization,” 2017.
- [84] B. Adlam and J. Pennington, “The neural tangent kernel in high dimensions: Triple descent and a multi-scale theory of generalization. arxiv [preprint]. <https://arxiv.org/pdf/2008.06786.pdf> (accessed Dec. 2021).” 2020.
- [85] S. Mei, A. Montanari, and P.-M. Nguyen, “A mean field view of the landscape of two-layer neural networks,” *Proc. Natl. Acad. Sci. U.S.A.*, vol. 115, no. 33, pp. E7665–E7671, 2018.
- [86] P.-M. Nguyen and H. T. Pham, “A rigorous framework for the mean field limit of multilayer neural networks. arxiv [preprint]. <https://arxiv.org/pdf/2001.11443.pdf> (accessed Jul. 2021).” 2021.
- [87] V. Pappayan, X. Y. Han, and D. L. Donoho, “Prevalence of neural collapse during the terminal phase of deep learning training,” *Proc. Natl. Acad. Sci. U.S.A.*, vol. 117, no. 40, pp. 24 652–24 663, 2020.
- [88] C. Fang, H. He, Q. Long, and W. J. Su, “Exploring deep neural networks via layer-peeled model: Minority collapse in imbalanced training,” *Proc. Natl. Acad. Sci. U.S.A.*, vol. 118, no. 43, 2021.
- [89] D. E. Rumelhart, G. E. Hinton, and R. J. Williams, “Learning representations by back-propagating errors,” *Nature*, vol. 323, no. 6088, pp. 533–536, 1986.
- [90] S. Shalev-Shwartz and S. Ben-David, *Understanding Machine Learning: From Theory to Algorithms*. New York, NY, USA: Cambridge Univ. Press, 2014.
- [91] W. E. C. Ma, S. Wojtowytsch, and L. Wu, “Towards a mathematical understanding of neural network-based machine learning: what we know and what we don’t,” 2020. [Online]. Available: <https://arxiv.org/pdf/2009.10713.pdf>
- [92] M. J. Wainwright, *High-Dimensional Statistics: A Non-Asymptotic Viewpoint*. Cambridge Univ. Press, 2019.
- [93] R. Vershynin, *High-Dimensional Probability: An Introduction with Applications in Data Science*. Cambridge Univ. Press, 2018.
- [94] T. M. Getu, N. T. Golmie, and D. W. Griffith, “Blind estimation of a doubly selective OFDM channel: A deep learning algorithm and theory,” 2022. [Online]. Available: <https://arxiv.org/pdf/2206.07483.pdf>
- [95] T. M. Getu, W. Saad, G. Kaddoum, and M. Bennis, “Performance limits of a deep learning-enabled text semantic communication under interference,” 2023. [Online]. Available: <https://arxiv.org/pdf/2302.14702.pdf>
- [96] J. G. Proakis, and M. Salehi, *Digital Communications*, 5th ed. New York, NY, USA: McGraw-Hill, 2008.
- [97] D. Elbrächter, D. Perekrestenko, P. Grohs, and H. Bölcskei, “Deep neural network approximation theory,” *IEEE Trans. Inf. Theory*, vol. 67, no. 5, pp. 2581–2623, 2021.
- [98] Wikipedia, “Probability space,” [Online]. [https://en.wikipedia.org/wiki/Probability\\_space](https://en.wikipedia.org/wiki/Probability_space) (accessed Mar. 2022).
- [99] D. P. Bertsekas and J. N. Tsitsiklis, *Introduction to Probability*, 2nd ed. Belmont, MA, USA: Athena Scientific, 2008.

- [100] A. Papoulis and S. U. Pillai, *Probability, Random Variables, and Stochastic Processes*, 4th ed. Boston, MA, USA: McGraw Hill, 2002.
- [101] Wikipedia, “Probability axioms,” [Online]. [https://en.wikipedia.org/wiki/Probability\\_axioms](https://en.wikipedia.org/wiki/Probability_axioms) (accessed Mar. 2022).
- [102] R. G. Gallager, *Stochastic Processes: Theory for Applications*. Cambridge, UK: Cambridge Univ. Press, 2013.
- [103] H. Kobayashi, B. L. Mark, and W. Turin, *Probability, Random Processes, and Statistical Analysis*. New York, NY, USA: Cambridge Univ. Press, 2012.
- [104] J. L. Devore, *Probability and Statistics for Engineering and the Sciences*, 8th ed. Brooks/Cole, 2010.
- [105] G. R. Grimmett and D. R. Stirzaker, *Probability and Random Processes*, 3rd ed. Oxford, UK: Oxford Univ. Press, 2001.
- [106] Wikipedia, “Law of total probability,” [Online]. [https://en.wikipedia.org/wiki/Law\\_of\\_total\\_probability](https://en.wikipedia.org/wiki/Law_of_total_probability) (accessed Mar. 2022).
- [107] H. Pishro-Nik, *Introduction to Probability, Statistics, and Random Processes*. Kappa Research, LLC, 2014.
- [108] K. He, X. Zhang, S. Ren, and J. Sun, “Delving deep into rectifiers: Surpassing human-level performance on ImageNet classification,” 2015. [Online]. Available: <https://arxiv.org/pdf/1502.01852.pdf>
- [109] Y. A. LeCun, L. Bottou, G. B. Orr, and K.-R. Müller, “Efficient backprop,” in *Neural Networks: Tricks of the Trade*, 2nd ed., G. Montavon, G. B. Orr, and K.-R. Müller, Eds. Berlin, Heidelberg: Springer, 2012, pp. 9–48.
- [110] Y. Bengio, “Practical recommendations for gradient-based training of deep architectures,” in *Neural Networks: Tricks of the Trade*, 2012.
- [111] S. Haykin, *Neural Networks and Learning Machines*, 3rd ed. Upper Saddle River, NJ, USA: Pearson, 2009.
- [112] Wolfram, “Wolfram MathWorld: Hyperbolic Tangent,” [Online]. <https://mathworld.wolfram.com/HyperbolicTangent.html> (accessed May 2022).
- [113] J. Peters, D. Janzing, and B. Schölkopf, *Elements of Causal Inference: Foundations and Learning Algorithms*. Cambridge, MA, USA: The MIT Press, 2017.
- [114] J. Kaddour, A. Lynch, Q. Liu, M. J. Kusner, and R. Silva, “Causal machine learning: A survey and open problems,” 2022. [Online]. Available: <https://arxiv.org/pdf/2206.15475.pdf>
- [115] G. Wang, G. B. Giannakis, and J. Chen, “Learning ReLU networks on linearly separable data: Algorithm, optimality, and generalization,” *IEEE Trans. Signal Process.*, vol. 67, pp. 2357–2370, 2019.
- [116] F. Chollet, *Deep Learning with Python*. Shelter Island, NY, USA: Manning, 2018.
- [117] G. Marcus, “Deep learning: A critical appraisal,” 2018. [Online]. Available: <https://arxiv.org/abs/1801.00631>
- [118] Wikipedia, “Matrix calculus,” last accessed Mar. 2023. [Online]. Available: [https://en.wikipedia.org/wiki/Matrix\\_calculus](https://en.wikipedia.org/wiki/Matrix_calculus)
- [119] T. Parr and J. Howard, “The matrix calculus you need for deep learning,” 2018. [Online]. Available: <https://arxiv.org/pdf/1802.01528.pdf>
- [120] Wolfram, “Wolfram MathWorld: Sign,” [Online]. <https://mathworld.wolfram.com/Sign.html> (accessed Apr. 2022).
- [121] H. V. Poor, *An Introduction to Signal Detection and Estimation*, 2nd ed. New York, NY, USA: Springer-Verlag, 1994.
- [122] D. P. Kingma and J. L. Ba, “Adam: A method for stochastic optimization,” in *Proc. ICLR*, 2015.